Seda SAKİ FABRICATION OF NANOCOMPOSITE MEMBRANES AND THEIR APPLICATIONS IN OILY WASTEWATER TREATMENT AGU 2017

FABRICATION OF NANOCOMPOSITE MEMBRANES AND THEIR APPLICATIONS IN OILY WASTEWATER TREATMENT

A THESIS
SUBMITTED TO THE DEPARTMENT OF ADVANCED MATERIALS AND NANOTECHNOLOGY
AND THE GRADUATE SCHOOL OF ENGINEERING AND SCIENCE
OF ABDULLAH GUL UNIVERSITY
IN PARTIAL FULFILLMENT OF THE REQUIREMENTS
FOR THE DEGREE OF
MASTER

By
Seda SAKİ
July 2017

GCRIS

FABRICATION OF NANOCOMPOSITE MEMBRANES AND THEIR APPLICATIONS IN OILY WASTEWATER TREATMENT

A THESIS

SUBMITTED TO THE DEPARTMENT OF

ADVANCED MATERIALS AND NANOTECHNOLOGY

AND THE GRADUATE SCHOOL OF ENGINEERING AND SCIENCE OF ABDULLAH GUL UNIVERSITY

IN PARTIAL FULFILLMENT OF THE REQUIREMENTS

FOR THE DEGREE OF

MASTER

By

Seda SAKİ

July 2017

GCRIS

SCIENTIFIC ETHICS COMPLIANCE

I hereby declare that all information in this document has been obtained in accordance with academic rules and ethical conduct. I also declare that, as required by these rules and conduct, I have fully cited and referenced all materials and results that are not original to this work.

Name-Surname: Seda SAKİ

Signature :

GCRIS

REGULATORY COMPLIANCE

M.Sc thesis titled **"Fabrication of nanocomposite membranes and their applications in oily wastewater treatment"** has been prepared in accordance with the Thesis Writing Guidelines of the Abdullah Gül University, Graduate School of Engineering & Science.

Prepared By;

Seda SAKİ

Advisor

Assoc. Prof. Dr. Niğmet UZAL

Head of the Advanced Materials and Nanotechnology Program

Prof. Dr. Murat DURANDURDU

ACCEPTANCE AND APPROVAL

M.Sc. thesis titled “Fabrication of nanocomposite membranes and their applications in oily wastewater treatment “and prepared by Seda Saki has been accepted by the jury in the Advanced Materials and Nanotechnology Graduate Program at Abdullah Gül University, Graduate School of Engineering & Science.

17/07/2017

JURY:

Advisor :Assoc. Prof. Dr. Niğmet UZAL

Member :Assoc. Prof. Dr. Nuray ATEŞ

Member :Assoc. Prof. Dr. Okan Tarık KOMESLİ

GCRIS

APPROVAL:

The acceptance of this M.Sc. thesis has been approved by the decision of the Abdullah Gül University, Graduate School of Engineering & Science, Executive Board dated ….. /….. / …… and numbered …….. .

…….. /…….. / ……..

Prof.İrfan ALAN

GCRIS

ABSTRACT

FABRICATION OF NANOCOMPOSITE MEMBRANES AND THEIR APPLICATIONS IN OILY WASTEWATER TREATMENT

Seda Saki

MSc. in Advanced Materials and Nanotechnology

Supervisor: Assoc. Prof. Dr. Nigmet Uzal

July, 2017

Industrial oily wastewaters are generated by various industries such as steel, food, textile, leather, petrochemical and metal milling and should be treated before discharging natural environment due to its serious environmental problems. With this view, membrane separation processes have promote a significant development of novel and green technology for oily wastewater treatment due to its clear advantages, for instance, ease in operation, efficient separation, low energy consumption and cost. Specially microfiltration (MF) and ultrafiltration (UF) membranes are playing a more prominent role in the oily wastewater treatments because of many advantages like as stable effluent quality, small area requirement, no chemicals addition, high chemical oxygen demand (COD) removal and low energy need. But the main drawback of membrane processes is the fouling problem. To overcome this problem, many researchers effort fabrication of high performance of membrane with higher hydrophilicity and antifouling properties. In this study, flat-sheet PSF/PEI nanocomposite membranes using Al_2O_3 and $CaCO_3$ nanoparticles were prepared by phase inversion method. The effect of Al_2O_3 and $CaCO_3$ nanoparticles were investigated on the structural properties and filtration performance of the nanocomposite membranes. Prepared membranes were characterized with scanning electron microscopy (SEM), fourier transform infrared spectroscopy (FT-IR), contact angle, porosity, water flux, thermogravimetric analysis (TGA), atomic force microscope

(AFM), X-ray diffraction (XRD), BSA rejection, tensile strength, and viscosity measurements. Membrane permeability performance and antifouling properties towards oil water emulsion separation of these new generation nanocomposite membranes were evaluated for synthetic and real industrial oily wastewater. The results showed that there is a great potential to use these nanocomposite membranes for oily water treatment with higher permeability and antifouling capacity. All Al_2O_3 and $CaCO_3$ nanocomposite membranes reached higher oil rejection ratios over 90%.

Keywords: nanocomposite membrane, Al_2O_3 and $CaCO_3$ nanoparticles, oil rejection, industrial oily wastewater

GCRIS

ÖZET

NANOKOMPOZİT MEMBRAN ÜRETİMİ VE YAĞ İÇEREN ATIKSULARIN ARITIMINDA UYGULANMASI

Seda Saki

İleri Malzemeler ve Nanoteknoloji Yüksek Lisans Pogramı

Tez Yöneticisi: Doç. Dr.Niğmet Uzal

Temmuz - 2017

Endüstriyel yağlı atıksular çelik, gıda, tekstil, deri, petrokimya ve metal gibi çeşitli endüstriler tarafından üretilmekte ve ciddi çevre sorunlarına sebep olmaları nedeniyle alıcı ortama deşarj edilmeden önce arıtılmaları gerekmektedir. Bu bağlamda; membran ayırma süreçlerinin kullanım kolaylığı, etkin ayırma kapasitesi, düşük enerji tüketimi ve maliyet gibi avantajları nedeniyle yağlı atık su arıtımında yeni ve yeşil bir teknoloji olarak gelişim göstermektedir. Özellikle mikrofiltrasyon (MF) ve ultrafiltrasyon (UF) membranları, stabil su kalitesi, küçük alan gereksinimi, kimyasal ilavesine gerek olmaması, yüksek kimyasal oksijen ihtiyacı (KOİ) giderimi ve düşük enerji gereksinimi gibi avantajlarından dolayı yağlı atık su arıtımlarında önemli bir rol oynamaktadır. Fakat membran proseslerin en büyük sorunu tıkanma problemidir. Bu sorunun üstesinden gelmek için, birçok araştırmacı daha yüksek hidrofiliklik ve tıkanma direnci özelliklerine sahip yüksek performanslı membran üretimi konusunda araştırmalarını yoğunlaştırmıştır. Bu çalışmada, Al_2O_3 ve $CaCO_3$ nanoparçacıkların kullanıldığı düz tabaka PSF/PEI nanokompozit membranlar faz dönüşümü yöntemi ile üretilmiştir. Üretilen anokompozit membranların yapısal özellikleri ve filtrasyon performansı üzerine Al_2O_3 ve $CaCO_3$ nanoparçacıklarının etkisi, araştırılmıştır. Üretilen yeni nesil nanokompozit membranlar taramalı elektron mikroskobu (SEM), Fourier dönüşümlü kızılötesi spektrometre (FTIR), temas açısı, gözeneklilik, su akısı, termogravimetrik analiz (TGA), atomik kuvvet mikroskopu (AFM), X-ışını kırınımı (XRD) , BSA reddi, gerilme mukavemeti ve viskozite ölçümleri ile karakterize edilmiştir. Yeni nesil nanokompozit membranların yağ/su emülsiyon ayrımına karşı membran geçirgenlik performansı ve tıkanmaya direnç özellikleri, sentetik ve gerçek sanayi yağlı atıksu için değerlendirilmiştir. Sonuçlar, yüksek permeabilite ve tıkanma direnci nedeni ile yağlı su

arıtımı için bu çalışmada üretilen nanokompozit membranların büyük bir potansiyeli olduğunu göstermiştir. Tüm Al_2O_3 ve $CaCO_3$ nanokompozit membranlar ile %90'ın üzerinde yağ giderimi elde edilmiştir.

Anahtar kelimeler: nanokompozit membran, Al_2O_3 ve $CaCO_3$ nanomalzemeler, yağ giderimi, endüstriyel yağlı atıksu

GCRIS

Acknowledgements

First of all, I would like to thank my supervisor, Assoc. Prof. Dr. Nigmet Uzal, for bringing me to this interesting and promising topic and her many valuable discussions and wonderful suggestions for my graduate work and her understanding, encouragement and numerous hours spent helping me to complete this thesis.

Next, I would like to thank Assoc. Prof. Dr. Burak Uzal and Assoc. Prof. Dr. Murat Gökçek for their precious time and valuable comments and suggestions during my thesis.

I'd also like to express my special thanks to the thesis committee, Assoc. Prof. Dr. Nuray Ates and Assoc. Prof. Dr. Okan Tarık Komesli for the efforts to provide valuable comments during my proposal presentation, for the their valuable time to review this thesis and for offering me an opportunity to defend in front of them.

Special thanks go to my colleague Y. Emre Bulbul for his support and motivation during the experimental studies. My appreciation is also extended to Mr. Furkan Yerli and Mr. Berk Ertem for helping me with the experimental set-up.

Especially thanks to the Scientific Research Foundation of Abdullah Gül University (Project No. FYL-2016-75) for funding this study.

Finally, I would like thank my parents for all of their concerns and supports.

TABLE OF CONTENTS

1. INTRODUCTION 1

2. LITERATURE REVIEW 3

2.1. Membrane Technology 3

2.2. Membrane Materials 7

2.2.1. Polymeric membranes 9

2.2.2. Polymeric nanocomposite membranes 10

2.3. Membrane Fabrication 14

2.3.1. Interfacial polymerization 15

2.3.2. Stretching 16

2.3.3. Track-etching 16

2.3.4. Electrospinning 17

2.3.5. Phase inversion 19

2.4. Membrane Separation Processes for Oily Wastewater Treatment 21

3. EXPERIMENTAL 24

3.1. Materials 24

3.2. Preparation of Membranes 25

3.3. Membrane Characterization 27

3.3.1. SEM 27

3.3.2. Water contact angle 28

3.3.3. Water filtration tests 29

3.3.4. BSA removal experiments 30

3.3.5. Oil removal experiments 31

3.3.6. Porosity 32

3.3.7. FT-IR 32

3.3.8. Mechanical strength 33

3.3.9. Viscosity measurements 34

3.3.10. Thermal stability 35

3.3.11. AFM analysis 35

3.3.12. XRD analysis 36

4. RESULTS AND DISCUSSIONS 37

4.1. The Effect of PSF Polymer Concentration 37

4.2. The Effect of PEI Concentration in PSF Membrane Matrix 38

4.3. PSF/PEI/ Al_2O_3 Nanocomposite Membranes 43

4.3.1. Viscosity of membrane dope solutions 43

4.3.2. Membrane morphology 45

4.3.3. Membrane hydrophilicity 47

4.3.4. Porosity 48

4.3.5. Mechanical properties 49

4.3.6. Thermal stability 50

4.3.7. FT-IR 51

4.3.8. Pure water flux 52

4.3.9. BSA rejection 54

4.4. PSF/PEI/$CaCO_3$ Nanocomposite Membranes 55

4.4.1. Viscosity of membrane dope solutions 56

4.4.2. Membrane morphology 57

4.4.3. Membrane hydrophilicity 59

4.4.4. Porosity 61

4.4.5. Mechanical properties 61

4.4.6. FT-IR 62

4.4.7. AFM 63

4.4.8. XRD 65

4.4.9. Pure water flux 66

4.4.10. BSA rejection 67

4.5. Oil Rejection Experiments 69

4.5.1. Oil rejection performance of Al_2O_3 membranes 69

4.5.2. Oil rejection of $CaCO_3$ membranes 72

5. CONCLUSIONS 78

BIBLIOGRAPHY 81

LIST OF TABLES

Table 2.1.Development of membrane technology since 1960s 5
Table 2.2.Membrane process, their driving force, mass transfer mechanism and applications 6
Table 3.1.Casting solution compositions of Al_2O_3 membranes..... 25
Table 3.2.Casting solution compositions of $CaCO_3$ membranes 26
Table 4.1.Contact angle and water flux values of 15 wt% PSF incorpareted with different concentrations of PEI 39
Table 4.2.Contact angle and water flux values of 20 wt% PSF incorporated with different concentration of PEI..... 42
Table 4.3.Casting solution compositions of PSF, PSF/PEI and PSF/PEI/Al_2O_3 membranes 43
Table 4.4.Contact angle, pure water flux (at 4 bar), and porosity of PSF, PSF/PEI (15/1 wt%) and PSF/PEI/Al_2O_3 (20 nm and 80 nm) nanocomposite membranes 48
Table 4.5. Weight loss (%) differences of PSF and PSF/PEI/Al_2O_3 nanocomposite membranes at 550°C 51
Table 4.6. Casting solution compositions of PSF, PSF/PEI (20/2 wt%) and PSF/PEI/$CaCO_3$ membranes 56
Table 4.7.Contact angle, pure water flux (at 2 bar) and porosity of PSF, PSF/PEI and PSF/PEI/$CaCO_3$ nanocomposite membranes..... 60
Table 4.8.The roughness properties of PSF, PSF/PEI (20/2 wt%) and PSF/PEI/$CaCO_3$ nanocomposite membranes. 65
Table 4.9.The BSA flux, BSA rejection and thickness of PSF (20 wt%), PSF/PEI (20/2 wt%) and PSF/PEI/$CaCO_3$ nanocomposite membranes. 68
Table 4.10.Wastewater characteristics..... 69
Table 4.11.pH and conductivities of the pemeates in filtrations with PSF/PEI and PSF/PEI/Al_2O_3 membranes 72
Table 4.12.Oil rejection ratio (%), FRR (%) and DR (%) values to PSF, PSF/PEI and PSF/PEI/$CaCO_3$ membranes of synthetic O/W emulsion filtration..... 74
Table 4.13.pH and conductivities of the feed of industrial wastewater filtrations with PSF/PEI and PSF/PEI/$CaCO_3$ membranes 77

LIST OF FIGURES

Figure 2.1.Schematic illustration of membrane separation 3
Figure 2.2.Schematic illustration of (a) dead-end and (b) cross-flow filtration 4
Figure 2.3. Schematic illutsration of the membrane materials and their structures..... 8
Figure 2.4.Fabrication of conventional nanocomposite membranes 11
Figure 2.5.Schematic illustration of IP process 15
Figure 2.6.Schematic illustration of streching process 16
Figure 2.7.Schematic illustration of track-etching process..... 17
Figure 2.8.Schematic illustration of electrospinning process 18
Figure 2.9.Schematic drawing illustrating of phase inversion process..... 20
Figure 3.1.Chemical structure of PSF and PEI 24
Figure 3.2.Schematic diagram for the preparation of PSF/PEI/Al_2O_3 membranes 26
Figure 3.3.Schematic diagram for the preparation of and PSF/PEI/$CaCO_3$ 27
Figure 3.4.Hydrophobic surface (left) and hydrophilic surface (right) 28
Figure 3.5.Optical contact angle and surface tension meter 28
Figure 3.6.Dead-end filtration set-up..... 30
Figure 3.7.UV-visible spectroscopy 31
Figure 3.8. FT-IR spectra..... 33
Figure 3.9. Tensile testing equipment..... 34
Figure 3.10. Rotational viscometer with variable temperature and shear capabilities ... 34
Figure 3.11. Thermogravimetric Analyzer 35
Figure 4.1.SEM images of top surface of; (a) 15 wt% PSF membrane, (b) 20 wt% PSF membrane and (c) 25wt% PSF membrane 38
Figure 4.2.SEM images of 15 wt% PSF membranes cross-section containing PEI with different concentrations: (a) 0.2 wt%, (b) 0.5 wt%, (c) 1 wt%, (d) 2 wt%..... 40
Figure 4.3.SEM images of PSF and PSF/PEI membranes: (a) PSF surface, (b) PSF/PEI surface, (c) PSF cross section, (d) PSF/PEI cross section. 41
Figure 4.4.SEM images of 20 wt% PSF membranes cross-section containing PEI with different concentrations: (a) 0 wt%, (b) 2wt%, (c) 4wt%, (d) 6wt%..... 42

Figure 4.5.Viscosity of the casting solutions for the PSF (15 wt %), PSF/PEI (15/1 wt%), and PSF/PEI/Al_2O_3 nanocomposite membranes (20 nm and 80 nm) 45
Figure 4.6.SEM images of PSF/PEI (15/1 wt%) membranes cross-sections containing 20 nm Al_2O_3 with different concentrations: (a) 0.2 wt%, (b) 1 wt%, (c) 5 wt%.... 46
Figure 4.7.Cross-section SEM images of PSF/PEI (15/1 wt%) membrane containing 5 wt% Al_2O_3 nanoparticles: (a) 20 nm Al_2O_3, (b) 80 nm Al_2O_3..... 47
Figure 4.8.Tensile strength of breaking point of PSF, PSF/PEI (15/1 wt%) and PSF/PEI/Al_2O_3 nanocomposite membranes 50
Figure 4.9.TGA curves of PSF, PSF/PEI (15/1 wt%) and PSF/PEI/Al_2O_3 nanocomposite membranes 51
Figure 4.10. FT-IR spectrum of PSF, PSF/PEI and PSF/PEI membrane containing 5 wt % Al_2O_3..... 52
Figure 4.11.Water fluxes of PSF, PSF/PEI and PSF/PEI/Al_2O_3 nanocomposite membranes at different pressures. 53
Figure 4.12.BSA rejection performance of PSF, PSF/PEI (15/1 wt%), and PSF/PEI/Al_2O_3 nanocomposite membranes 54
Figure 4.13. BSA rejection performance of PSF, PSF/PEI (15/1 wt%), and PSF/PEI/Al_2O_3 nanocomposite membranes. 55
Figure 4.14.The casting solution viscosity values of PSF/PEI (20/2 wt%) and PSF/PEI/$CaCO_3$ nanocomposite membranes..... 57
Figure 4.15.Surface SEM images of PSF/PEI (20/2 wt%) membrane containing $CaCO_3$ nanoparticles: (a) 0.2 wt%, (b) 1 wt%, (c) 5 wt%, (d) 10 wt% 58
Figure 4.16.Cross-section SEM images of PSF/PEI membrane containing $CaCO_3$ nanoparticles: (a) 0.2 wt%, (b) 1 wt%, (c) 5 wt%, (d) 10 wt% 59
Figure 4.17.Contact angle images of PSF/PEI membrane containing $CaCO_3$ nanoparticles: (a) 0.2 wt%, (b) 1 wt%, (c) 5 wt%, (d) 10 wt% 60
Figure 4.18. Strain-stress curve of PSF and PSF/PEI/$CaCO_3$ membranes 62
Figure 4.19.FT-IR spectrum of PSF and PSF/PEI/$CaCO_3$ nanocomposite membranes. 63
Figure 4.20.AFM images of (a) PSF (20 wt%), (b) PSF/PEI (20/2 wt%) and PSF/PEI/$CaCO_3$ nanocomposite membranes containing (c) 1 wt% $CaCO_3$ nanoparticles, (d) 2 wt% $CaCO_3$ nanoparticles, (e) 5 wt% $CaCO_3$ nanoparticles, (f) 10 wt% $CaCO_3$ nanoparticles..... 64
Figure 4.21.XRD graphs of PSF and PSF/PEI membrane containing 10 wt% $CaCO_3$ nanoparticle..... 66

Figure 4.22.Pure water flux of PSF/PEI/$CaCO_3$ nanocomposite membranes 67
Figure 4.23.BSA flux of PSF/PEI/$CaCO_3$ nanocomposite membranes..... 68
Figure 4.24.Oil rejection ratio of BSA flux of PSF/PEI/Al_2O_3 nanocomposite membranes 70
Figure 4.25.Synthetic vacuum oily feed solution and filtreted permeate 70
Figure 4.26.Industrial wastewater and filtreted water with Al_2O_3 membranes at 25 ± 5 °C, TMP: 2 bar..... 71
Figure 4.27.Oil rejection ratio of PSF, PSF/PEI and PSF/PEI/$CaCO_3$ membranes of synthetic O/W emulsion and ındustrial wastewater..... 73
Figure 4.28.Flux changes of PSF, PSF/PEI and PSF/PEI/$CaCO_3$ membranes of pure water, synthetic oily water and cleaned membrane fluxes 74
Figure 4.29. Industrial wastewater and filtered water with $CaCO_3$ nanocomposite membranes at 25 ± 5 °C, TMP: 2 bar 75
Figure 4.30. SEM images of the top surface view fouled membranes of after industrial oily water filtration; PSF/PEI membrane containing $CaCO_3$ nanoparticles: (a) 0.2 wt%, (b) 1 wt%, (c) 5 wt%, (d) 10 wt% 76

GCRIS

LIST OF ABBREVIATIONS

AFM	Atomic force microscope
BSA	Bovine serum albumin
CA	Cellulose acetate
CNTs	Carbon-nanotubes
COD	Chemical oxygen demand
DGDE	Diethylene glycol dimethyl ether
DMAc	Dimethyl acetamide
DMF	Dimethyl Formamide
DR	Decay ratio
FRR	Flux recovery ratio
FT-IR	Fourier transform infrared spectroscopy
GBL	γ-Butyrolactone
GO	Graphene oxide
HA	Humic acids
IP	Interfacial polymerization
MF	Microfiltration
MPD	M-phenylenediamine
MWCNTs	Multiwalled carbon nanotubes
NF	Nanofiltration
NMP	N-Methyl pyrrolidone
O/W	Oil/Water

GCRIS

OA	Oleicacid
PA	Polyamide
PAN	Poly (acrylonitrile)
PDA	Polydopamine
PE	Polyethelene
PEG	Polyethelene glycol
PEI	Polyethyleneimine
PEO	Polyethylene oxide
PES	Polyethersulphone
PI	Phase inversion
PP	Polypropilene
PPMM	Polypropylene microfiltration membrane
PRO	Pressure retarded osmosis
PSF	Polysulfone
PU	Polyurethane
PVA	Polyvinyl alcohol
PVDF	Poly(vinylidine fluoride)
PVP	Polyvinylpyrrolidone
RO	Reverse osmosis
SDS	Sodium dodecylsulfate
SEM	Scanning electron microscopy
SZP Particles	Zr-doped hybrid silica particles
TFC	Thin-film composite
TFN	Thin-film nanocomposite
TGA	Thermogravimetric analysis

TMC	Trimesoyl chloride
UF	Ultrafiltration
VRR	Volume reduction ratio
WPU	Waterborne polyurethane

GCRIS

Chapter 1

1. INTRODUCTION

Oily wastewaters are mainly produced from the food, leather, metallurgical, petrochemical and cosmetic industries, and petroleum refineries [1-4], in the typical range of 100–1000 mg/L oil in effluent which lead to serious environmental problems [5-7]. Furthermore it needs to be reduced to the environmental standards of 10–15 mg/L for safely discharge to receiving water bodies [5, 8, 9]. Gravitational separation [10], coagulation/flocculation [11], electric field [12], and air flotation are the conventional technologies used to remove oil from wastewtaters. However, these methods can not treate stable oil/water (O/W) emulsions (size≤20 μm) effectively [13, 14]. With this view, membrane separation have promote a significant development of novel and green technology for oily wastewater treatment due to its clear advantages, for instance, ease in operation, efficient separation, low energy consumption and sustention cost [15-17].

Among all membrane methods, ultrafiltration (UF) process, which has pore sizes of 2–50 nm range, has gradually become an attractive technology for oil removal [18-20]. Polymeric membranes were widely used to produce UF membranes such as polysulfone (PSF) [21], polyethersulfone (PES) [22], polyvinylidene fluoride (PVDF) [23] and polyacrylonitrile (PAN) in the application of oily water treatment.

PSF is commonly used to fabricate membranes and preferred due to its mechanical robustness, structural and chemical stability, large range of solubility, and thermal resistance [24, 25]. Besides the advantages of PSF, it needs to be modified to reduce its hydrophobic characteristics and increase its permeability and antifouling capacity for treating oily wastewaters [26-29]. Fouling is the major problem of the membranes, which is caused by deposition and adsorption of foulants on the membrane surfaces or within pore channels, results in flux and rejection decline [30-32]. Membrane hydrophilicity effect membrane fouling directly, i.e. the higher hydrophilicity generally shows the more antifouling capacity [33, 34]. To enhance antifouling property, hydrophilic additives such as hydrophilic polymers as cellulose acetate (CA) [35], and

polyvinyl alcohol (PVA) [36], polyethylenimine (PEI) [37], polyethyleneglycol (PEG) [38], and polyvinylpyrrolidone (PVP) [39]; and inorganic nanoparticles as Fe_2O_3 [40], TiO_2 [41], Al_2O_3[42], SiO2 [43], ZnO_2 [44], bentonite and $CaCO_3$ [45] have been performed.

Among these additives, PEI is shown to be a favorable polymeric amine with special features, and it is mostly used as a macrovoid formation agent [46, 47]. However, the addition of hydrophilic polymers, including PEI, can decrease the mechanical strength, stability, and selectivity of the membrane [48]. To overcome these problems, blending the polymer with inorganic nano-additives has also become a popular approach for the design of new PSF membranes with desirable properties [49, 50]. PSF membranes with inorganic nano-additives have better permeability, selectivity, and mechanical strength than pure PSF membranes. The incorporation of nano-additives in the polymer matrix also enhances the membrane's permeability, selectivity, tensile strength, and thermal and chemical resistance [51-54].

This study focuses on fabricating PSF/PEI nanocomposite membranes using two different particle sizes of Al_2O_3 nanoparticles (20 and 80 nm) and one size of $CaCO_3$ (100 nm) via the phase inversion method. To the best of our knowledge, there are no reported data on using a PSF/PEI/Al_2O_3 and PSF/PEI/$CaCO_3$ blended substrate to fabricate polymeric nanocomposite membranes for treating oily wastewater, and the effect of the Al_2O_3 and $CaCO_3$ nanoparticles on PSF/PEI membranes has not been examined. The effects of the nanoparticle size and concentration on the performance of membranes were thus investigated. The membrane properties were evaluated by scanning electron microscopy (SEM), fourier transform infrared spectroscopy (FT-IR), contact angle, porosity, water flux, thermogravimetric analysis (TGA), atomic force microscope (AFM), X-ray diffraction (XRD), BSA rejection, tensile strength, and viscosity measurements. To examine the membrane permeability performance and antifouling properties towards O/W emulsion separation, and industrial wastewater filtration experiment was also carried out accordingly. The findings provide new insight that may contribute to the development of better nanocomposite membranes for water-based filtration applications.

Chapter 2

2.LITERATURE REVIEW

2.1. Membrane Technology

Membranes have gained an important role in many technically and commercially relevant separation processes including sea and brackish water desalination, separation of gases and vapors and energy conversion and storage systems [55-57]. Membranes simply defined as selective barriers between two phases that feed and permeate can control transport mechanism of solution between the two compartments [58-60] (Fig. 2.1).

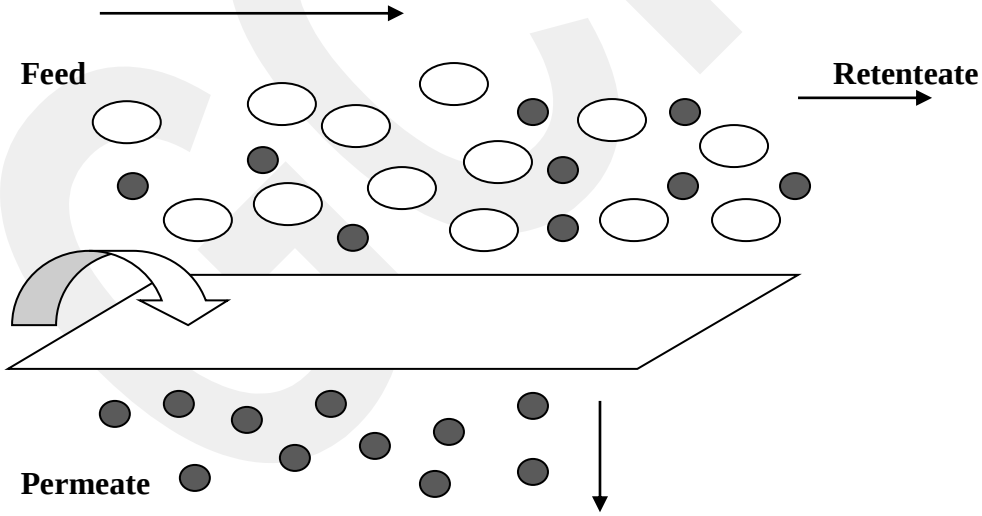

Figure 2.1.Schematic illustration of membrane separation

In membrane seperation systems there are two types of filtration processes; dead-end and cross-flow filtrations. Dead-end applications are the most basic form, which is the liquid, filtered directly through the membrane surface, so that the filtered solution is

accumulated on the surface of the membrane. Although this accumulation is known as a fouling of dead-end filtration, can be effective technique for concentrating compounds to be removed is low or the packing tendency [61, 62]. On the other hand, high concentrations of particles or macromolecules will rapidly compact on the membrane surface to excess unacceptable level in a dead-end filtration. A cross-flow system contributes the means to maintain stable filtration rates. With cross-flow filtration a flow along the membrane which prevents the accumulation of solution on the membrane surface [63-65]. In cross-flow filtration, feed passes tangentially through the membrane surface. Hovewer the smaller components than the pores pass the membrane; larger components than the filter pores are retained and run through the membrane surface and flowing back to the feed tank when pressure applied. Dead-end and cross-flow filtrations schematic illustration was given in Fig.2.2.

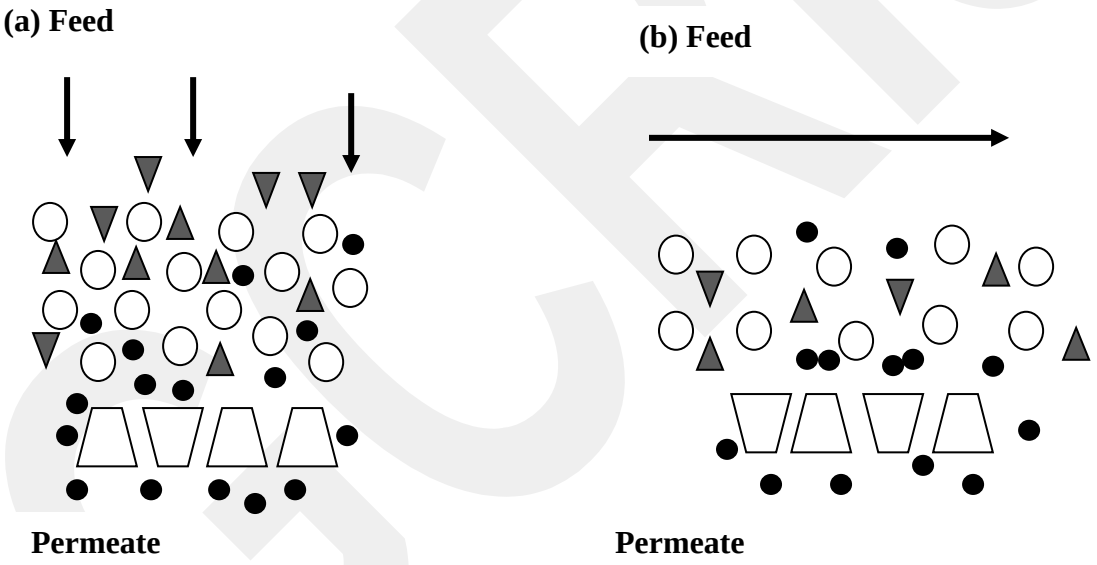

Figure 2.2.Schematic illustration of (a) dead-end and (b) cross-flow filtration

First use of membranes in clean water was at the end of World War II. US Army sponsored the significant research effort to develop of membranes. In the early 1960s, membrane separation system was discovered in academia and industry [66]. During the 1960s–1970s, different membrane based separation processes have been developed [67]. Since 1960s, increasing trend of membrane developments are listed Table 2.1.

Table 2.1.Development of membrane technology since 1960s [13]

Year	Applications
1960s	Reproducible membranes development Development of anisotropic reverse osmosis (RO) membrane
1970s	Membrane materials improvement (CA, PSF) Module design Thin film nanocomposite membrane fabrication Propose of pressure-retarded osmosis (PRO) process
1980s	Membrane system hardware improvement commercial inorganic (ceramic) membranes development Development of the mixed-matrix membranes
1990s	Improvement of hydrodynamics of microfiltration membranes Functionalized membranes (ion exchange) Forward osmosis (FO) membrane fabrication Pilot-scale FO

The transport through of membranes is provided by driving forces like as chemical potential, temperature gradient, pressure, or electrical field [68, 69]. Membrane technology has attracted growing attention because of their high selectivity, low energy consumption, do not need additives, simplicity of operation, performed at low temperatues in many application areas (Table 2.2) [68, 70]. And also, membrane processes can be easily intagrated into other separation or reaction processes.

Table 2.2.Membrane process, their driving force, mass transfer mechanism and applications [17]

Membrane process	Driving force	Mass transfer mechanism	Applications
Microfiltration	Pressure	Convection	Clarification
Ultrafiltration	Pressure	Convection	Concentration/fractionation
Nanofiltration	Pressure	Convection/diffusion	Concetration/purification
Reverse osmosis	Pressure	Diffusion/solubilization	Concentartion/desalination
Electrodialysis	Electrical potential	Ion exchange	Ions and non ionic solutes seperation
Pervaporation	Concentration	Diffusion/absorbtion	Volatile liquids seperation
Membrane distilattion	Partial pressure	Diffusion/evaporation	Desalination/concentration

Pressure-driven membrane processes as reverse osmosis (RO), nanofiltration (NF) ultrafiltration (UF) and microfiltration (MF) are used in water and wastewater treatment [71, 72]. These membranes generally used in pressure driven processes and show different pore sizes ranges from 1 nm for NF and 0.1 to 10 μm for MF. MF is used for turbidity decreasing and contaminants removal such as particles and bacteria which are the lowest energy consuming filtration process [28, 73, 74]. UF is promising process for macromolecule concentration and fractionation in many industrial processes [75-77]. UF membranes are defined by their molecular weight cut-off which knowns to the molecular weight solute which is 90% rejected by the membrane. UF can remove the contaminants, high removal rate of turbidity, organic matters and virus [78, 79] from the drinking water, with low cost [75]. Demineralization and small organic molecules concentration are applied by NF membranes [80-82]. NF membrane surface generally negatively charged due to Donnan effect to reject multivalent ions. RO membranes are nonporous and their separation mechanism depends on the “solution-diffusion” model [83]. RO is widely used desalination to overcome disadvantages of conventional thermal technology. Commercial RO technology has had many improvements such as

developments in membrane materials and module design, energy recovery, lower energy consumption [84-86].

2.2. Membrane Materials

Membranes are preffered because of their high permeability and selectivity with thermal, chemical and mechanical stabilities. Metals, ceramics, polymers, and glass are widely used for membrane preparation in many fields. In practice, usage of membrane materials have some limitations depending on their chemical and physical properties [71]. Conventionally organic polymers are used in pressure-driven membrane processes. Polymeric membranes are widely used because of the advantages of their formation ability, elasticity, toughness, high rejection performance and lower cost [87-89].

New types of inorganic membranes can be classified by ceramic membranes and metal membranes for gas separation at high temperatures. Ceramic membranes have been used for environmental applications because of low cost and high performance. They can separate colloidal, suspended particles from water and wastewaters, including clean water, industrial solvents and oil economically let to recylling and reusing of these solvents and oil. Ceramic membranes have narrow pore size distribution thus; they can succesfully to purificate of drinking water sources, higher thermal and harsh chemicals stability during membrane cleaning. Ceramic MF, UF and NF membranes are relatively novel materials for the treatment of produced water and alumina, zirconia, titania, and silica are widely used to fabricate the ceramic membranes [90, 91]. In addition porous ceramic membranes, dense ones such as perovskite, bismuth and solid-electrolyte, have been improved and commercialized [92].

Metal membranes are used to seperate of hydrogen from gas mixtures. Metal membranes generally form dense structure with palladium-based material at a thickness greater than 0.1 mm and use in electronic, metallurgic and chemical industries. Metal membranes have some limitation because of their cost, low permability chemical stability [93, 94]. Metallic membranes have been attractive during the last few years for MF application. MF metal membranes generally fabricate by sintering method with a diameter between 1.5 and 80 μm. These membranes have higher termal and chemical

stability in wide range of environments, and their robustness provide longer lifetimes than the conventional polymeric or ceramic membranes. However, metallic membranes cost is much more than polymeric or ceramic membranes [95].

Furthermore, membrane materials, synthetic membranes can be divided in four groups:
(1) porous films,
(2) homogeneous solid films,
(3) barriers carrying electrical charges,
(4) liquid or solid films containing selective carriers.

Moreover, membranes come in two typical structural configurations: their structure can be symmetric or asymmetric. The schematic drawing of Fig. 2.3 shows the membrane morphology and materials of synthetic membranes.

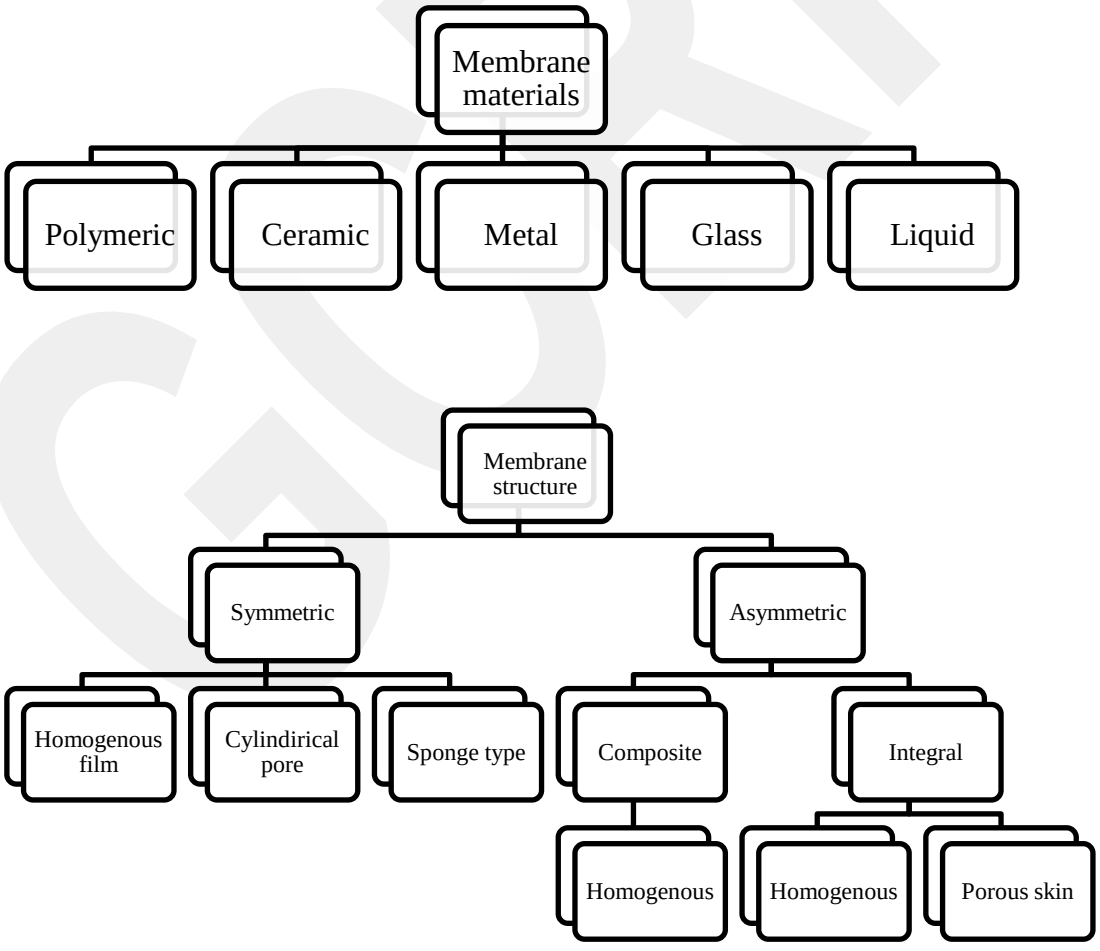

Figure 2.3. Schematic illutsration of the membrane materials and their structures [19]

2.2.1. Polymeric membranes

Polymeric membranes are used in many fields of water and wastewater treatment due to their permeability and selectivity properites for the effective seperations [96-98]. They generally include selective layer, which controls the separation capabilities, and a support layer which response for the mechanical stability.

Various polymeric materials such as CA, PSF, PVDF, PAN and PES are used in membrane fabrication. PSF has excellent properties such as solubility in a large range solvents, high thermal, chemical and mechanical resistance. PSF polymer has phenylene rings repeating units which provide to high degree of seperation capacity, high rigidity, and three dimensional stability and hence widely used in many applications. However, PSF polymer has limitations due to its hydrophobicity which results in lower water permeability and serious membrane fouling. It can be improved by modification methods, through blending and surface modification with hyrdophilic polymers and inorganic nanoparticles [24, 25]. In this view, PSF membranes were prepared with different concentration (1, 5, 10 wt%) of high molecular weight PVP additives to reduce the miscibility of casting solutions and thermodynamic enhancement. Also PVP increases the solution viscosity, which causes kinetic limitation during phase separation. At 5 wt.% PVP concentration, althogh macrovoid structure enlarge and membrane permeability increases, further increment of PVP shows that the thermodynamic enhancement is reached by the rheological limitations in demixing of the solution [99]. Similarly, for a different polymer, PAN, UF membranes were prepared to investigate crucial parameters like as polymer concentration, solvent and additives in membrane matrix. To get better combination of flux and rejection, N-methyl pyrrolidone (NMP) was determined as optimal solvent. Increasing the polymer concentration does not siginificanlty effect the membrane pore sizes [100].

UF membranes made by CA were modified with PEG to improve chemical, mechanical and thermal resistance. It is found that the CA concentration and hydrophilic PEG

additives changed the porosity and pore size of membranes. When increasing PEG concentration, permeate flux as well as percentage protein rejection ratio, thermal stability were developed. Prepared membrane which was including 21.25% CA and 6.25% PEG offered maximum rejection of bovine serum albumin (BSA) and pepsin at about 77% and 49%, respectively. However; CA degradation started at 260 °C, with PEG addition thermal degradation started at as high as 300°C [101]. Phelane et al. [52] prepared and characterize PSF nanocomposite membranes incorperated with silver, cobalt and nickel nanoparticles. Characterization results showed that unmodified PSF membranes contact angle values were decreased from 87.5º to 50º with the addition metal nanoparticles. Depending on electro-chemical impedance spectroscopy, low frequency and low potential values supplied more than 50% improvement in fouling performance [102]. In another study, Esfahani et al. [103] fabricated PSF membranes via phase inversion process to improve antifouling capacity using adsorption isotherms, flux declines and flux recovery ratio (FRR). Humic acid (HA) and BSA protein were used a foulnats and their concentrations affects were determined on membranes fouling behaviors. For both HA and BSA, fouling was effected by filtration time considerably at low concentrations compared to high concentrations, whereas FRR and flux decline and pore blocking were certainly occurring [103].

2.2.2. Polymeric nanocomposite membranes

Nanocomposite membranes enhanced as emerging alternative membranes, which offer higher permeability, hyropilicity, chemical, thermal, and fouling resistance. Nanocomposite membrane materials combined via blending nanoparticles and organic materials are remarkable for the preparation new generation of composites and nanocomposite materials with new or enhanced properties [104-107].

In water and wastewater treatment applications conventional nanocomposite and thin-film nanocomposite (TFN) membranes found more common areas [108]. Phase inversion (PI) method is mostly used to fabricate of conventional nanocomposite membranes that blend nanomaterial in polymer solution, and generally be prepared in flat sheet or hollow fiber types (Fig.2.4). Membrane pore size and porosity are determined by permeability and rejection in pressure-driven processes [109, 110]. In

addition, surface hydrophilicity and roughness commonly are controlled by membrane fouling characteristics. Incorporation of nanomaterials in polymer matrix is changing the membrane structural and morphological properties. Also hydrophilic nanomaterials presence in dope solution cause solvent and non-solvent exchange to form more porous structure. This porous structure enhances surface hydrophilicity, porosity and pore size of membranes, permeability and solute rejection. In addition porous structure, nanomaterials contribute membrane mechanical, thermal and chemical stability due to good compatibility between fillers and polymer [41, 111, 112].

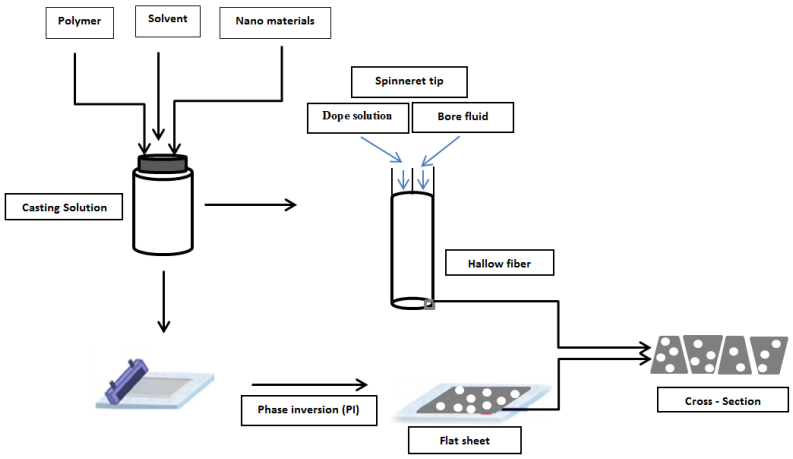

Figure 2.4.Fabrication of conventional nanocomposite membranes

Besides conventional nanocomposite membrane, TFN membranes are also gathering more attention in membrane fabrication. TFNs consist of an ultra-thin top layer and a more porous supporting layer. TFN membranes are widely used in desalination, removal of heavy metals, organic pollutants and pharmaceutically active compounds [113, 114]. Soon after the development of FO/PRO processes have required enhancement of TFC membranes to generate electricity. Many studies have been devoted to develop TFC membranes properties. New generation of nanocomposite membranes has been developed based on dispersing nanomaterials which including Ag, TiO_2, zeolites, CNTs, silica into the ultra-thin top layer to improve membrane performance for seperation [113, 115]. The *in-situ* interfacial polymerization (IP) process occurs between aqueous m-phenylenediamine (MPD) and trimesoyl chloride (TMC) organic solution. Dipersion of nanoparticles either in aqueous or in organic phase increases membrane hydrophilicity and based on the solution-diffusion theory

[116, 117], mass transfer through the membrane to increase water flux [118]. Besides lower contact angle, thinner top layer thickness and lower degree of cross-linking result high permeability and salt rejection [119]. Loading of nanoparticle into the polyamide (PA) layer leads to reduce the cross-linking due to decreasing reaction potential between amine groups and acyl chloride groups. Incoperation of hydrophilic nanoparticle into the PA layer decreases contact angle value and enhance antifouling and anti-biofouling capacity. Furthermore, the amide connection in PA TFC membranes supply chlorine resistane [120, 121].

Reecntly, nanoparticle blended membranes is getting more and more popularity on creating synergistic effect or functionality corparation nanoparticless into polymeric matrix [122, 123]. The superior properties of nanomaterials compared to bulk particles have many specific advantages due to their specific functional groups, which is backbone with polymer chain. Generally functional groups of nanoparticles are an ionic form or have lone-pair electrons [124]. The incorporation of nanomaterials with conventional polymers not only changed structural and morphological properties (e.g. hydrophilicity, porosity, thermal, and mechanical stability) which are Al_2O_3, TiO_2, SiO_2, $CaCO_3$, nanoclay and zeolite of membranes, but also gain unique functionalities (e.g. antibacterial property and photocatalytic capability) which are nano-Ag, CNTs and bi-metallic nanoparticles into the membranes [125, 126].

Many studies have examined the effect of metal oxide nano additives to provide immense changes in the performance of polymeric nanocomposite membranes. Particularly, Al_2O_3 is one of the most suitable nano-additives for altering the hydrophilicity and mechanical resistance, and it is non-toxic [127]. Hydrophilic Al_2O_3 nanoparticles exhibit desirable compatibility with a polymer matrix, controllable design, and minimal aggregation at different particle sizes and concentrations [128, 129]. The use of inorganic nanoparticles in a membrane matrix could provide synergistic effects on the membrane performance [130-133]. Wide range of inorganic nanoparticles used, $CaCO_3$ is also often studied in academic and industrial research studies because of its manageable operation and reactivity and well-known chemical properties. $CaCO_3$ nanomaterial is used in many industries like as plastics, paints, paper, medicine and food [134] because of their superior properties: easier synthesis, cheaper, hydrophilic,

super mechanical properties and high thermal stability and compatibility with polymer matrix [135-137].

Maximous et al. [24] embedded Al_2O_3 nanoparticle in PES UF to apply activated sludge filtration and to observe fouling resistance. As well as membrane performance, solvent evaporation time and polymer concentration were identified as the most important parameter for fitting membrane properties. The results showed the 18% polymer concentration and 15 s solvent evaporation time were optimum. Al_2O_3 addition improved membrane porosity and the decreasing interaction between the membrane surface and foulants. Also, 0.05 wt % Al_2O_3 loading showed better antifouling stability in MBR application.

The presence of Al_2O_3 nanoparticles alters the phase inversion process and affects the structure and performance of the obtained nanocomposite membrane with a threshold value for Al_2O_3 nanoparticles. Yan et al. [138] studied the effect of 10-nm Al_2O_3 nanoparticles on the performance of PVDF ultrafiltration membranes. They demonstrated that the addition of 2 wt% Al_2O_3 nanoparticles to the PVDF polymer matrix significantly improved the hydrophilicity, water flux, and mechanical stability of the membranes. Although an excessive amount of inorganic Al_2O_3 particles in the casting solution (3-4 wt%) caused the membrane elasticity and flux to decline, it did not affect the hydrophilicity and porosity. Homayoonfal et al. [139] fabricated Al_2O_3/PSF nanocomposite membranes via phase inversion method with the aim of reducing biofouling in membrane bioreactors. Al_2O_3 nanoparticle improved membrane hydrophilicity, roughness and reduced the biofilm formation. Nanoparticle presence resulted much higher flux and 83% reduction in biofouling. 0.03 wt % Al_2O_3 concentration in polymer matrix showed higher membrane performance with 2075 L/m^2h water flux, 91% dye rejection, 90% COD reduction and 12 L/m^2h permeation flux in MBR application. Mojtahedi et al. [140] were investigated the effect of coating and blending fabrication methods of PSF/PEG/Al_2O_3 nanocomposite membrane in terms of filtration performance. Blending method modified membrane had higher dye rejection, while coating method modified membrane illustrated higher dye flux. Dai et al. [141] investigated the preparation of PVDF/polyurethane (PU)/Al_2O_3 nanocomposite membrane via the thermally induced phase separation method. PVDF/PU/Al_2O_3 nanocomposite membrane had lower roughness with attributed lower fouling resistance

than pure PVDF membeanes and pure water flux and tensile strength were increased from 846 to 1028 L/m^2h and from 5.5 to 7.8 N, repectively.

Hou et al. [142] prepared PVDF membranes for membrane distillation with hydrophilic polyester nonwoven fabric support. To investigate the effects of $CaCO_3$ on membrane property in terms of pore size and distribution, hydrophobicity, porosity, thermal properties and permeability. $CaCO_3$ addition enlarged pore size and enhanced membrane surface roughness and hyrdophilicity. Nonetheless, membrane structure deteriorated and porosity and pore size reduced at the nanoparticle loading excess 4.5 wt%. During the membrane distillation, for 35 g/L sodium chloride feed solution permeate flux was 49.37 kg/m^2h at 83 ºC. Fujihara et al. [143] reported that, nanocomposite polycaprolactone/$CaCO_3$ nanofibers has high tensile strength and osteoblast was attachment succesfully.

Gao et al. [137] were fabricated, waterborne polyurethane (WPU)/$CaCO_3$ nanocomposites via in situ polymerization to enhance the dispersion and increase the compatibility between nanoparticles and WPU matrix. $CaCO_3$ was modified with oleic acid (OA). Experimental results showed that, modified OA/$CaCO_3$ was well dispersed in WPU matrix, WPU thermal stability was improved significantly and also the tensile strength was enhanced from 3.6 MPa to 10 MPa. Zhi et al. [144] prepared PVDF/poly(acrylicacid)/$CaCO_3$ composite membranes by mineralization method. The mineralization condition was optimized and membranes performance evaluated. Although pure PVDF contact angle was about 92°, after the mineralization it decreased 20°. Moreover, for the mineralzied membranes pure water fluxes were improved three times and they exhibited high dye rejection (99.85%).

2.3. Membrane Fabrication

There are several ways for the fabrication of polymeric membranes, like as sintering, interfacial polymerization, track etching, electrospinning and phase inversion methods.

2.3.1. Interfacial polymerization

Interfacial polymerization (IP) is the most common process for produced of TFC RO and NF membranes. Cadotte et al. [145] fabricated and performed the first IP TFC RO membrane. The main methodolgy of IP includes immersing a microporous polymer support in a polymeric amine solution and then the amine impregnated membrane soaking into a solution of a di-isocyanate in hexane. Amine and di-isocyanate cross-linkange was provide by heat-treatment between 70 -110 °C [145]. After development of IP technique, the TFC membranes have better rejection ratios than asymmetric membranes with high water fluxes [80]. Most of NF and RO membranes, which have PA thin layer on top of the membrane support, were fabricated by IP method. MPD and TMC widely used as a active monomers to form functional PA layer in RO/NF membranes (Fig. 2.5). Other amine monomers for production of TFC PA membranes include: p-phenylenediamine [146], piperazine [147], triethylenetetramine [148], and poly(ethyleneimine) [149]. These monomers functional or polar groups make the prepared membranes smoother or hydrophilic, which is advantageous on membrane permeability and antifouling capacity. Monomer concentrations, solvent type, reaction time and post-treatment conditions affect the structure and composition of membrane layer [150, 151]. Because of the superiority of IP technique membrane selective and support layer can be preapered independently so that the novel TFC membranes skin layer and microporous substrate layer have been successfully improved [116, 152].

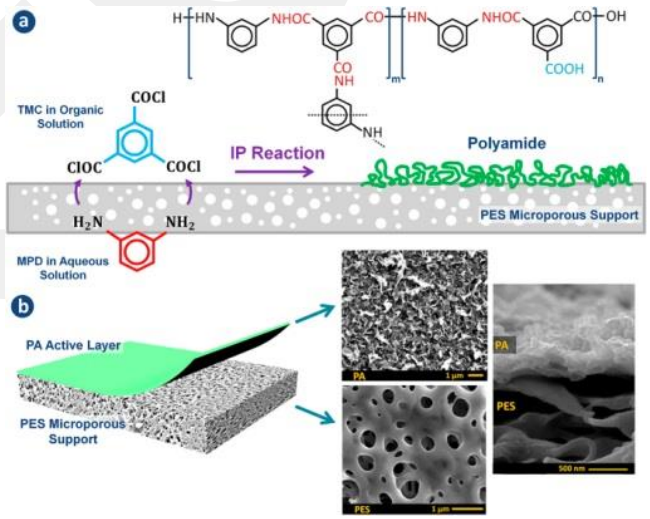

Figure 2.5.Schematic illustration of IP process [104]

2.3.2. Stretching

Since 1970s, stretching technique has been used generally in microporous membranes fabrication. Celgard® is known as commercial producer of polyetilene (PE) and polypropilene (PP) based membranes to use energy storage equipments [153]. This technique consist of polymer heating over the melting temperature and then extruded into thin sheet forms followed by stretching to occur porous structure [154, 155]. Stretching technique is solvent free process, which provides protection of crystalline regions of the polymer. Stretching method follows cold stretching which nucleate the micropores in the precursor film and then the hot stretching which increase pore structure. In this process, material's physical properties (like crystallinity, melting point, tensile strength etc.) and the applied processing parameters tailor the sample porous structure and properties of the membranes (Fig.2.6) [154].

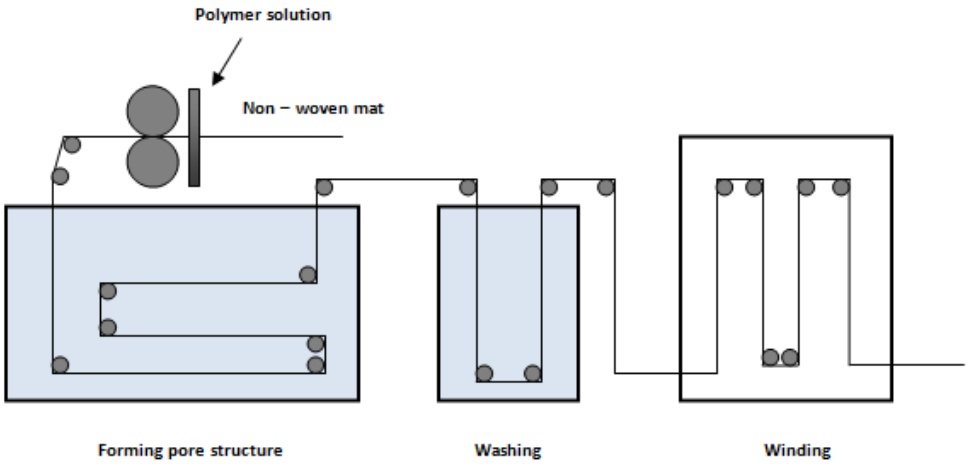

Figure 2.6.Schematic illustration of streching process [108]

2.3.3. Track-etching

Track-etch membranes used in industrial applications and offer definite benefite over conventional membranes because of their controlled structure. Depending on transport and retention characteristics, track-etch membranes pore size, shape and density can be determined. The nanoscale structures superior properties (electronic, optical, magnetic, mechanical, smaller size) present significant potential in variable areas due to their

flexibility to produce nanowires with a different composition [156]. A nonporous polymeric film forms irradition of energetic heavy nuclei such as californium or uranium [157] (Fig. 2.7). Exposing a uranium converter to a neutron flux from a nuclear reactor starts the fission of 235U. The other method is to fabricate track-etching membrane based on the use of ion beams from accelerators. These techniques are available to control pore size, pore size distribution and pore density, which is related water transport properties. The membrane pore size is determined by the duration of irradiation and temperature [158].

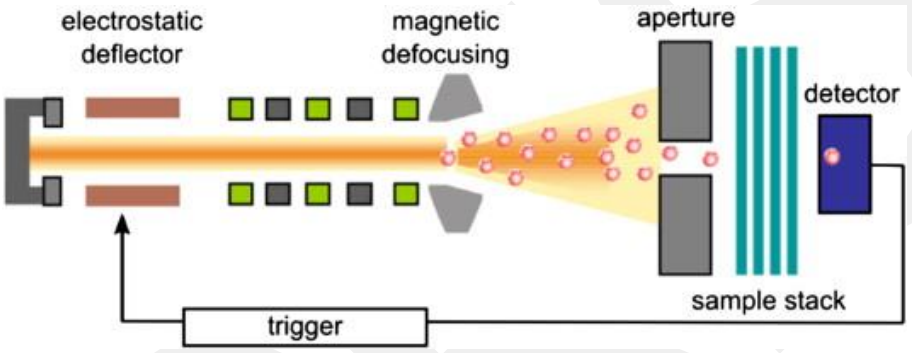

Figure 2.7.Schematic illustration of track-etching process [112]

2.3.4. Electrospinning

Electrospinning has recently attracted a great deal of attention in many areas due to their potential use in many applications such as protective clothing, advanced composites, sensors, tissue engineering, pharmaceutical industries and air filters [159-161]. A high potential voltage is applied between the polymer solution and the collector. Membrane structural parameter like as porosity, hydrophobicity and morphology can be controled by applied voltage and the distance of the needle tip to collector (Fig.2.8) [162]. Due to the superior properties, electrospun fibrous membranes have been used for filtration and membrane distillation purposes [163, 164]. Zong et al. [165] demostrated that applied potential strength, polymer solution viscosity, solution feed rate and conductivity of solution have significant effects on the fiber diameter and nanostructured morphology of fibers. Optimum potential difference was reported between 12 to 20 kV to form a stable jet. Potential difference can be changed and depend on feed rate, polymer solution concentration and distance. Applying high potential above 20 kV causes more

beaded structure on the fibers. Viscosity is another important parameter to get bead free smooth fibers. The optimum viscosity values provide with the selection of polymers and its molecular weights and salt addition. The most important problem of electrospun nanofiber membranes is low mechanical strength that it is difficult to handle. To overcome this problem, the thickness of the electrospin membrane could be increased with additional support to contribute mechanical strength, unlike conventional cast membranes. Thus, today much of the applications of electrospnning nanofiber membranes in membrane separation technology are based on hybrid systems which are prepared mix matrix membrane via electrospin coating. In Burmann et al. [166] study, inorganic and organic-inorganic types of fillers with different pore size and structure, were embedded in PSF matrix via spin coating to test H_2/CH_4 and O_2/N_2 mixed gas separations. Optimal parameters were adjusted and metal-organic material with 0.34 nm pore size coated membrane achieved higher than 60% H_2/CH_4 and O_2/N_2 separations. An the another metal-organic material with 0.75 nm pore size coated membrane increased permeability from 12.7 to 51.4 Barrer for H_2, and from 2.0 to 6.1 Barrer for O_2.

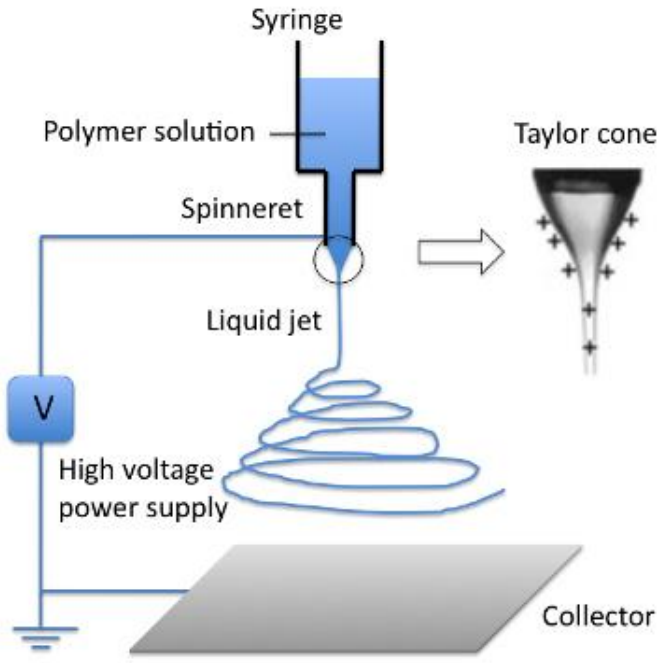

Figure 2.8.Schematic illustration of electrospinning process [121]

2.3.5. Phase inversion

The phase inversion process is generally used for preparing asymmetric polymeric membranes, which have a dense top layer and a porous or nonporous sublayer [167-169]. Membrane substrate immerses in a coagulation bath and solvent-nonsolvent exchanged occurs. In phase separation processes, a liquid polymer solution is precipitated two phases. Polymer-rich, solid phase forms the membrane matrix and the other polymer-poor phase forms the membrane pores (Fig.2.9). The membrane formation has many variables such as dope solutions composition, coagulation bath temperature and additives [170-172].

For phase inversion process, the ideal polymer is an amorphous, tought but not brittle, thermo plastic, higher molecular weights, soluble in water or solvent. CA, PSF, PVDF polyetherimide, and aromatic PA are some of the polymer which has these specifications [172-175]. Moreover polymer casting solution concentration is the other parameter and generally porous UF membranes are in the range of 15–20 wt%, RO membranes are avarge 25 wt%, and spin membranes are about 35 wt% [173]. The casting solution solvents such as dimethyl formamide (DMF), NMP, and dimethyl acetamide (DMAc) are used to dissolve a wide range of polymers [176, 177]. These solvents provide rapid precipitatation of casting solutions in coagulation bath to give porous, asymmetric membranes. Low-soluble solvents, such as tetrahydrofuran, acetone, dioxane, and ethyl formate cause slow precipitation to give nonporous membranes that causes lower porosity and flux. For the effect of membrane structure precipitation medium composition changes can be an alternative. Although the water is a typical coagulation bath, some organic solvents like as methanol or isopropanol could be added in water to get denser, less anisotropic membranes because of slow pore formation. Also temperature of the coagulation bath is important. Low temperature precipitation make membrane denser, cold water is used for preparation of RO membranes. During the fabrication of asymmetric membranes, small amounts of modifiers, which can be 5–10 wt%, are used to improve membrane properties significantly [178, 179]. Salt such as zinc chloride and lithium chloride and hydrophilic polymer as commonly PVP [180] or PEG [69] addition provide more porous membranes. Although a portion of additives are removed in precipitation and cleaning of the membrane, the final membrane would be more hydrophilic and often less brittle.

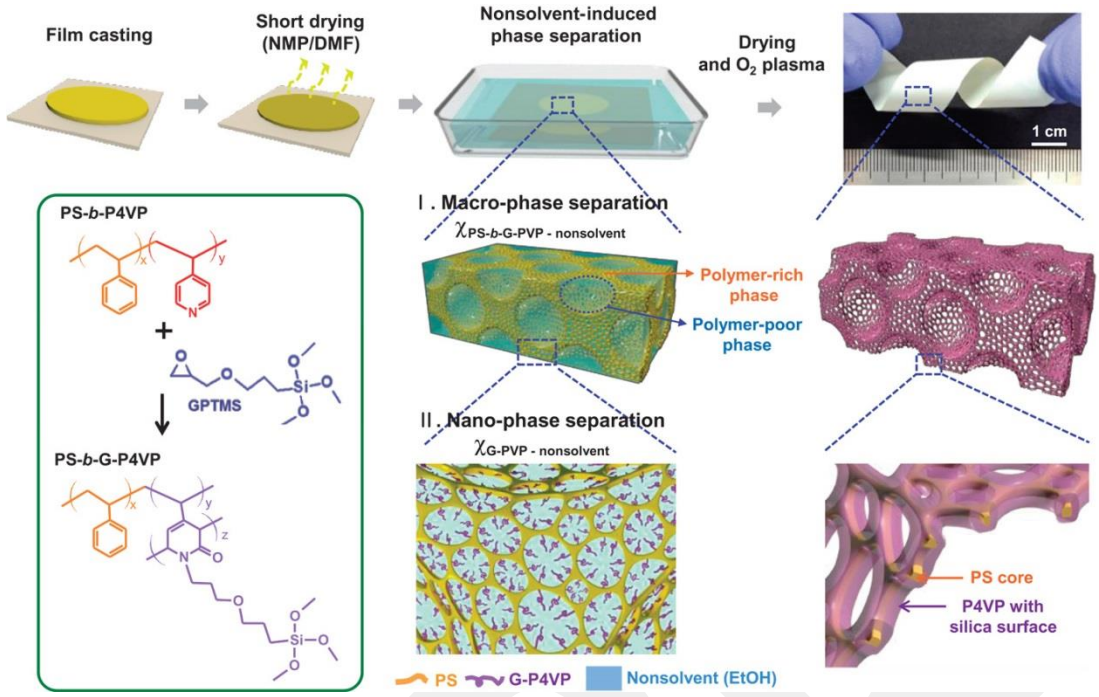

Figure 2.9.Schematic drawing illustrating of phase inversion process [136]

Han [181] prepared PSF membranes by phase inversion method with 75% relative humidity. Propionic acid was used to improve precipitation rate, and resulted in enhancement in water permeate flux was obtained. The overall results explained that in the optimum PSF concentration of 15 wt%, the propionic acid added in the casting solution works as a remarkable pore former in the phase inversion process. Musale et al. [182] fabricated chitosan composite UF and NF membrane on PAN by phase inversion. PAN poor solubility in various solvents which not allow the reduction of the pore size. So that, the pore size of the PAN membrane cannot be reduced significantly by the phase inversion process.

In another study, additive and solvent affect on membrane performance was investigated. PSF/NMP/PEG casting solutions were characterized to optimize PEG and NMP ratios by SEM images, water flux, viscosity and PEG (12 000 and 35 000 g/mol) rejection tests. It is reported that, increasing PEG and NMP ratios, casting solution was thermodynamically less stable because of higher porosity and bigger pore sizes formed on membrane surface. Besides this, increasing PEG and NMP ratios increased membrane flux but PEG rejection ratios decreased [183]. Kim and Lee [184] fabricated asymmetric PSF membranes with 1,4-dioxane, diethylene glycol dimethyl ether

(DGDE), acetone, and γ-butyrolactone (GBL) as additives by soaking coagulation bath. Experiment results demostrated that, because low miscibility of 1,4-dioxane, DGDE, and acetone, membrane pore sizes decreased. However, GBL loading increased the membrane pore size because of its higher miscibility. Additives did not change the cross-section of membrane; however, the top surface formed very packed and closed structure.

2.4. Membrane Separation Processes for Oily Wastewater Treatment

Steel, food, textile, leather, petrochemical and metal industries produce high oil containing wastewaters. Industrial wastewaters containing high oil should be treated before discharging through receving environments due to its serious environmental problems. Regulations that govern the accaptable discharge of oily water municipal treatment plants and surface waters are becoming increasingly thight. In these wastewaters besides high oil content there are serious pollutants such as organic matters, total suspended solids, total phosphorus and total nitrogen. In the treatment of these wastewaters application of conventional physicochemical treatment methods is limited due to low separation efficiencies, secondary pollutants, high energy and operating costs. These disadvantages necessitated the development of new processes for the treatment of oily wastewaters. Limitations of traditional methods changes and varies in permeate quality, huge volume of sludge, high chemical required and operational cost, large footprint. To overcome these disadvantages, membrane separation processes have been promoted for oily wastewater treatment [185-187]. In recent years, membrane-based separation technologies such as MF and UF have been used for various applications due to low energy requirements, continuous operation, low space requirements, low additional chemical requirements and high chemical oxygen demand (COD) removal efficiencies.

Membrane science has been developed and adapted to purification of oily water. With different pore sizes, membranes provide alternative method to separate stable emulsions and dissolved oil. Nevertheless, membrane fouling is a major problem which decreases the selectivity and efficiency. Commercial membranes can not seperate emulsions effectively and required some modifications such as coating, etching, freze drying, self

assembly etc. And many experimets have focused on enhancement of commercial membrane properties. Commercial MF PVDF membrane was modified by surface-initiated atom transfer radical polymerization (SI-ATRP) technique for oily water treatment. A zwitterionic polyelectrolyte was used a modifier agent and make membrane surface superhydrophic. Modified membranes removed oil with ultrahigh efficiency with higher antifouling performance [188]. Yang et al [145] modified polypropylene microfiltration membrane (PPMM) via co-deposition of mussel-inspired polydopamine (PDA) and PEI. However, PDA coating was improved the membrane hydrophilicity significantly, PDA/PEI deposition showed high water permeability under low pressure and better stability in alkaline enviroment [189]. Reuse the enhancement of oil water separation, novel approach has developed with high separation capacity, high selectivity and stable performance to supply growing demands.

The production of membranes, which has a key role in membrane processes, is of great importance to separate oily water treatment to meet the requirement of discharging limit. Special membranes can be designed and prepared with polymeric materials and inorganic nanoparticles to enhance oil seperation performance.

Yang et al. [190] showed that the performance of PSF UF membranes modified by TiO_2 nanoparticles for oily water treatment. Their results revealed the effectivity of TiO_2 nanomaterials in improving membrane properties in terms of water permeate flux, hydrophilicity as well as mechanical strength and fouling resistance. Yi et al. [16] fabricated PVDF UF membrane incoperated with nano-sized TiO_2/Al_2O_3 to improve antifoluing capacity. Their results showed that TiO_2/Al_2O_3 addition supply better antifouling capacity and hydrophilicity and also desirable flux recovery after washing. On the other hand, Yuliwati and Ismail [41, 191] prepared PVDF UF membrane incorporated with hydrophobic TiO_2 nanoparticles to evaluate the performance of oily wastewater purification. The effect of TiO_2 nanoparticles concentration was investigated on spinning dope and their experimental findings showed that the concentration of TiO_2 at around 1.95 wt% showed 98.8% oil removal with the highest permeability of 82.5 L/m^2 h bar.

In another study, Zhang et al. [192] used PSF membranes with Zr-doped hybrid silica particles (SZP particles) for oily wastewater treatment. SZP particles improved the PSF membrane hydrophilicity, anti-fouling capacity and mechanical strength significantly.

The contact angle of the membrane decreased from 78.0° to 45.5°. Also oil retention was 92% with 116 L/m^2h flux value at 0.1 MPa. Similarly, Zhang et al. [193] conducted a study that focused on enhancement the hydrophilic and antifouling capability of PSF membranes assisted with sulfated zirconia particles for treating oily wastewater. Experiments showed that the permation oil concentration decreased from 80 mg/L to 0.67 mg/L, which satisfies the recycle standards.

In another study, functionalized SiO_2 nanoparticles with PSF mixed matrix membrane was prepared for the separation of O/W emulsion. Modified membrane with SiO_2 nanoparticles showed 17.32 L/m^2h^1 permeate flux when compared to unmodified PSF membranes with a flux of 1.08 L/m^2h^1. With SiO_2 nanoparticles addition, water flux, hydrophilicity and antifouling properties were improved with the formation of larger pores [194]. Vatanpour et al. [195] fabricated PES membranes incorporated with coated multiwalled carbon nanotubes (MWCNTs) by TiO_2 and oxidized MWCNTs for oily wastewater treatment. TiO_2 coated MWCNTs membrane showed better anti-biofouling, hydrophilicity and pure water flux then oxidized MWCNTs blended membranes.

GCRIS

Chapter 3

3.EXPERIMENTAL

3.1. Materials

PSF with a weight average molecular weight of 60,000 was purchased from Acros Organics. An aqueous solution of branched PEI with a weight-average molecular weight of 25,000 was obtained from Sigma-Aldrich and used as a modifying agent. Chemical structure of PSF and PEI were given Fig.3.1. DMF (Merck, anhydrous, 99.8%) and NMP (Merck) were used as solvents. Hydrophilic Al_2O_3 nanoparticles with sizes of 20 and 80 nm and $CaCO_3$ nanoparticles with 100 nm were supplied from Nanografi, Turkey, and used as additives for the PSF/PEI solutions. BSA was used as a foulant and supplied from Amresco Inc. (USA). Sodium dodecylsulfate (SDS) was used a emulsifier and was purchased from Serva. Vacuum pump oil (G-19) was purchased from Edwards (UK). Hexane was used for industrial oily wastewater analysis and was purchased from Merck. All of the organic and inorganic reagents were of analytical grade and used as standard.

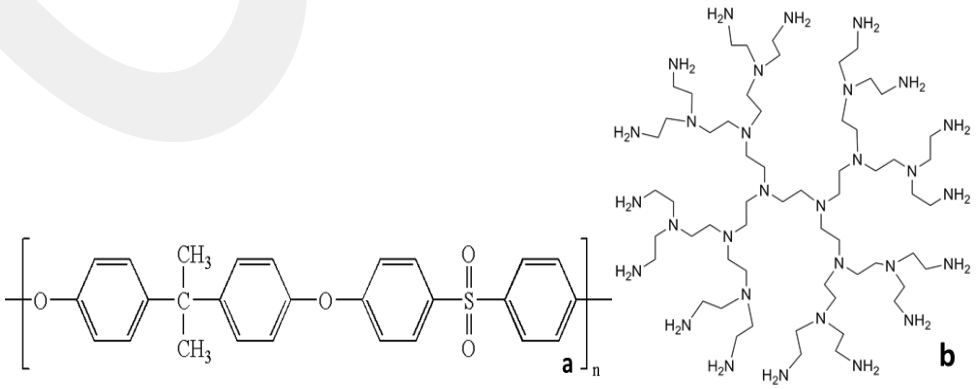

Figure 3.1.Chemical structure of (a) PSF and (b) PEI polymers [202] [203]

3.2. Preparation of Membranes

For the fabrication of the membranes, the 20 nm and 80 nm and Al_2O_3 were first dissolved in an NMP solution at three different concentrations of 0.2, 1, 5 wt% Al_2O_3. The mixture was then sonicated for 2 hours. Next, the Al_2O_3 nanoparticles were added to the mixture containing 15 wt% PSF and 1 wt% PEI polymer prepared in DMF and NMP. The final solution was mixed for one day at 400 rpm using a magnetic stirrer to make it homogeneous. The polymer suspension was then sonicated for at least 2 hours at 25°C. The details of the casting solution compositions are shown in Table 3.1.

Table 3.1.Casting solution compositions of Al_2O_3 membranes

Substrate	PSF (wt%)	PEI (wt%)	20 nm Al_2O_3 (wt%)	80 nm Al_2O_3 (wt%)
M201	15	1	0.2	-
M202	15	1	1	-
M203	15	1	5	-
M801	15	1	-	0.2
M802	15	1	-	1
M803	15	1	-	5

All casting solutions were allowed to stand for 1 hour to remove all air bubbles, and then they were cast onto a clean glass plate (20-30 cm) with a steel casting knife. The fixed thickness of the cast film was 350±20 μm. The film was immediately immersed in a coagulation bath for 2 min to remove the residual solvents and for solidification. Schematic diagram of PSF/PEI/Al_2O_3 membranes preparation procedure was given in Fig.3.2. All prepared membranes were stored in a bottle of DI water at 4°C.

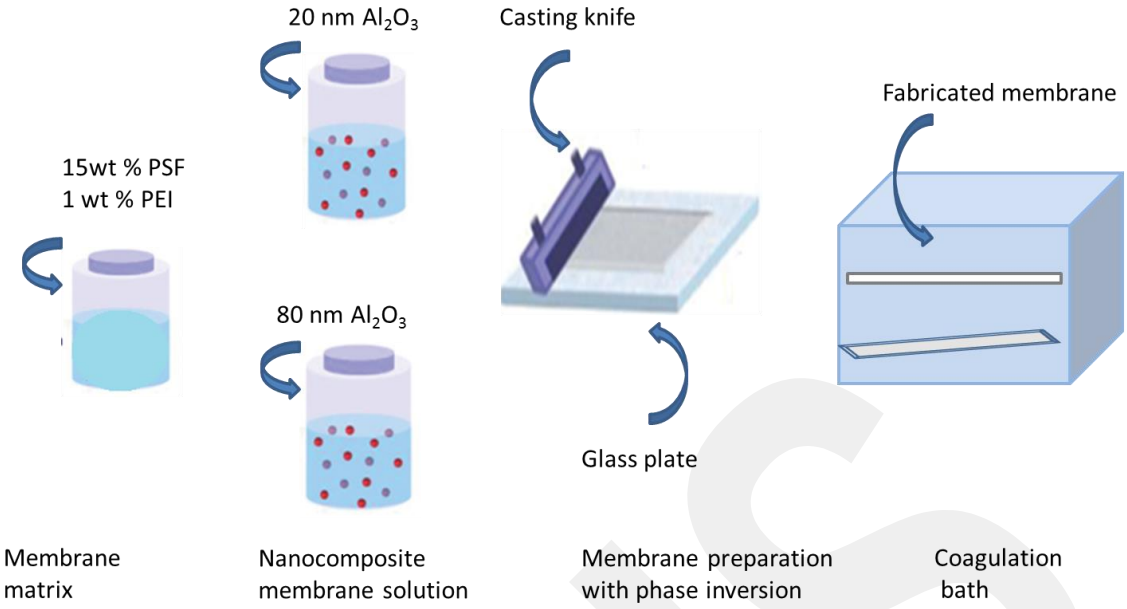

Figure 3.2.Schematic diagram for the preparation of PSF/PEI/Al_2O_3 membranes

$CaCO_3$ (100 nm) were first dissolved in an NMP solution at three different concentrations of 1, 2, 5 and 10 wt% $CaCO_3$. The mixture was then sonicated for 2 hours. Next, the $CaCO_3$ nanoparticles were dissolved with 20 wt% PSF and 2 wt% PEI in DMF and NMP mixture to form casting solutions. The final solution was than mixed for one day at 400 rpm using a magnetic stirrer to make the solution homogeneous. The polymer suspension was then sonicated for at least 2 hours. The details of the casting solution compositions are shown in Table 3.2.

Table 3.2.Casting solution compositions of $CaCO_3$ membranes

Substrate	PSF (wt%)	PEI (wt%)	$CaCO_3$ (wt%)
PSF	20	0	0
PSF/PEI	20	2	0
C1	20	2	1
C2	20	2	2
C5	20	2	5
C10	20	2	10

All casting solutions were allowed to stand for 1 hour to remove all air bubbles, and then they were cast onto a clean glass plate (20-30 cm) with a steel-casting knife. The fixed thickness of the cast film was 75±5 μm. The film was immediately immersed in a distilled water bath for 2 min to remove the residual solvents and for solidification. Schematic diagram of PSF/PEI/$CaCO_3$ membranes preparation procedure was given in Fig.3.3. All prepared membranes were stored in a bottle of DI water at 4°C.

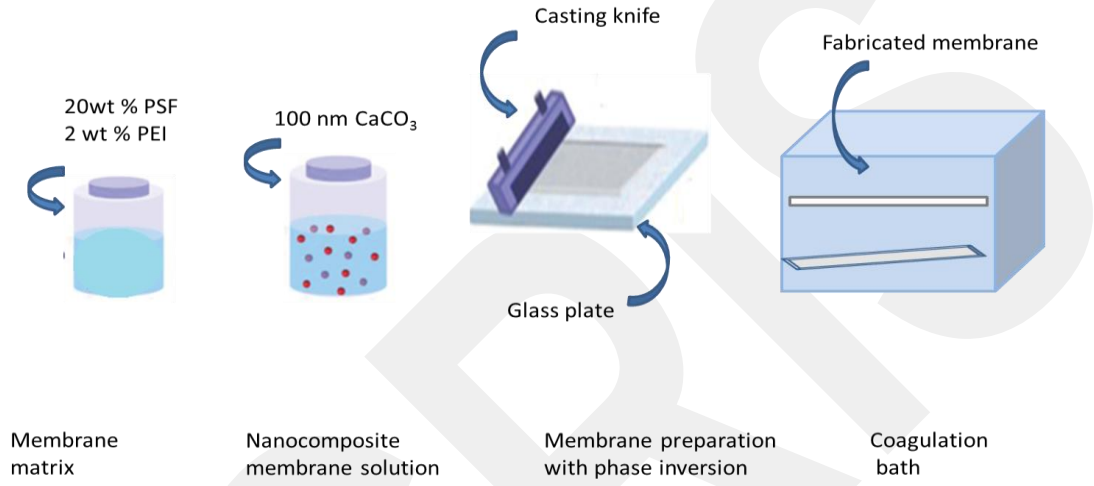

Figure 3.3.Schematic diagram for the preparation of and PSF/PEI/$CaCO_3$

3.3. Membrane Characterization

3.3.1. SEM

SEM affords the optical information of the membrane morphology in terms of pore structure, distribution and density. The top-surface and cross-section morphologies of the membranes were observed using a Zeiss Evo LS10 scanning electron microscope. The membranes were carefully sectioned with an avarage 0.5 mm width and 3 mm length and then mounted onto the SEM grid. Before the analysis, each sample was coated with platinum, and the samples were analyzed at 10 kV.

3.3.2. Water contact angle

Membrane hydrophilicity directly relate with membrane permeability and fouling. Hydrophilicity can be characterized by contact angle experiments generally with sessile drop method. Hydrophilic membrane indicates with less than 90° of contact angle and hydrophobic is over 90°. Smaller contact angle causes more hydrophilic membrane. The Fig. 3.4 demonstrates the difference between hydrophobicity and hydrophilicity.

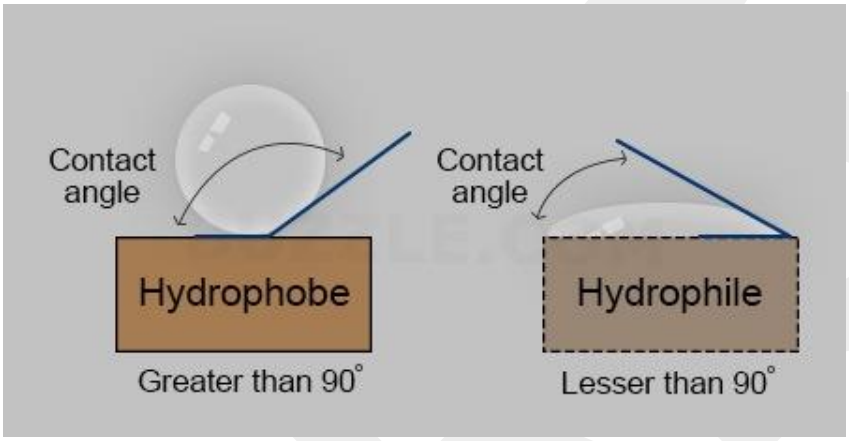

Figure 3.4.Hydrophobic surface (left) and hydrophilic surface (right), figures adapted from Chemistry LibreTexts [204]Fig. 3.5 represents the instrument used in contact angle measurements. The principle of this instrument that water is dropled on the membrane surface and a camera records an image of water droplet. Then the angles between surface and droplets are determined. Contact angle can be measurement several times on the different points of membrane surface and then mean value of the contact angles are calculated.

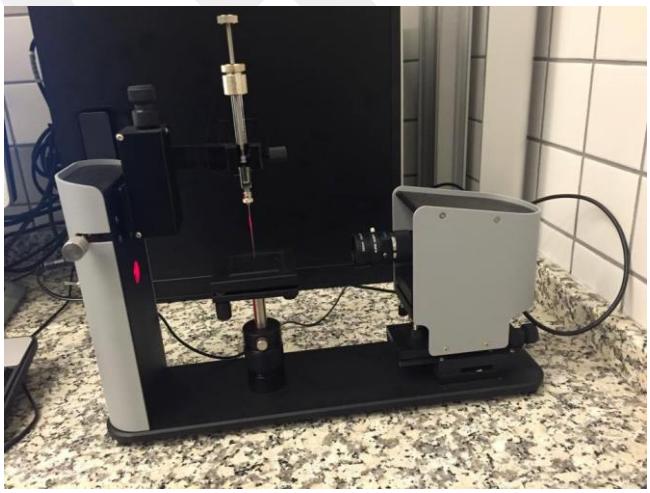

Figure 3.5.Optical contact angle and surface tension meter

The surface hydrophilicity of the membranes was measured using a contact angle meter (Attention-Theta Lite, Biolin Scientific, Finland). DI water was used to compare the hydrophilicity of the pure PSF, PSF/PEI, PSF/PEI/Al_2O_3 and PSF/PEI/$CaCO_3$ membranes. For each measurement, at least three readings from different surface locations were taken, and the reported contact angles are the average values. All of the membranes were fully dried before measuring the contact angle to avoid issues with water interaction.

3.3.3. Water filtration tests

A dead-end stirred cell filtration system (Sterlitech, HP4750) was used to determine the membranes' intrinsic separation properties (i.e., water flux and rejection). Filtration cell connected with a nitrogen gas cylinder and consisted of a filtration cell with a volume of 300 mL. The effective membrane area for the system was 14.6 cm^2. The feed side of the system was presurrized by nitrogen gas (Fig.3.6). In the water filtration test, 3 different transmembrane pressures (TMP) were applied (2, 4, and 6 bar) for PSF/PEI/Al_2O_3 membranes and 2 bar constant TMP for PSF/PEI/$CaCO_3$ membranes, stirring speed were carried out at 300 rpm and the temperature was kept at room temperature (25±3ºC). The water fluxes of the prepared membranes were calculated using Eq. 1:

$$J = \frac{V}{A \times t} \quad (1)$$

where, J is the water flux (L/m^2h), V is the permeate volume (L), A is the effective membrane area (m^2), and t is time (h). In the second step, O/W emulsion refilled the stirred cell reservoir. The flux for O/W emulsion J_1 (L/m^2 h) was measured based on the pure water flux calculation.

Figure 3.6.Dead-end filtration set-up

3.3.4. BSA removal experiments

The rejection experiments were carried out at 2 bar TMP in the dead-end filtration module. The membranes' BSA rejection performance was determined using aqueous solutions containing 2.5 g/L of BSA [196]. The solutions were prepared using DI water at room temperature. BSA concentrations were analyzed using UV-visible spectroscopy (UV-1800, Shimadzu, China) at a wavelength of 280 nm. The BSA and oil rejections (R) were calculated by Eq. 2:

$$\%R = 1 - \frac{\mathrm{Cp}}{\mathrm{Cf}} \times 100 \qquad (2)$$

where Cp is the concentration of BSA in the permeate, and C_f is the concentration of BSA in the feed solution. The volume reduction ratio (VRR) is calculated using the following formula:

$$\mathrm{VRR} = \frac{\mathrm{V0}}{\mathrm{VR}} \qquad (3)$$

where, V_0 and V_R are the initial feed volume and retentate volume, respectively.

3.3.5. Oil removal experiments

The vacuum pump oil (G-19) was used for preparation synthetic O/W emulsion. The oil rejection tests were carried out at 2 bar TMP in the dead-end filtration module. The emulsion were combined with oil and surfactant SDS in a ratio of 9:1 (w/w), and then added to 500 mL DI water by mixing for 30 min to homogenous. The emulsion was stored at room temperature. After UF of O/W emulsion, the membranes were cleaned with DI water 20 min, then the water flux of cleaned membranes J_2 (L/m^2 h) was measured again synthetic oily water concentrations were analyzed using UV-visible spectroscopy (UV-1800, Shimadzu, China) at a wavelength of 283 nm, and UV analyzer as shown in Fig. 3.7.

The oil rejections (R) were calculated same as BSA rejection by Eq. 2. and where Cp is the concentration of oil in the permeate, and C_f is the concentration of oil in the feed solution. The volume reduction ratio (VRR) is calculated using the Eq 3.

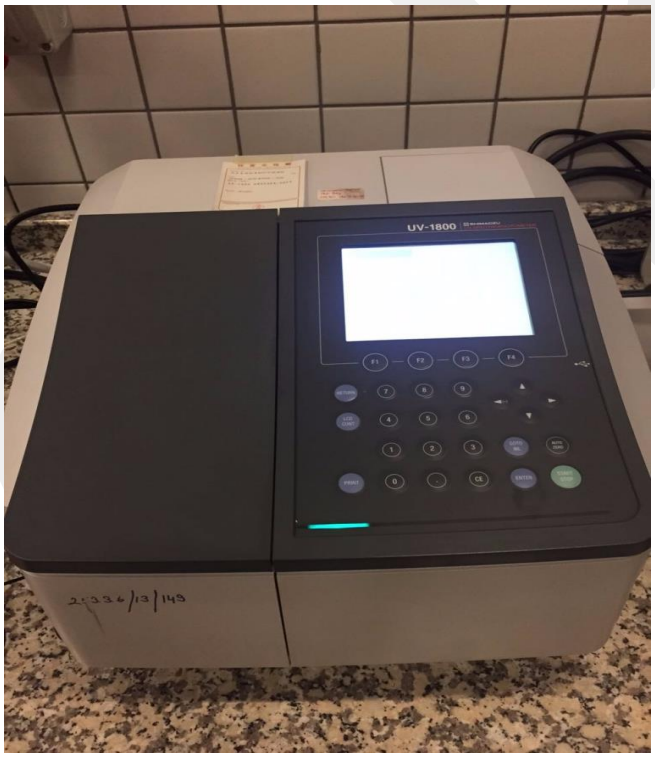

Figure 3.7.UV-visible spectroscopy

Fouling resistance of membranes was evaluated by oil water emulsion flux decay ratio (DR) and flux recovery ratio (FRR) and was calculated using the following equations [35, 197]:

$$DR = \frac{J-J1}{J} \times 100 \quad (4)$$

$$FRR = \frac{J2}{J1} \times 100 \quad (5)$$

The lower DR and higher FRR values mean that better antifouling capacity of the membrane in oil water emulsion filtration efficiency.

Industrial wastewater was obtained from a tank containing a mixture of oily solutions at a metal equipment producing industry in Kayseri with aproximately 500-700 m^3 of wastewater per day. COD was analyzed by Hach DR 6000 spectrophotometer.

3.3.6. Porosity

For the porosity measurements, dry membranes were immersed in ethanol for 2 hours, and the liquid on the surfaces of the membranes was removed using filter paper. The membrane porosity (ε) was calculated using Eq. 6 [198]:

$$\varepsilon = \frac{(\omega 1-\omega 2)/d\omega}{\frac{\omega 1-\omega 2}{d\omega}+\omega 2\ /dp} \quad (6)$$

where ω_1 is the weight of the wet membrane (g), ω_2 the weight of the dry membrane (g), dω is the density of pure water (0.998 g/cm^3) ,and dp is the polymer density (1.24 g/cm^3).

3.3.7. FT-IR

The FT-IR spectroscopy has provided easy method to determine of the relative amounts of different polymeric membrane with time-resolution down to nanoseconds. The spectrum changes represent the average composition of membrane layers, therefore structural changes after in modified and non-modified membranes. FT-IR spectra were employed for functional identification of PEI, Al_2O_3 and $CaCO_3$ nanoparticles using an FT-IR spectrometer (Thermo Nicolet Avatar 370) and the instrument used in measurements was given in Fig 3.8. Prior to the FT-IR measurements, the samples were dried in a drying oven for 15 minutes at 120°C.

Figure 3.8. FT-IR spectra

3.3.8. Mechanical strength

Mechanical properties of polymeric nanocomposite membranes are related to their structure which dispersion of additives in the polymer matrix. Better dispersion of the nanoparticles without any aggregation in the polymer matrix generally improve mechanical strength, but significantly reduced ductility of pure polymer [199]. The mechanical strength of the prepared membranes was measured using an AGS-J tensile testing machine (Shimadzu, Japan) and the instrument used in mechanical tests was given in Fig. 3.9. The measurements were carried out according to the ASTM D 882 standard by applying a 500-N load at a crosshead speed of 1 mm/min. All the samples were sectioned with dimensions of 6×2 cm^2. The sample thicknesses were measured with an electronic micrometer with ±0.1 μm precision (No. 293-561, Mitutoyo, Japan). The average values of mechanical strength were obtained from the results of three measurements.

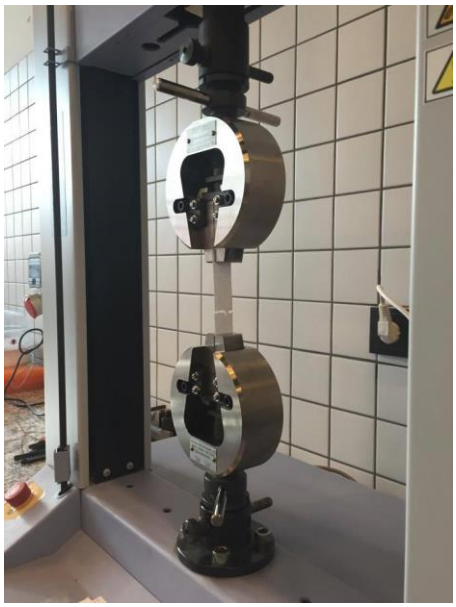

Figure 3.9. Tensile testing equipment

3.3.9. Viscosity measurements

The average viscosity of the dope solution was measured with a Rapid Visco Analyzer (Pertem, RVA 4500) and the instrument used for viscosity measurements was shown in Fig 3.10. The viscosity was measured at room temperature (25±3°C). To ensure complete uniformity of the samples to be analyzed, the rotation of the RVA was set to 60 rpm for 120 seconds.

Figure 3.10. Rotational viscometer with variable temperature and shear capabilities

3.3.10. Thermal stability

The thermal stability of the membranes was determined by thermogravimetric analysis (TGA) (DTG-60H, Shimadzu) and the instrument was given in Fig. 3.11. TGA measures the amount of weight change of a material depending on temperature increasing under nitrogen gas. Sample pan is supported by a precision balance and it is heated during the experiment and weight loss of the sample is monitored during the experiment. In order to remove the residual solvent from the membranes, 5–10 mg membrane samples were kept at 50°C for 12 hours under vacuum and then heated under N_2 atmosphere from 30 to 700°C at 10°C min^{-1}.

Figure 3.11. Thermogravimetric Analyzer

3.3.11. AFM analysis

AFM is important analysis to determine surface roughness (Ra, Rq, and Rmax) at the nanoscale. AFM tip scan membrane surface and when tip closers the surface, force will occur between the surface and the tip which cause the cantilever to deflect towards the surface. Membrane surface roughness was characterized by MultiMode 8-HR, Veeco operated in tapping mode (Model: RTESP-300). The membranes were dried overnight at 80°C to evaporate of liquid completely from the membrane surfaces and pores. The analysis was performed using a 5 µm ×5 µm image size, a 3.4 Hz scan rate. The

roughness parameters of each membrane are reported as the average of at least three measurements on membranes.

3.3.12. XRD analysis

The XRD analysis were carried out by using XRD Bruker D8 advance with a 40kV scaled copper tube as source and a graphite crystal as monochromator. Diffraction angles were 2θ, 5-90°. Through this analysis it is possible to show the evidence of structural changes caused by the blending PEI and Al_2O_3 and $CaCO_3$ nanoparticles on the PSF membrane.

GCRIS

Chapter 4

4. RESULTS AND DISCUSSIONS

Fabrication and characterization of nanocomposite membranes with pore former and nanoparticles and the examination of these membranes in oily wastewater treatment were investigated. In this context, the experiments were performed at five stages. Firstly, the polymer concentration of membrane was optimized using PSF polymer. Secondly, the concentration of PEI as a pore former in membrane dope solutions was optimized. Thirdly, the concentrations of two different nanoparticles $CaCO_3$ and Al_2O_3 in nanocomposite membrane dope solutions were optimized. In the fourth stage all fabricated nanocomposite membranes were characterized in terms of viscosity, membrane morphology (SEM, AFM), porosity, chemical structure (FTIR, XRD), water contact angle, thermal properties (TGA) and mechanical strength. Finally, performances of fabricated PSF/PEI/Al_2O_3 and PSF/PEI/$CaCO_3$ nanocomposite membranes were filtred at dead end system using pure water, BSA and oily wastewater.

4.1. The Effect of PSF Polymer Concentration

Polymer concentration is one of the most important parameters of membranes and has a significant effect on membrane performance. The effect of PSF polymer concentration was investigated for three different concentrations of 15 wt%, 20 wt %, 25 wt% PSF. The effect of PSF polymer concentration is analyzed in terms of pure water flux and SEM analysis. Although 15 wt% and 20 wt % PSF membrane had 20 and 3 L/m^2h pure water flux, no flux value was not observed in 25 wt% PSF membrane at 2 bar. As the polymer dosage increased the membrane structure became more and more dense and can be seen clearly from Fig. 4.1. Lohokare et al. [200] has investigated the effect of membrane preparation conditions on membrane morphology and filtration performance. They obtained that increasing of polymer concentration in dope solution resulted higher selectivity but lower pure water flux. 25 wt% polymer concentration were more brittle,

but 5-10 wt% PSF were transparent and very sensitive to pressure; they shrank very easily upon drying. Therefore, higher polymer concentration can be caused lower water permeation and any flux value could not observed 25 wt% PSF membrane. A denser and thicker membrane structure as soon as showed well porous structure. According to these results; 15 wt% and 20 wt% PSF polymer concentrations were chosen as concentrations for Al_2O_3 and $CaCO_3$ membranes to get UF/MF and tight UF membranes, respectively.

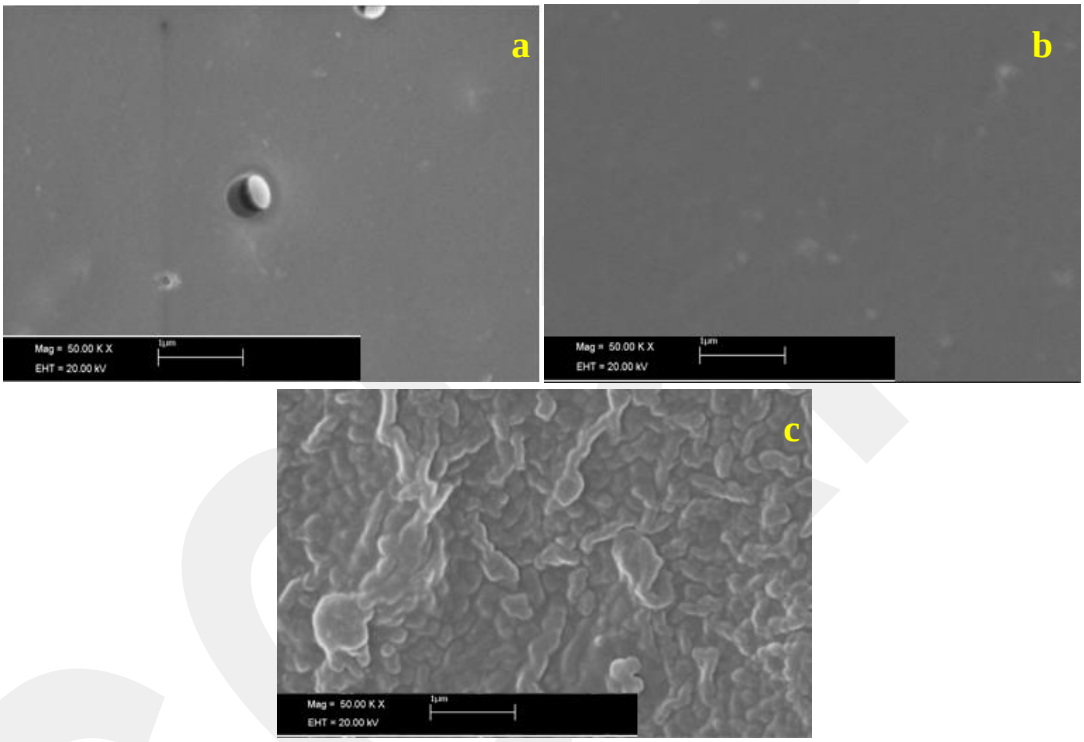

Figure 4.1.SEM images of top surface of; (a) 15 wt% PSF membrane, (b) 20 wt% PSF membrane and (c) 25wt% PSF membrane

4.2. The Effect of PEI Concentration in PSF Membrane Matrix

Phase inversion of symmetric and asymmetric polymeric membrane characteristics depended on many factors and pore former addition in polymer matrix is one of the major factors to adjust formation of membrane structure by macrovoid formation, porosity and hydrophilicity. The frequently used additives as pore formers are organic polymer such as PVP, PEG, polyethylene oxide (PEO) and PEI. PEI is generally

preferred in membrane fabrication due to branched structure and water-solubility properties [201]. Besides this, PEI can develop connection between pores on the surface and porous layer of the asymmetric structure during the phase inversion [202].

The effect of PEI concentration on the performance of PSF membrane was also investigated. In this context, four different concentrations of PEI (0.2, 0.5, 1, 2 and 3 wt%) was blended in 15 wt % PSF membrane matrix and three different concentrations of PEI (2, 4 and 6 wt%) was blended in 20 wt % PSF membrane matrix.

In membrane fabrication with phase inversion process, DMF/NMP solvent mixture flow out of polymer-rich body and PEI flow in solvent-rich body. The polymer-rich part would rapidly solidify into the membrane surface while the solvent-rich phase would dissolve in non-solvent and develop the macrovoids in the membrane sub-layer. In addition, PEI would also increase the hydrophilicity of PSF membrane because of their hydroxyl groups [203]. The effect of PEI polymer concentration is analyzed interms of pure water flux and hydrophilicity. The results of membrane hydrophilicity and pure water fluxes were given in Table 4.1. As shown in Table 4.1, pure water fluxes of membranes increased with PEI loading due to more macrovoids formations. Although, increasing PEI in membrane matrix improve hydrophilicity of membranes up to 1 wt%, above this concentration no significant change has been obtained on membrane hydrophilicity. This can be explained with pore former threshold limit for surface location.

Table 4.1.Contact angle and water flux values of 15 wt% PSF incorpareted with different concentrations of PEI

Substrate (PEI)	**0.2 wt%**	**0.5 wt%**	**1 wt%**	**2 wt%**	**3 wt%**
Water flux (L/m^{2}h)	80	144	317	1220	1761
Contact angle (°)	75	71	64	67	69

Cross-section SEM images of 15 wt% PSF membranes containing different concentrations PEI are given in Fig. 4.2. However; increasing the PEI concentration resulted in formation of new pore structures; above 2 wt% PEI concentration, membrane deformations were observed.

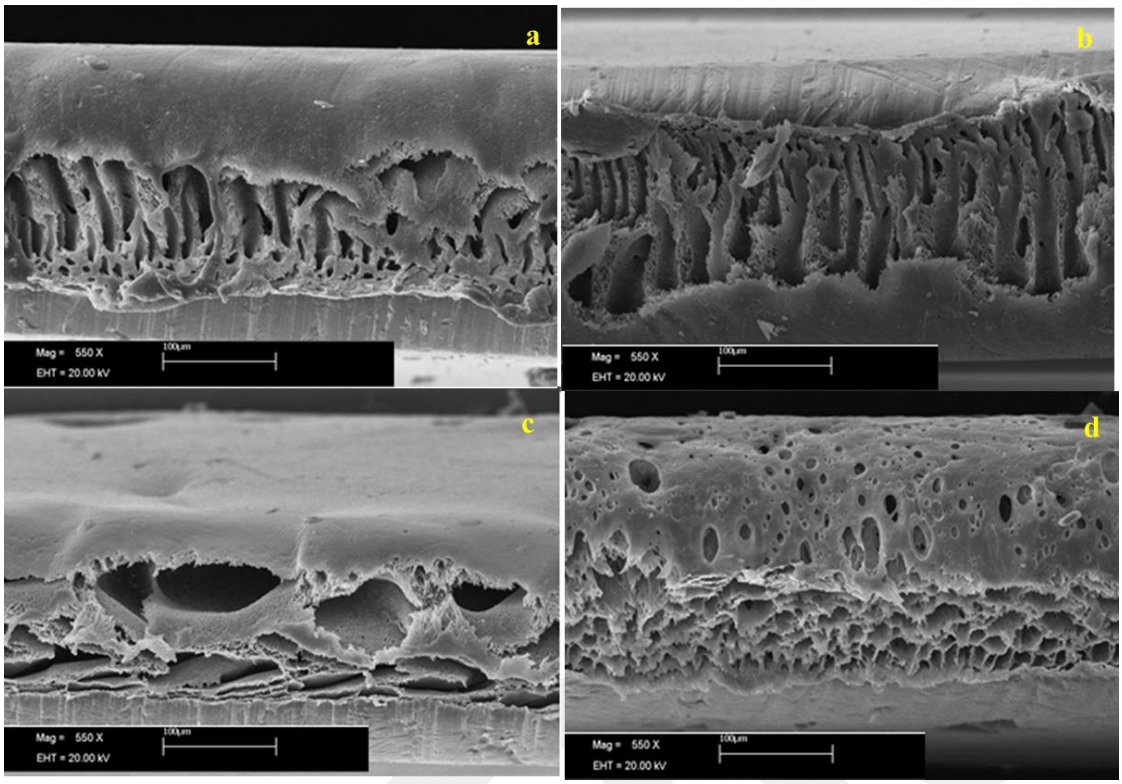

Figure 4.2.SEM images of 15 wt% PSF membranes cross-section containing PEI with different concentrations: (a) 0.2 wt%, (b) 0.5 wt%, (c) 1 wt%, (d) 2 wt%

Like as morphological characteristics, hydrophilicity and water flux directly affect membrane performance. Thus, 1 wt% PEI concentration was chosen as additive concentration for 15 wt% PSF membrane casting solution because of lowest contact angle and acceptable water flux was obtained for this. More than 1 wt% PEI addition; membrane structure deformation was also started (Fig.22 d).

Images of the PSF and PSF/PEI (15/1 wt%) membrane surfaces and cross sections are shown in Fig. 4.3. As shown in Fig. 4.3a, a uniform surface without nodules was formed during the fabrication of the pure 15 wt% PSF membrane. However, the surface was completely different and had small pores when 1 wt% PEI was added to the polymer matrix (Fig. 4.3b). The PSF membrane exhibited a very dense structure and few macrovoids, which results in mechanical support. During the phase inversion process, the fast solvent–non-solvent exchange occurs, and repulsive forces between PSF and water cause immediate precipitation on the polymer structure (Fig. 4.3c) [204, 205]. The addition of PEI to the polymer matrix results in the formation of an asymmetric

structure consisting of a thin and dense top layer and a finger-like macroviod structure at the bottom layer (Fig. 4.3d) [206].

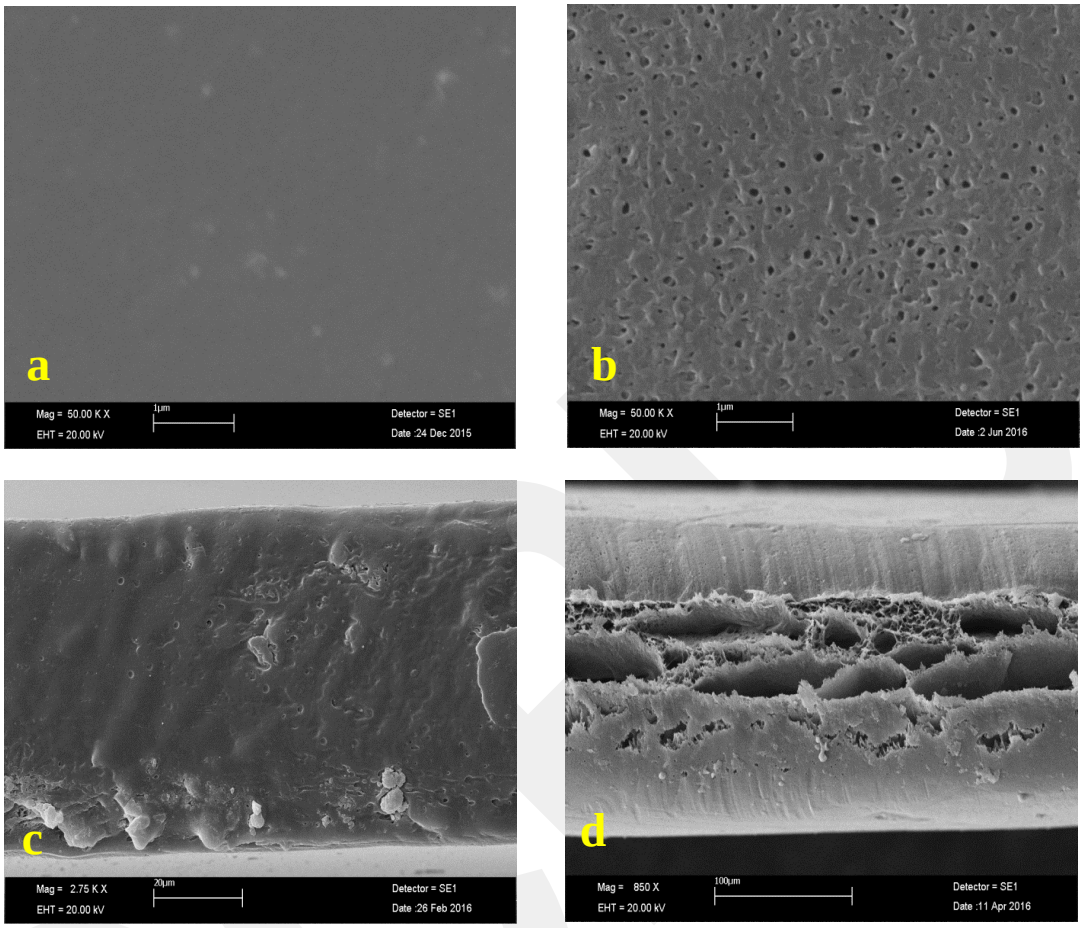

Figure 4.3.SEM images of PSF and PSF/PEI (15/1 wt%) membranes: (a) PSF surface, (b) PSF/PEI surface, (c) PSF cross section, (d) PSF/PEI cross section.

For the 20 wt % PSF membranes, PEI concentrations were increased and the effect of three different concentrations of PEI (2, 4 and 6 wt%) on the performance of membranes was evaluated. The effect of polymer concentration is analyzed in terms of SEM analysis, pure water flux and hydrophilicity parameters. The results of membrane hydrophilicity and pure water fluxes were given in Table 4.2. According to the pure water flux and contact angle measurements, no significant change has been observed with the increase in PEI concentration.

Table 4.2.Contact angle and water flux values of 20 wt% PSF incorporated with different concentration of PEI

Substrate (PEI)	2 wt%	4 wt%	6 wt%
Water flux (L/m^{2}h)	236	214	240
Contact angle (°)	76	76	78

Fig. 4.4 shows top surface images of 20 wt% PSF and PSF/PEI membrane with 2, 4 and 6 wt% PEI addition to the polymer matrix. However, 20 wt% PSF has uniform surface without nodules (Fig. 4.4a), the surface pore structure was completely changed and had small pores when 2 wt% PEI was added to the polymer matrix (Fig. 4.4b). No significant change was observed on membrane flux and hydrophilicity for the different PEI concentrations tested. It can be also seen in Fig.4.4 when PEI loading reached over 2 wt%, bigger macrovoids even visible space formed on membrane surface. Depending on experimental results obtained, SEM images, flux and contact angle values the lowest PEI concentration (2 wt%) was chosen to protect of dense packaging UF structure.

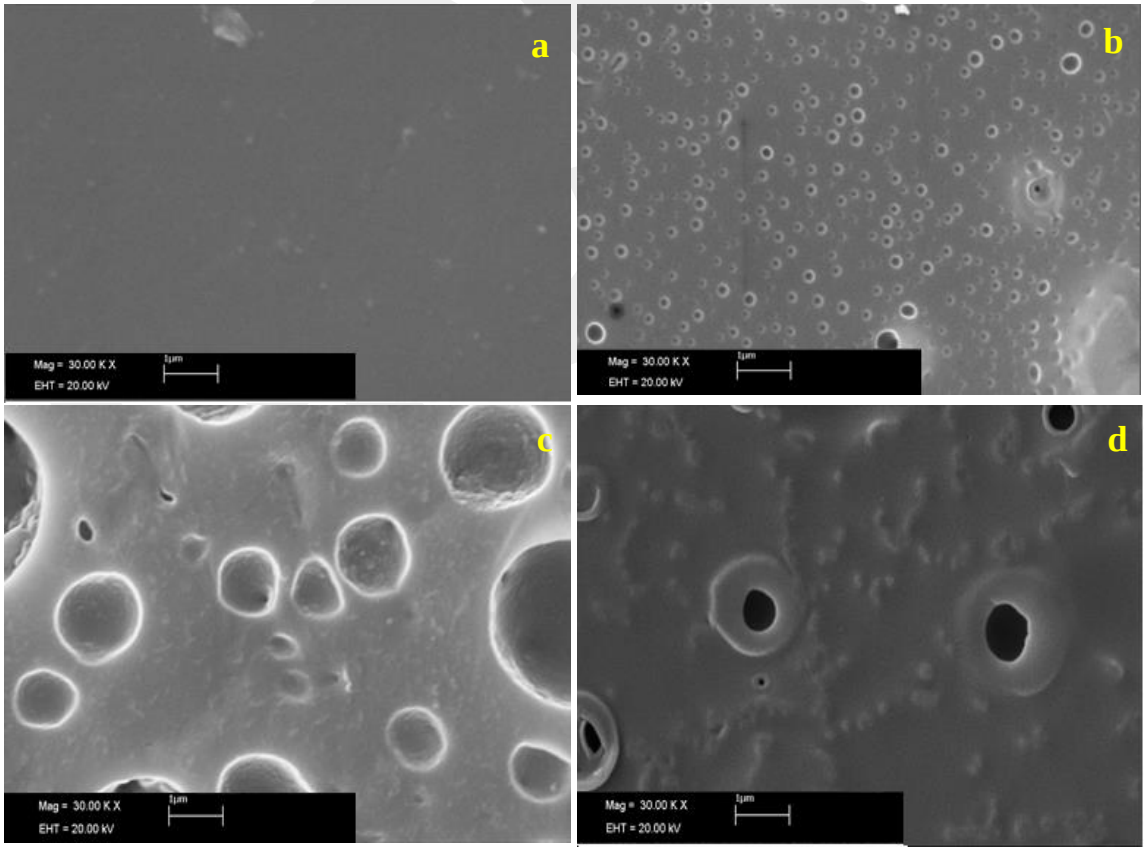

Figure 4.4.SEM images of 20 wt% PSF membranes cross-section containing PEI with different concentrations: (a) 0 wt%, (b) 2wt%, (c) 4wt%, (d) 6wt%

4.3. PSF/PEI/ Al_2O_3 Nanocomposite Membranes

Al_2O_3 nanoparticle is widespread inorganic polymer filler because of its superior properties such as hydrophilicity, anti-fouling resistance and improvement of structural property of polymeric membranes. Within this context, novel flat sheet PSF nanocomposite membranes were prepared by phase inversion method with addition of PEI and Al_2O_3 nanoparticles to increase flux and hydrophilicity and enhance the performance of membranes for oily water treatment. Al_2O_3 nanoparticles were added to the membrane matrix to improve permeability, selectivity, mechanical resistance and antifouling capacity. Two different sizes of 20 nm and 80 nm Al_2O_3 nanoparticles were used with different weight percentages of 0.2 wt%, 1 wt% and 5 wt%. The effect of size and concentration of Al_2O_3 nanoparticles were investigated on the structural properties and filtration performance of the membranes. Compositions of casting solutions were demostrated in Table 4.3.

Table 4.3.Casting solution compositions of PSF, PSF/PEI and PSF/PEI/Al_2O_3 membranes

Substrate	PSF (wt%)	PEI (wt%)	Al_2O_3 (wt%) (20 nm)	Al_2O_3 (wt%) (80 nm)
M201	15	1	0.2	-
M202	15	1	1	-
M203	15	1	5	-
M801	15	1	-	0.2
M802	15	1	-	1
M803	15	1	-	5

4.3.1. Viscosity of membrane dope solutions

Viscosity is one of the most important parameters for membrane fabrication because it affects the solvent–non-solvent exchange rate and the final morphology of the formed membranes [207]. Fig. 4.5 shows viscosity values of the casting solutions used in

fabrication of PSF/PEI/Al_2O_3 nanocomposite membranes. The results show that the addition of PEI and Al_2O_3 increased the viscosity of all solutions and also with increasing Al_2O_3 loading for both sizes of nanoparticles. The addition of 1 wt% PEI increased the viscosity from 170 to 278 cp for 15 wt % PSF. Ananth et al. [202] also investigated the effect of PEI concentration increase in PES membrane matrix and they reported that viscosity of membrane solutions were increased with PEI loading. When PEI amount was 5 wt% dope solution viscosity values were increased from 500 cp to 1600 cp.

As shown in Fig. 4.5, increasing the Al_2O_3 concentration also increased the viscosity from 320 cp to 540 cp and from 265cp to 495 cp for the 20 nm and 80 nm particles, respectively. The highest viscosity was obtained from the PSF/PEI solution containing 5 wt% 20 nm Al_2O_3 nanoparticles as 540 cp. This result can be explained in terms of the adsorption between the polymeric chains and the exposed hydroxyl groups at the surface of the nanoparticles, which have high specific surface area and surface energy [190, 208]. White and Crowder [209] and Taurozzi et al. [210] also reported an increase in the viscosity of the solution when the amount of nanoparticles was higher and when the nanoparticles were smaller. The effects of the nanoparticle concentration and size were contributed to the change in the elastic modulus and recovery of the mixture. The results were also correlated with the literature reported that the polymer–nanoparticle interfacial surface area is affected by both the amount and the size of the TiO_2 nanoparticles [190].

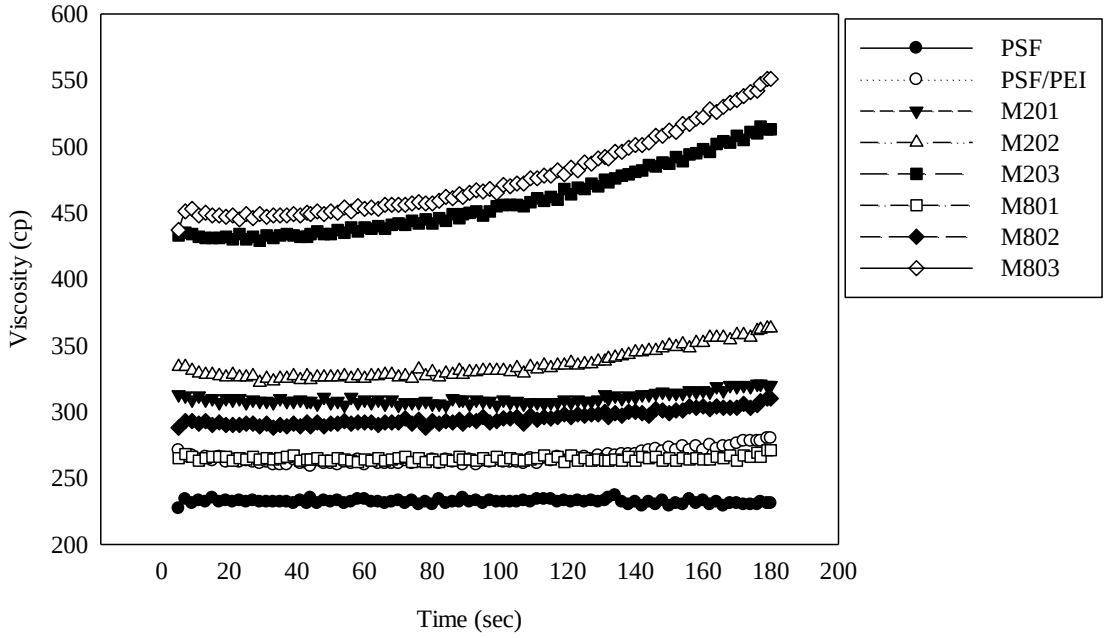

Figure 4.5.Viscosity of the casting solutions for the PSF (15 wt %), PSF/PEI (15/1 wt%), and PSF/PEI/Al_2O_3 nanocomposite membranes (20 nm and 80 nm)

4.3.2. Membrane morphology

Morphology analysis is another very important tool for the development of membranes. The morphology is influenced by various factors, including the interaction, viscosity, and diffusion rate of casting solution [211]. The rates of solidification and coagulation of PSF polymer determine the membrane matrix formation [212]. To investigate the morphological changes associated with the addition of PEI and Al_2O_3 nanoparticles, images of the top and cross sections of the membranes were obtained by SEM.

Cross-section images of the PSF/PEI (15/1 wt%) membranes with different concentrations of 20 nm Al_2O_3 (0.2, 1, 5 wt%) are shown in Fig. 26. The membrane morphology changed significantly with the increasing nanoparticle concentration. Compared to the pure PSF membrane (Fig. 4.5c), the Al_2O_3 nanoparticles result in the development of a long finger-like structure in the cross section. With increasing content of Al_2O_3, the amount of finger-like pores enhanced, and the clear boundary between the sub-layer and center of the membrane disappeared with the addition of 5 wt% Al_2O_3 (Fig. 4.5c) [213].

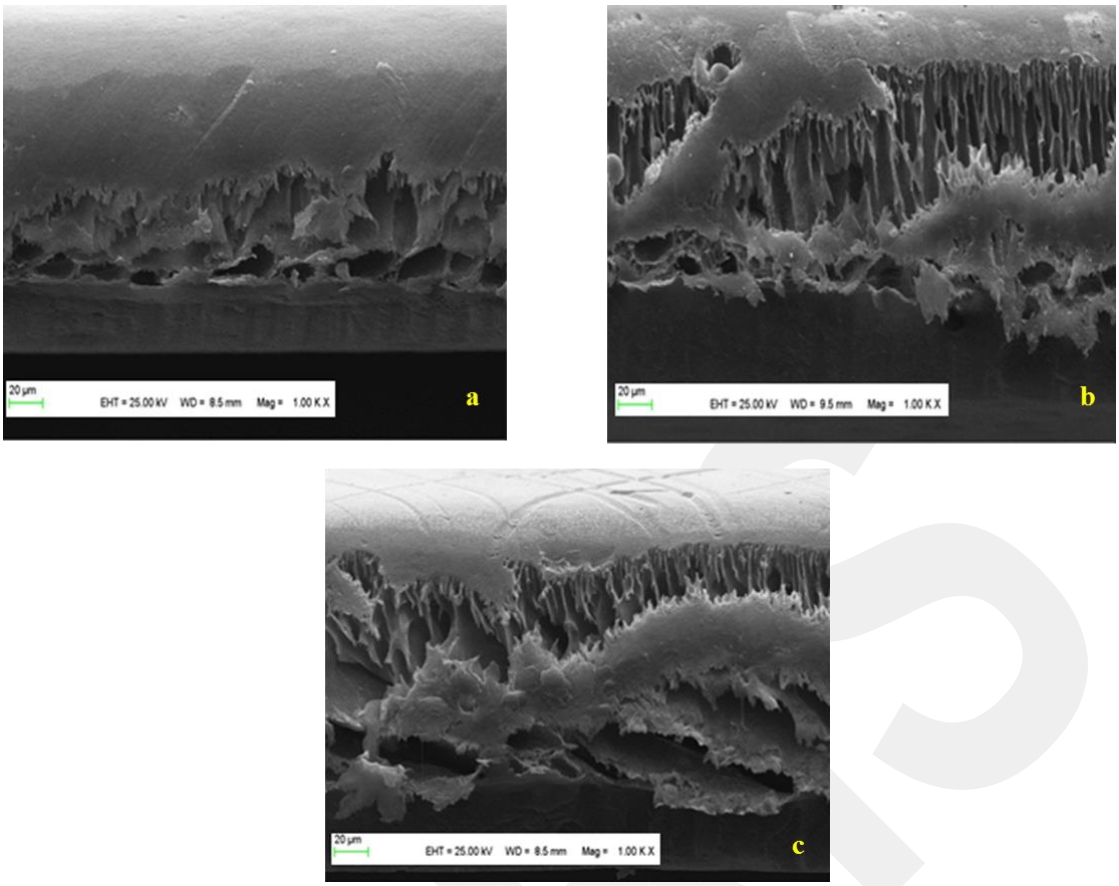

Figure 4.6.SEM images of PSF/PEI (15/1 wt%) membranes cross-sections containing 20 nm Al_2O_3 with different concentrations: (a) 0.2 wt%, (b) 1 wt%, (c) 5 wt%

Fig. 4.7 compares the cross-section SEM images of the 20 nm and 80 nm Al_2O_3 at 5 wt%. The 20 nm Al_2O_3 was dispersed uniformly in the polymer matrix (Fig. 4.7a), but the 80 nm Al_2O_3 membrane had many short finger-like structures in the center, which were covered with dense top and bottom layers. This is attributed to the high loading amount of 80 nm nanoparticle resulting in unstable distribution in the PSF/PEI membrane matrix (Fig. 4.7b) [105]. This could be explained by the high viscosity of the casting solution when the 20 nm Al_2O_3 is added, as well as the high affinity of the 20 nm nanoparticles to the polymeric phase [214].

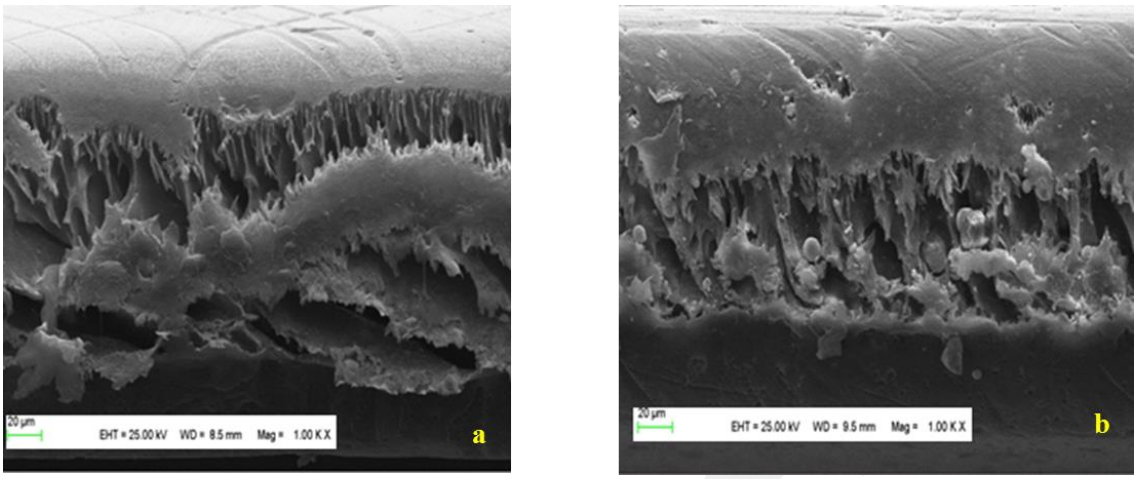

Figure 4.7.Cross-section SEM images of PSF/PEI (15/1 wt%) membrane containing 5 wt% Al_2O_3 nanoparticles: (a) 20 nm Al_2O_3, (b) 80 nm Al_2O_3

4.3.3. Membrane hydrophilicity

Hydrophilicity is directly related to the flux and antifouling property of a membrane. The hydrophilicity of the PSF/PEI/Al_2O_3 nanocomposite membranes was evaluated by the contact angle measurements using the sessile drop method, as shown in Table 4.4. The pure PSF membrane's contact angle was 87°, but PEI addition decreased the contact angle to 67º (Table 4.4). The contact angles were 72°, 65°, and 56° for membranes with 20 nm Al_2O_3 nanoparticles at 0.2, 1, and 5 wt % loadings, respectively. For 80 nm Al_2O_3 nanoparticles, the contact angles were 81°, 77°, and 55° for 0.2, 1, and 5 wt % loadings, respectively. The contact angles of the PSF/PEI/Al_2O_3 nanocomposite membranes were higher than 1, and 5 wt % loadings for 0.2 wt % concentration at both sizes of Al_2O_3 nanoparticles. When the amount was increased to 5 wt%, the contact angles decreased for both sizes of Al_2O_3 nanoparticles blended membranes. This could be due to greater migration of nanoparticles to the surface during the phase inversion process at high concentration [215, 216]. The membrane hydrophilicity was positively affected by increasing the nanoparticle loading, but the particle size had no significant effect.

Table 4.4.Contact angle, pure water flux (at 4 bar), and porosity of PSF, PSF/PEI (15/1 wt%) and PSF/PEI/Al_2O_3 (20 nm and 80 nm) nanocomposite membranes

Substrate	CA (°)	Water flux (L/m^2h)	Porosity (%)
PSF	87±2	20.5	63±3
PSF/PEI	64±4	317.7	95±4
M201	72±5	236	71±2
M202	65±2	1289.1	77±5
M203	56±3	1336.6	79±6
M801	81±6	103.2	68±3
M802	77±3	1027.1	73±2
M803	55±2	901.3	65±4

4.3.4. Porosity

In general, membrane porosity is dependent on the mass transfer of the dope solution during the phase inversion [217]. The hydrophilic functional groups from the nanoparticles speed up the membrane formation process by accelerating the exchange rate between the solvent and non-solvent [218]. Al_2O_3 membranes porosities were given in Table 4.4. Consequently, the pore formation process would be enhanced with addition nanoparticle to the membrane matrix. As shown in Table 4.4, the porosity of membranes increased from 63% for the pure PSF membrane to 79% and 65% for membranes with 5 wt% 20 nm and 80 nm Al_2O_3 nanoparticles, respectively. All the blended membranes showed improved porosity, but there was a small decrease for the 80 nm Al_2O_3 at 5 wt%. This might have been caused by pore blockage due to the high particle size and amount of Al_2O_3 [219].

The improvements of the porosity of the nanocomposite membranes were attributed to the lower viscosity of the blending solution with the addition of hydrophilic Al_2O_3, which led to a faster occurrance of the phase inversion process. These results may be expressed by the slow solution demixing and improved kinetic limitations, which increased the viscosity. The increased viscosity caused higher diffusion rate into the cast

membrane, resulting in lower porosity [206, 215, 220]. This results are also in agreement with findings by Choi et al. [221], who prepared nanocomposite UF membranes from PSF casting solutions loaded with different amounts of MWCNTs.

4.3.5. Mechanical properties

Adding the nanoparticles improved the morphological and structural parameters of the PSF/PEI/Al_2O_3 membrane, as well as the mechanical resistance. The tensile strength of the Al_2O_3 membranes is shown in Fig. 4.8. The tensile strength of the pure PSF membrane was 3.18 MPa, which decreased to 3.02 MPa with the addition of PEI due to the increased pore formation [222]. Incorporating 0.2, 1, and 5 wt% 20 nm Al_2O_3 nanoparticles increased the tensile strength to 3.2, 3.7, and 4.1 MPa, respectively. This could be explained by the interaction between the nanoparticles and the PSF/PEI matrix. Al_2O_3 could act as a cross-linking point to connect the polymer chains and increase their rigidity. Therefore, more energy would be needed to break down the bonds between the Al_2O_3 and PSF, and the tensile strength was improved [223]. With increasing amount of Al_2O_3, the tensile strength values increased slightly. As shown in Fig. 4.8, the tensile strength with 0.2 and 1 wt% 80 nm Al_2O_3 increased but declined for 5 wt% Al_2O_3. When adding 5 wt% 80 nm Al_2O_3, the tensile strength decreased from 4.7 MPa to 3.2 MPa. Excessive concentration may cause nanoparticle aggregation and resulted as a decrease in tensile strength. Kumar et al. [224] prepared a study on PSF membrane containing graphene oxide (GO)–TiO_2 nanoparticles by a blending method. They found that the tensile strength was enhanced with lower amounts of GO–TiO_2 of up to 2 wt%, but it decreased when the loading was further increased to 5 wt%.

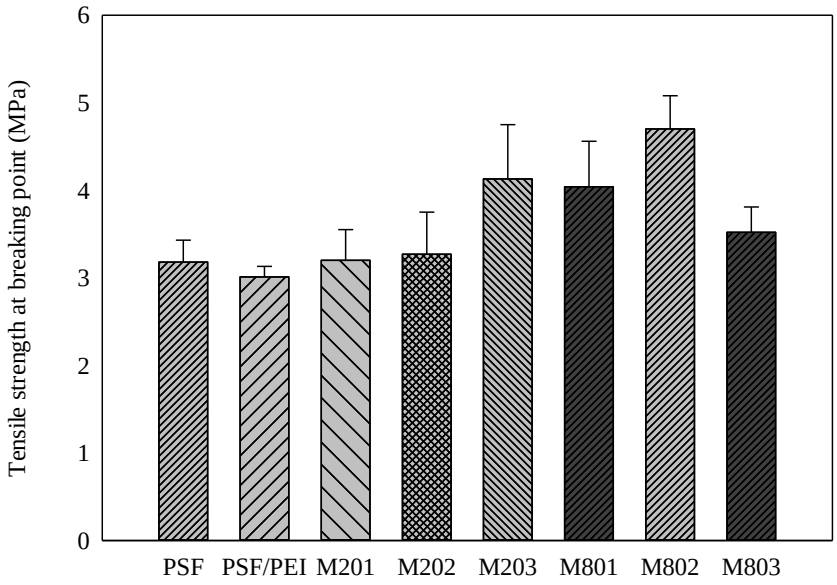

Figure 4.8.Tensile strength of breaking point of PSF, PSF/PEI (15/1 wt%) and PSF/PEI/Al_2O_3 nanocomposite membranes

4.3.6. Thermal stability

The thermal stabilities of the membranes were measured by TGA, as shown in Fig. 4.9. The thermal decomposition temperatures were in the range of 500-550°C. The TGA measurement results confirmed that PSF is a thermally stable polymer due to its fully aromatic structure [225]. As shown in the TGA curves, the nanoparticles have no significant effect on the thermal decomposition temperature.

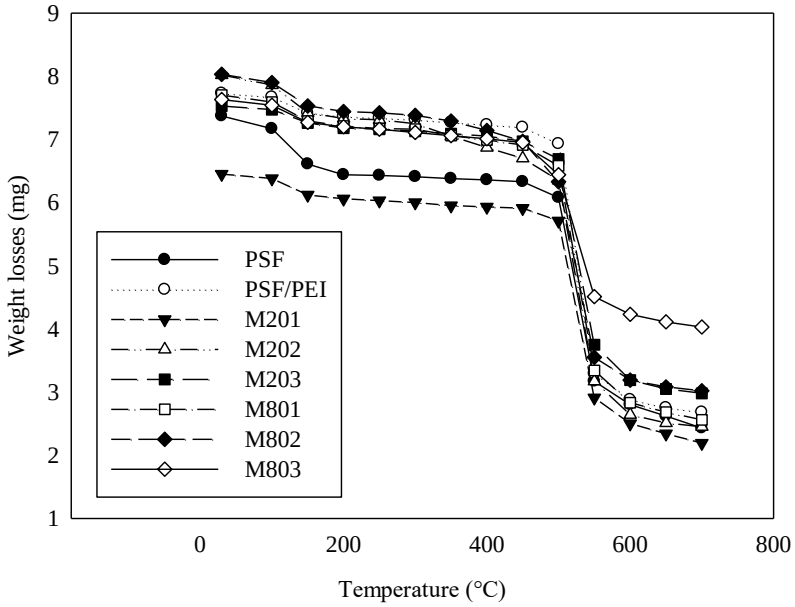

Figure 4.9.TGA curves of PSF, PSF/PEI (15/1 wt%) and PSF/PEI/Al_2O_3 nanocomposite membranes

The decomposition weight losses of prepared Al_2O_3 membranes decreased with increasing Al_2O_3 concentration and weight loss of membranes as shown in Table 4.5. Although the maximum weight loss ratio was obtained for pure PSF with 67%, adding 5 wt% 80 nm Al_2O_3 the minimum weight loss was observed with 47% in the temperature range of 500–550 ◦C. This could be arising from the fact that Al_2O_3 has higher thermal stability compared to pure PSF. Similar decrease was observed the decomposition loss with nanoparticle addition by Jadav et al.[226].

Table 4.5. Weight loss (%) differences of PSF and PSF/PEI/Al_2O_3 nanocomposite membranes at 550°C

Substrate	PSF	M201	M202	M203	M801	M802	M803
Weight loss (%)	67	66	64	60	66	62	47

4.3.7. FT-IR

The surface functional groups and chemical composition of the membranes were determined by FT-IR spectroscopy, as shown in Fig. 4.10. The characteristic absorption peaks of PSF were around 1149 cm^{-1} and 1168 cm^{-1} (SO_2 symmetrical stretching), 1244

cm^{-1} (aryl-O-aryl C–O stretching), 1582 cm^{-1} (SO_2 asymmetric stretching), 1677 cm^{-1} (asymmetric–CH_3), and 2151 cm^{-1} (C=C) for both figures [227, 228].

A new peak occurred at 3700 cm^{-1} in the spectrum of Al_2O_3 nanoparticle membranes, which is related to the –OH and Al–O functional groups of the Al_2O_3 nanoparticles [213]. This can be attributed to the successful interaction between the base polymer and inorganic phases. All of the membranes also had the same basic structure of PSF. Comparison between the spectrum of the PSF membrane and nanocomposite membrane showed a similar PSF characteristic peak in the area of 1000–3500 cm^{-1} because of the high PSF concentration. Thus, it is assumed that the membrane was successfully modified based on the higher peak obtained (Fig 4.10).

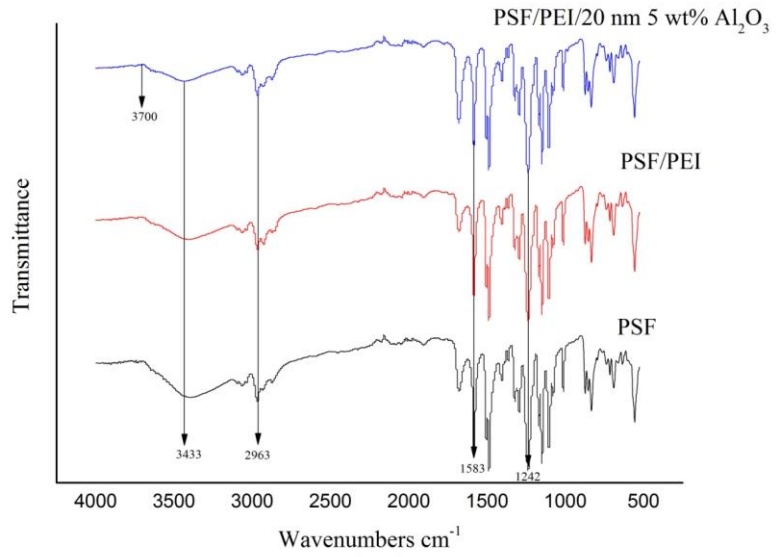

Figure 4.10. FT-IR spectrum of PSF, PSF/PEI and PSF/PEI membrane containing 5 wt % Al_2O_3

4.3.8. Pure water flux

The water fluxes of the membranes were determined at 3 different pressures (2, 4, and 6 bar), as shown in Fig. 4.11. The pure PSF membrane showed the lowest water flux of 20.51 L/m^2h at 0.4 MPa, and the highest water flux was obtained for the membranes with 5 wt% 20 nm Al_2O_3 nanoparticles as 1336.6 L/m^2h at 4 bar. This result could be explained by the enhancing potential of Al_2O_3 nanoparticle in terms of the hydrophilicity (Table 4.4) and porosity compared to the pure PSF membranes [108, 229].

Although increasing the amount of 20 nm Al_2O_3 nanoparticles enhanced the water flux of membranes, increasing the amount of 80 nm nanoparticles to 5 wt% adversely affected the water flux of membranes. This might be a result of pore blockage by the large nanoparticles [50, 230]. Therefore, either agglomeration or the slower exchange of solvent and non-solvent could not be prevented during the phase inversion process [108, 231].

These findings also might be supported by the porosity data. Higher porosity results in higher water flux values [232, 233]. Esfahani et al. [234] reported that the pure water flux was increased from 10 to 210 L/m^{2}h at 0.16 MPa by incorporation of 1 wt% multi-walled CNTs. In our study, the pure water flux increased from 12.6 to 171 L/m^{2}h at 2 bar by incorporation of 1 wt% Al_2O_3 (20 nm). Moreover, when the Al_2O_3 nanoparticle concentration increased to 5 wt%, the water flux increased to 850.2 L/m^{2}h at 2 bar TMP. These results demonstrate that the Al_2O_3 nanoparticles have a more remarkable effect on the pure water flux than MWCNTs.

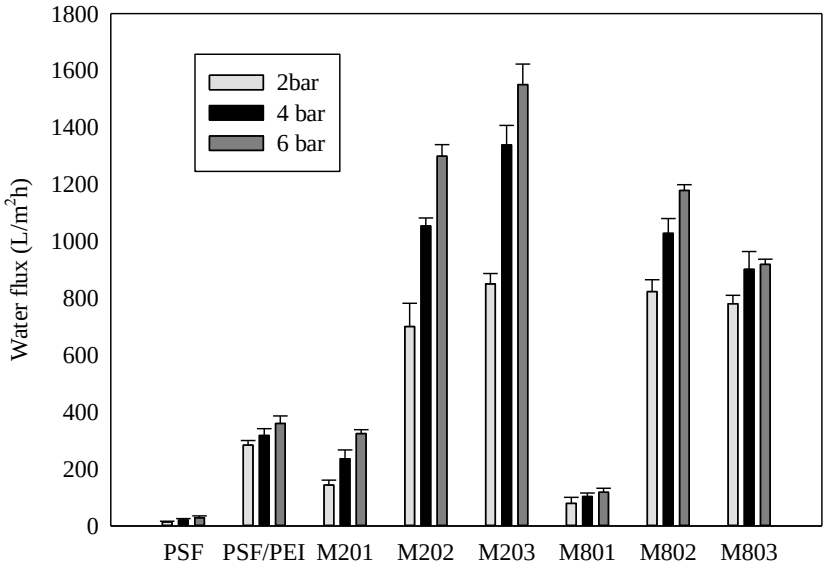

Figure 4.11.Water fluxes of PSF, PSF/PEI and PSF/PEI/Al_2O_3 nanocomposite membranes at different pressures.

4.3.9. BSA rejection

BSA filtration experiments were carried out using 2.5 g/L BSA solution was used because of its hydrophobic nature and appropriate molecular size to evaluate the separation performance. Properties of BSA were adapted from [235] molecular mass is average 67.000-69.000 mg/L. BSA rejection performance results are given in Fig. 4.12. The BSA rejection values of the pure PSF and PSF/PEI membranes were 83% and 72%, respectively. The PSF/PEI membrane had the lowest BSA rejection because of its higher porosity and consequently lower selectivity [236]. All of the prepared PSF/PEI/Al_2O_3 nanocomposite membranes rejected more than 90% of the BSA. The results are also comparable with literature given by Nair et al. [237], who achieved maximum BSA rejections of 88% to 94% using PSF membranes with $CaCO_3$ nanoparticles.

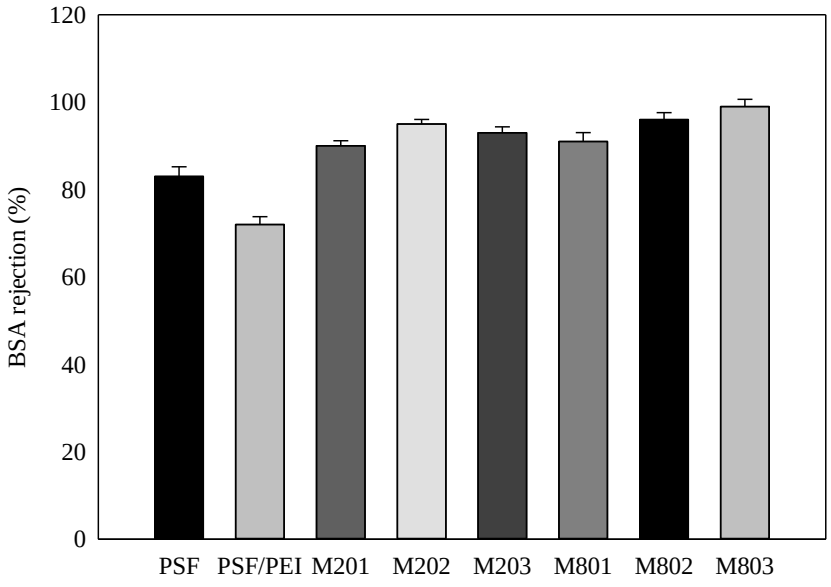

Figure 4.12.BSA rejection performance of PSF, PSF/PEI (15/1 wt%), and PSF/PEI/Al_2O_3 nanocomposite membranes

Figure 4.13 shows the variation of the BSA flux versus VRR at an operating pressure of 2 bar. As shown in Fig. 4.13, the fouling of the Al_2O_3 containing membranes were significantly reduced compared to pure PSF membranes. The flux reduced fast at the beginning of filtration for all membranes, after VRR values reached 1.5 all

nanocomposite membranes showed a steady state in the permeation rate. The nanocomposite membranes with 5 wt% and 1 wt% 20 nm Al_2O_3 showed the highest flux values.

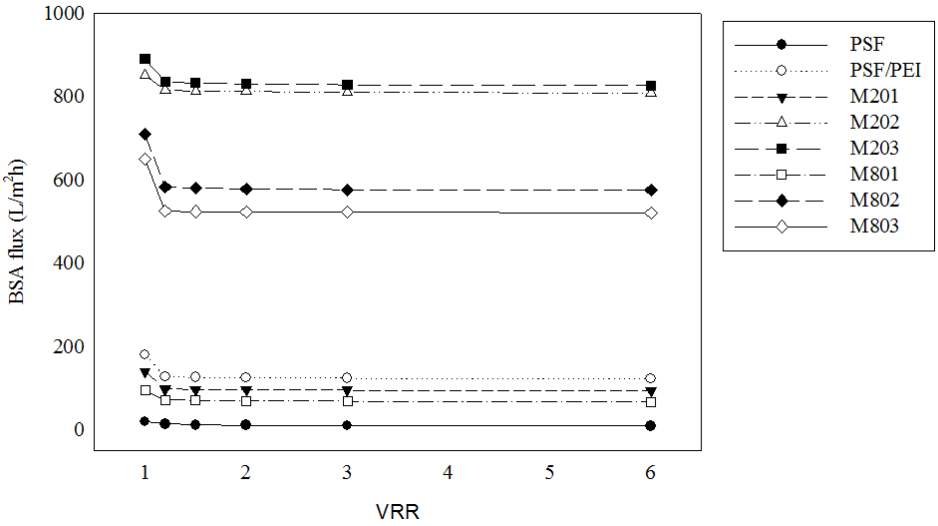

Figure 4.13. BSA rejection performance of PSF, PSF/PEI (15/1 wt%), and PSF/PEI/Al_2O_3 nanocomposite membranes.

4.4. PSF/PEI/$CaCO_3$ Nanocomposite Membranes

$CaCO_3$ has attracted considerable attention in water and wastewater treatment because of its non-toxicity, enviromental friendly, commercial availability and low cost, and ease of preparation properties [238]. Additionally, $CaCO_3$ surface properties can improve membrane hydrophilicity and water permeation due to its carboxylic groups [239]. Within this context, PSF/PEI/$CaCO_3$ nanocomposite membranes were prepared via phase inversion process with PEI and $CaCO_3$ nanoparticles additives to increase flux and hydrophilicity of membranes and improve their performance for oily water treatment. 100 nm $CaCO_3$ nanoparticles was used in membrane matrix with different weight percentages of 1 wt%, 2 wt% 5 wt% and 10 wt%. The effect of concentration of $CaCO_3$ nanoparticle on the structural properties and filtration performance of the membranes was investigated. $CaCO_3$ membranes casting solution compositions were given in Table 4.6.

Table 4.6. Casting solution compositions of PSF, PSF/PEI (20/2 wt%) and PSF/PEI/$CaCO_3$ membranes

Substrate	PSF (wt%)	PEI (wt%)	$CaCO_3$ (wt%)
PSF	20	0	0
PSF/PEI	20	2	0
C1	20	2	1
C2	20	2	2
C5	20	2	5
C10	20	2	10

4.4.1. Viscosity of membrane dope solutions

PSF/PEI (20/2 wt%), and PSF/PEI/$CaCO_3$ nanocomposite membranes viscosity values were shown in Fig.4.14. The casting solutions viscosity values were increased significantly with increasing $CaCO_3$ nanoparticles loading because of higher shear stress. As shown in Fig 4.14, increasing the $CaCO_3$ concentration from 1wt% to 10wt %, increased the viscosity from 680 to 2530 cp. The highest viscosity was obtained for the PSF/PEI solution containing 10 wt% $CaCO_3$ nanoparticles. This result can be explained in terms of the adsorption between the polymeric chains and the exposed hydroxyl groups at the surface of the nanoparticles, which have high specific surface area and surface energy [190, 208]. Nair et al. [237] also showed that the addition of $CaCO_3$ nanoparticles in PSF membrane increases the viscosity values from 800 to 1397 cP.

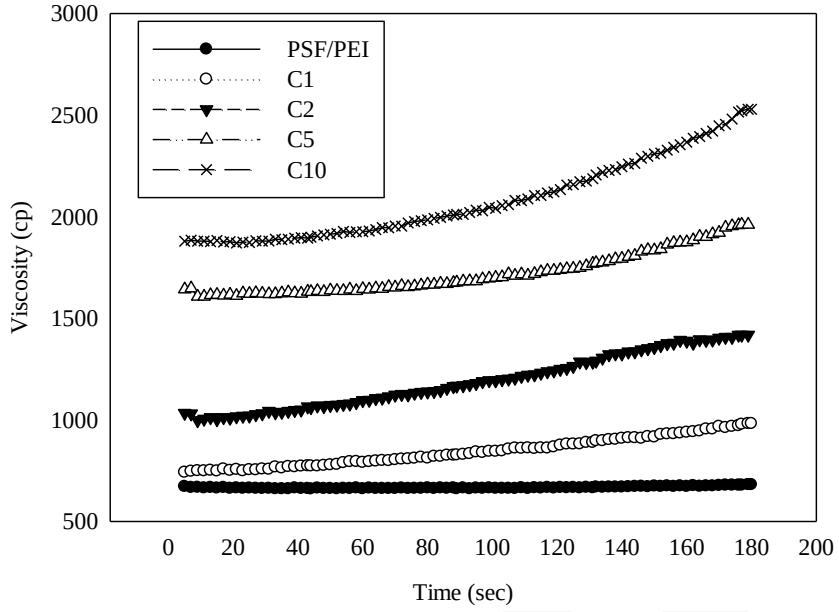

Figure 4.14.The casting solution viscosity values of PSF/PEI (20/2 wt%) and PSF/PEI/$CaCO_3$ nanocomposite membranes

4.4.2. Membrane morphology

Prepared $CaCO_3$ membrane top and cross-section structures were investigated by SEM. Surface images of the PSF/PEI (20/2 wt%) membranes with different concentrations of $CaCO_3$ (1, 2, 5, 10 wt%) are shown in Fig. 4.15. As shown in Fig. 4.15, although the concentration of $CaCO_3$ nanoparticles was high, agglomeration problem was not observed. Chan et al. [240] got similar results when $CaCO_3$ content was lower than 20 wt% in membrane matrix. However, for 27 wt% $CaCO_3$ loading more aggregates were reported on the surface of PP membranes. The membrane morphology also changed significantly with the increase in nanoparticle concentration. Compared to the pure PSF membrane (Fig. 4.15a), the $CaCO_3$ nanoparticles result in the development more porous structure on the membrane surface.

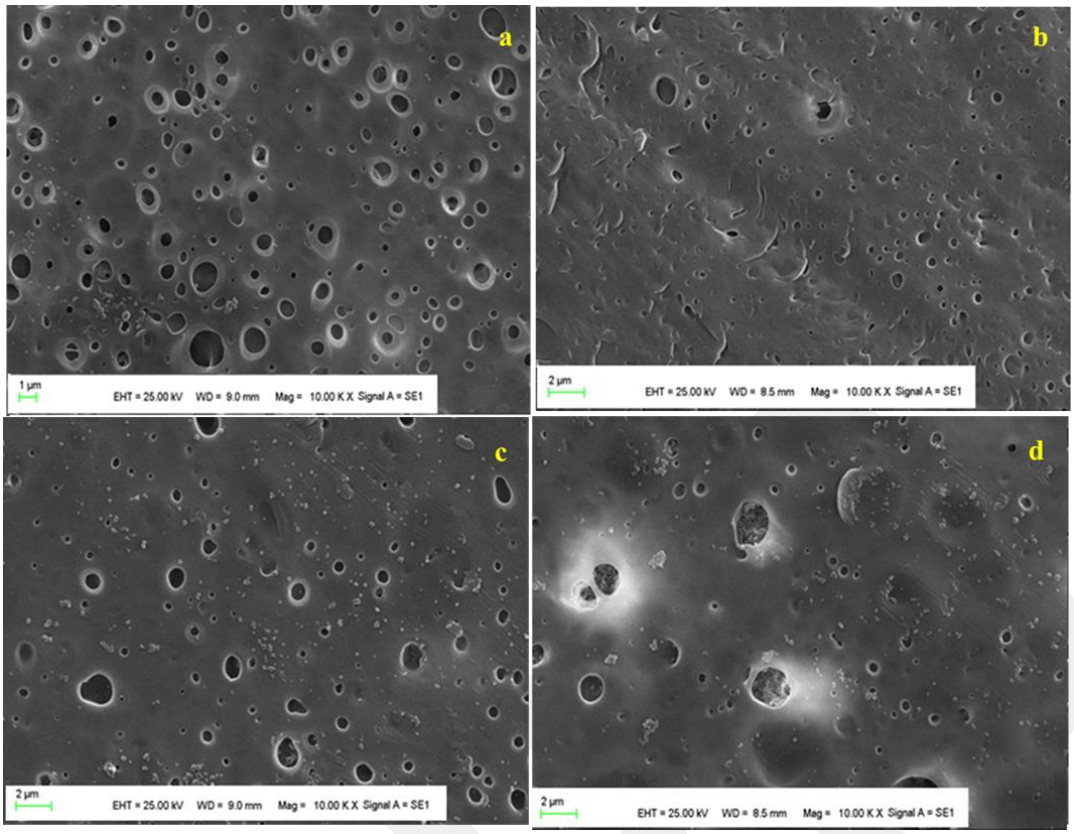

Figure 4.15.Surface SEM images of PSF/PEI (20/2 wt%) membrane containing $CaCO_3$ nanoparticles: (a) 0.2 wt%, (b) 1 wt%, (c) 5 wt%, (d) 10 wt%

Cross-section images of PSF/PEI/$CaCO_3$ nanocomposite membranes were given in Fig.4.16. Similar cross-section structure was observed in $CaCO_3$ nanocomposite membrane. Higher range of viscosity values between C1 and C10 nanocomposite membrane could be caused significant differences because of diffusion kinetic changes between components in the phase inversion. As shown in closer magnitutation of images (Fig.4.16 a and d), the higher viscosity induces slower exchange between solvent and non-solvent for the formation of porous structure, as a result smaller pore sizes will be formed. On the other hand, the hydrophilic PEI and $CaCO_3$ content in membrane matrix should have resulted in fast exchange because of higher viscosity which resulted microporous membranes structure during the phase inversion. [241]. Another possibility can be increasing concentration of $CaCO_3$ so that decreasing thermodynamic resistance of the membrane solution.

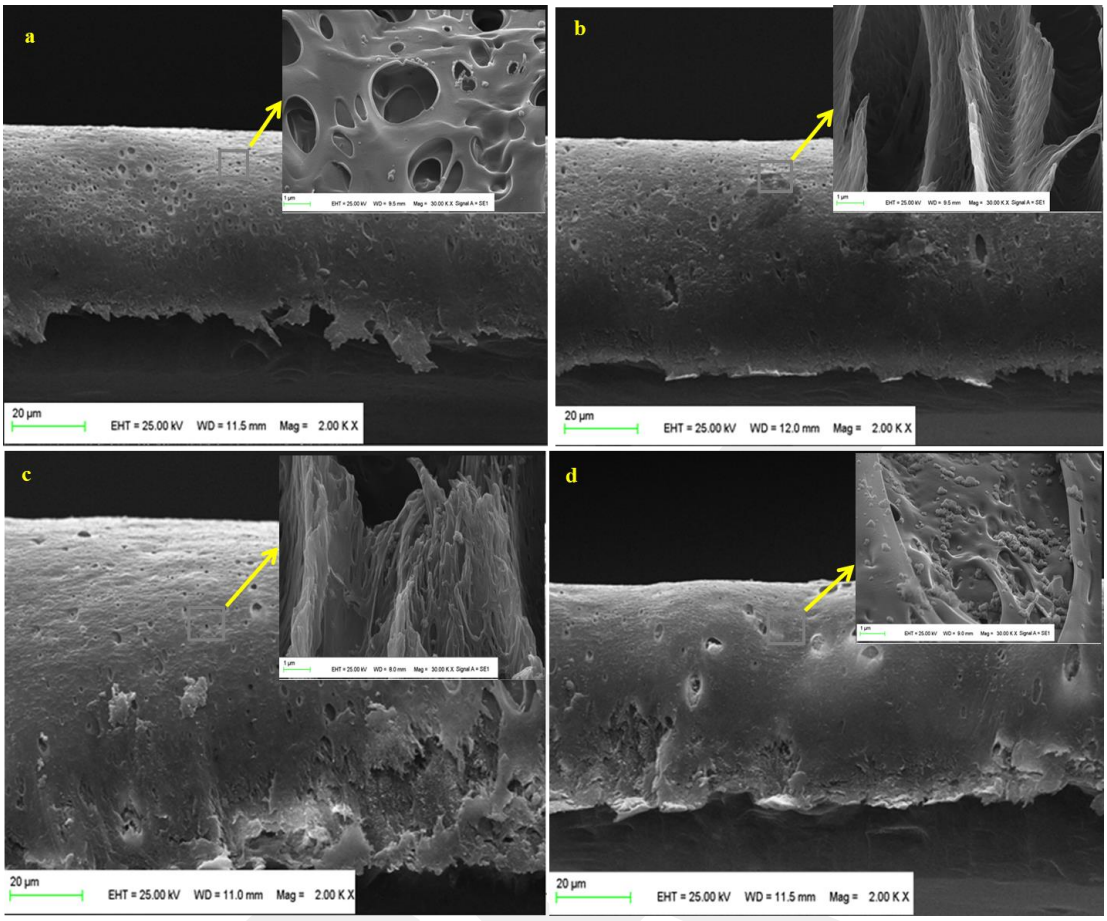

Figure 4.16.Cross-section SEM images of PSF/PEI membrane containing $CaCO_3$ nanoparticles: (a) 0.2 wt%, (b) 1 wt%, (c) 5 wt%, (d) 10 wt%

4.4.3. Membrane hydrophilicity

$CaCO_3$ membranes hydrophilicity was measured by contant angles and results of the measurements of different concentrations of $CaCO_3$ are given in Table 4.7. 2 wt% incorporation of $CaCO_3$ decreased contact angle from 92° for pure PSF membrane to 80°. The decrease in contact angle values with addition of $CaCO_3$ nanoparticles, is a clear indication of increasing hydrophilicity of the membranes. This hydrophilicity improvement can be attributed to the natural hydrophilicity of the $CaCO_3$ nanoparticles and also OH groups' formation on the membrane surface.

Table 4.7.Contact angle, pure water flux (at 2 bar) and porosity of PSF, PSF/PEI and PSF/PEI/$CaCO_3$ nanocomposite membranes

Substrate	CA (°)	Water flux (L/m^2h)	Porosity (%)
PSF	92±5	3.3±0.2	27±3
PSF/PEI	85±4	236±13	58±5
C1	87±7	85.5±12	74±8
C2	86±5	52.3±8	76±3
C5	80±6	103±26	75±6
C10	84±8	197±21	70±2

$CaCO_3$ lead to hydroxylated to form Ca–OH groups with water; this may result in a increasing of hydrophilicity [239]. And also, Fig. 4.17 illustrated the images of water droplets in contact with the surface of PSF/PEI/$CaCO_3$ nanocomposite membranes.

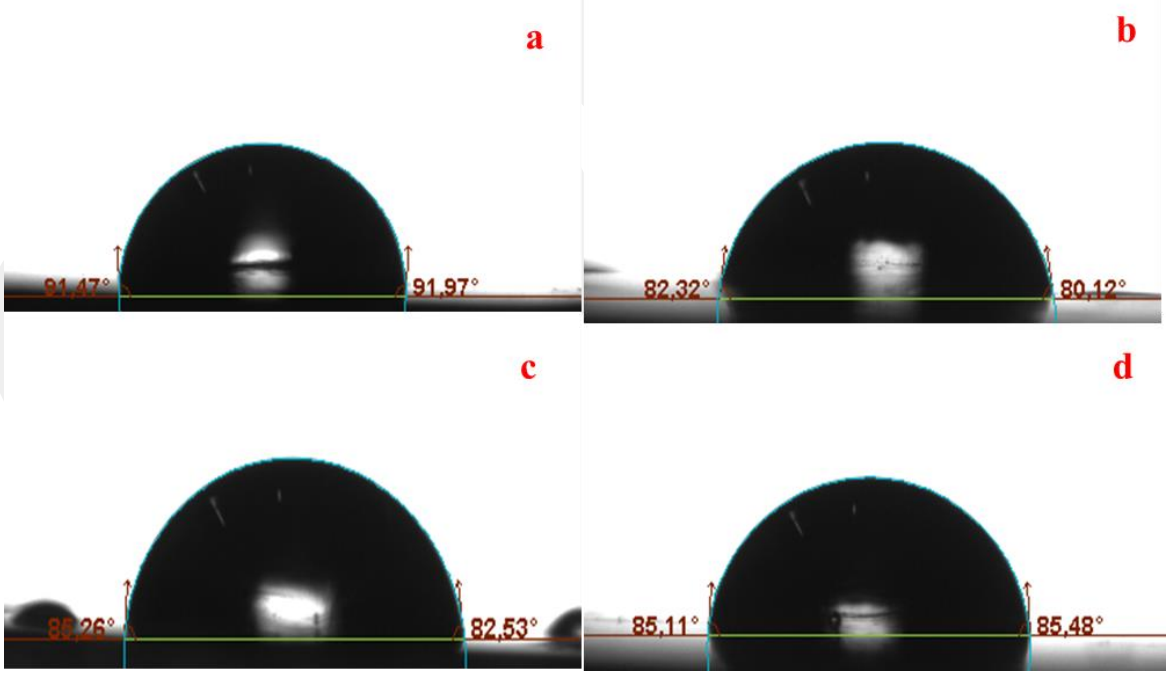

Figure 4.17.Contact angle images of PSF/PEI membrane containing $CaCO_3$ nanoparticles: (a) 0.2 wt%, (b) 1 wt%, (c) 5 wt%, (d) 10 wt%

4.4.4. Porosity

In PSF/PEI/$CaCO_3$ membranes $CaCO_3$ is well dispersed with different weight ratios in membrane structure and porous $CaCO_3$ exhibits distinct porosity that are very promising for water treatment [242, 243]. It can be seen that in Table 4.7, porosity significantly increases with $CaCO_3$ loading when compared to the PSF and PSF/PEI membranes. PSF and PSF/PEI (20/2 wt%) dense structure causes the lowest porosity with 27% and 58%, respectively. However, all nanocomposite membranes have similar porosity values; the maximum porosity was observed 76% at 2 wt% of $CaCO_3$ content.

4.4.5. Mechanical properties

Hydrophilic $CaCO_3$ addition in polymer matrix could enhance membrane morphology as well as mechanical properties especially tensile strength. $CaCO_3$ has been used as an important filler in polymeric materials [244]. The mechanical properties of the polymeric materials can be developed significantly and this will improve the compatibility between the filler and polymer [240]. Fig. 4.18 illustrated strain-stress curve of of PSF and PSF/PEI/$CaCO_3$ membranes. Tensile stress increased with $CaCO_3$ addition, when the $CaCO_3$ content is at 10 wt %, the tensile strength increased 7.8 MPa. Moreover, the tensile strength of pure PSF is 4.1 MPa.

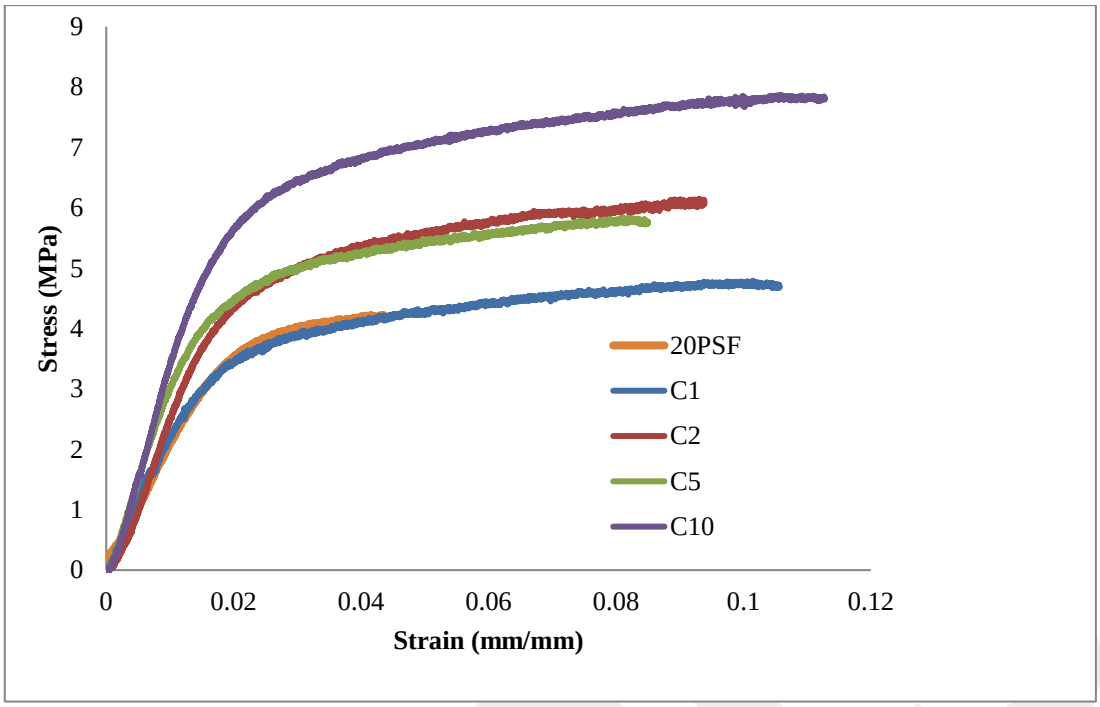

Figure 4.18. Strain-stress curve of PSF and PSF/PEI/$CaCO_3$ membranes

4.4.6. FT-IR

The surface chemical compositions of PSF/PEI/$CaCO_3$ nanocomposite membranes were determined by FT-IR spectroscopy, as shown in Fig. 4.19. The PSF characteristic peaks were around 1149 cm^{-1} and 1168 cm^{-1} (SO_2 symmetrical stretching), 1244 cm^{-1} (aryl-O-aryl C–O stretching), 1582 cm^{-1} (SO_2 asymmetric stretching), 1677 cm^{-1} (asymmetric–CH_3), and 2151 cm^{-1} (C=C) [227, 228]. After $CaCO_3$ addition, the peak intensities of 871 cm^{-1} and 1408 cm^{-1} increase because these two peaks are also described to the characteristic vibration of $CaCO_3$ (asymmetric stretching vibration and out-of-plane bending vibration of carbonate group). At the same time, a shoulder peak near 1408 cm^{-1} is corresponding to amorphous. In addition, the peak at 1664 cm^{-1} is assigned to the vibration of water molecules bounded on the $CaCO_3$ particles [142, 144, 245]. Very important, in order to demonstrate the presence of $CaCO_3$ in nanocomposite membranes, are the peaks at 869 and 704 cm^{-1} [246]. As the concentration of $CaCO_3$ increases from 5 wt% to 10 wt% the merged peaks became more obvious, this is evident the successful linkage of $CaCO_3$ in PSF.

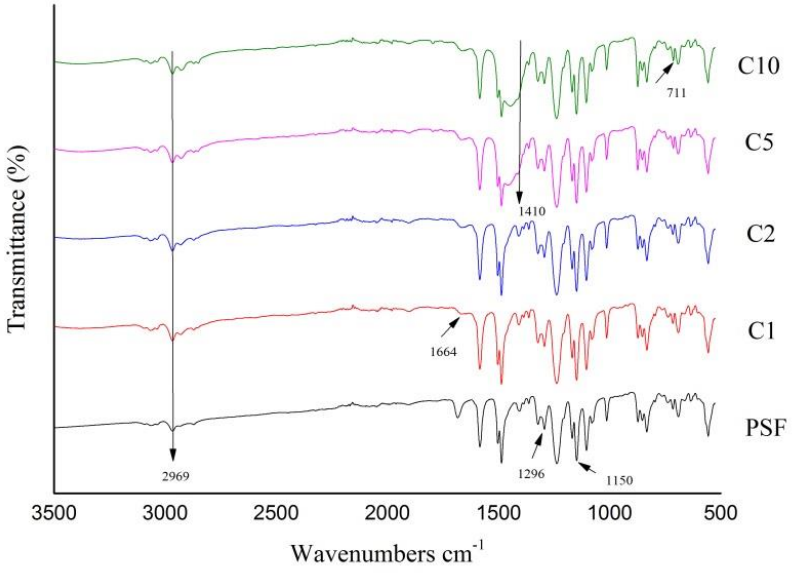

Figure 4.19.FT-IR spectrum of PSF and PSF/PEI/$CaCO_3$ nanocomposite membranes

4.4.7. AFM

The three-dimensional images of AFM analysis are shown in Fig. 4.20 and clearly observed from AFM images PSF smoother structure changed significantly addition with $CaCO_3$ nanoparticles.

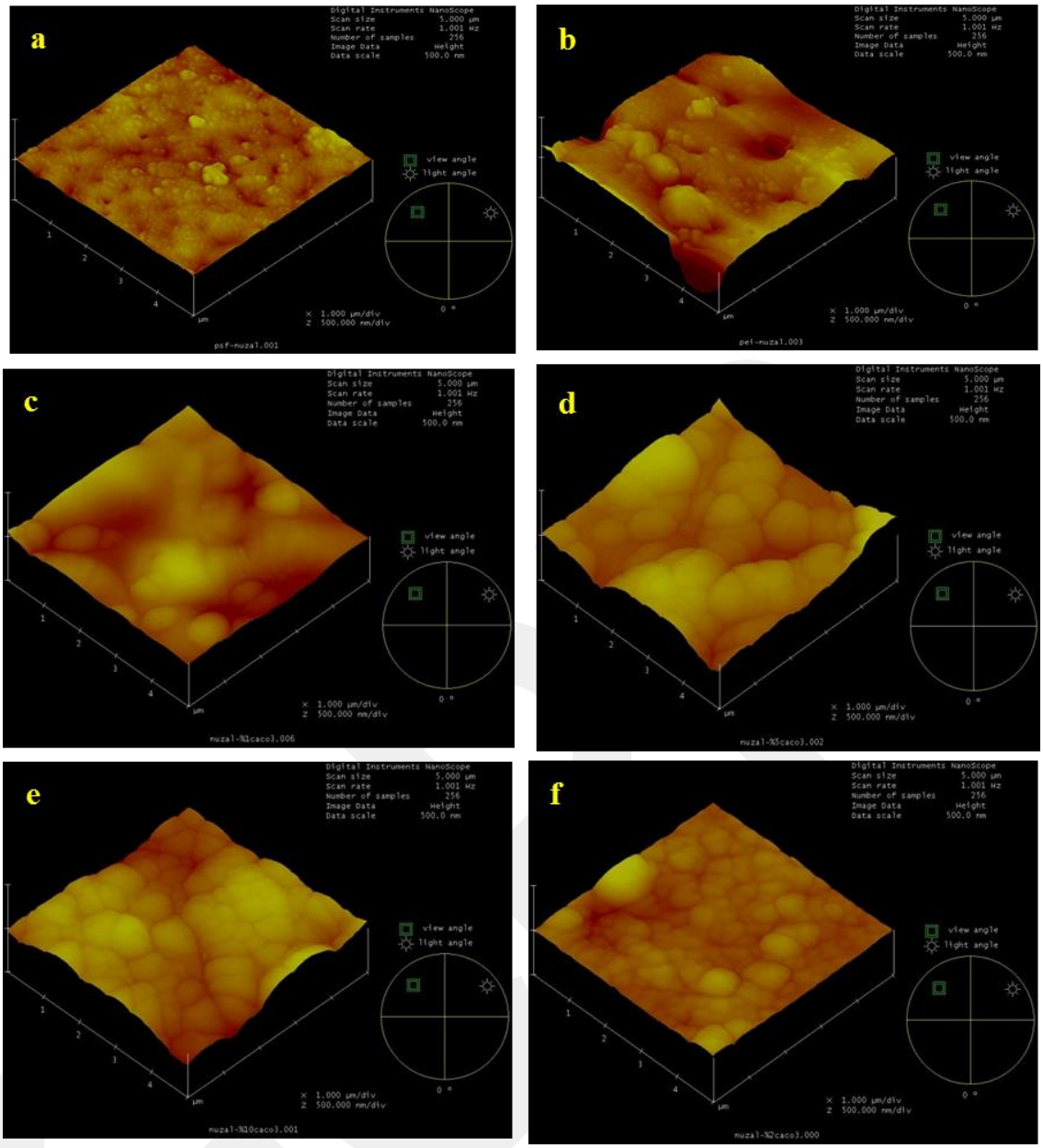

Figure 4.20.AFM images of (a) PSF (20 wt%), (b) PSF/PEI (20/2 wt%) and PSF/PEI/$CaCO_3$ nanocomposite membranes containing (c) 1 wt% $CaCO_3$ nanoparticles, (d) 2 wt% $CaCO_3$ nanoparticles, (e) 5 wt% $CaCO_3$ nanoparticles, (f) 10 wt% $CaCO_3$ nanoparticles

The roughness parameters, Rq, Ra and Rmax are given in Table 4.8 shows and its increase with the $CaCO_3$ nanoparticles loading. PSF/PEI/5wt% $CaCO_3$ exhibited Ra value as high as 97 nm in comparison to 9 nm shown by PSF membrane and this results similar with the data given in literature [237]. The surface roughness of the blend membranes was apparently higher than that of the pure PSF membrane. Moreover, the membrane roughness increased with $CaCO_3$ addition. Although PSF/PEI membrane showed higher Ra value than C1 and C2 membranes, this can be explain by PEI could

increase the solvent evaporation time during phase inversion and this value is also supported by Khayet et al. [247].The reduction in surface roughness may be assigned to the increase in membrane porosity.

Table 4.8.The roughness properties of PSF, PSF/PEI (20/2 wt%) and PSF/PEI/$CaCO_3$ nanocomposite membranes.

	Rq (nm)	Ra (nm)	Rmax (nm)
PSF	12	9	137
PSF/PEI	57	40	522
C1	35	25	316
C2	24	18	153
C5	44	97	308
C10	59	48	386

4.4.8. XRD

The microstructures of PSF and nanocomposite membranes were studied by X-ray diffraction analysis. XRD analysis was possible to determine the structural modification PSF membrane with PEI and $CaCO_3$ nanoparticle. XRD graph was shown in Fig. 4.21 which was observed from 2θ range of 5˚ to 80˚ at 40 kV. Fig. 4.21 illustrates a PSF and PSF/PEI/10 wt% $CaCO_3$ nanocomposite membranes XRD patterns.

The PSF is known to be an amorphous polymer with rigid structure. The typical broad band of amorphous polymer with slight peak of crystalinity was found for PSF. The crystalinity of a PSF membrane peaks changed with the addition of $CaCO_3$ nanoparticles. Additional diffraction peaks of $CaCO_3$ were observed at 36° and 40° on the XRD patterns. According to these results and in agreement with Campos observations [248] , it seemed that adding of $CaCO_3$ lead to change of the crystalline the PSF polymer matrix [249].

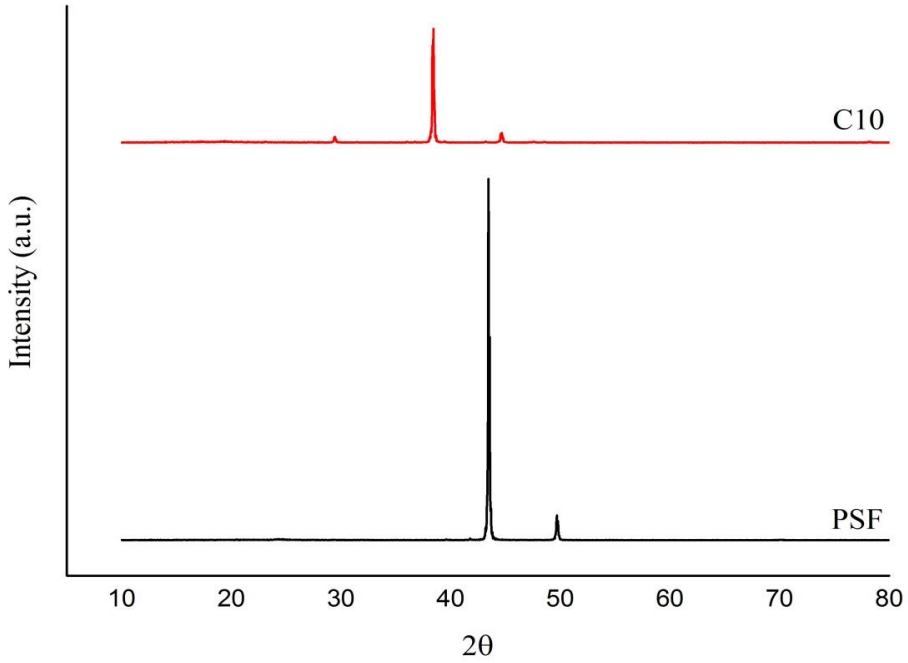

Figure 4.21.XRD graphs of PSF and PSF/PEI membrane containing 10 wt% $CaCO_3$ nanoparticle

4.4.9. Pure water flux

The water fluxes of the membranes were determined at 2 bar as shown in Fig. 4.22. The pure PSF membrane showed the lowest water flux of 3.3 L/m^2h, and the highest water flux was obtained for the membranes with 10 wt% $CaCO_3$ nanoparticles (C10) as 197 L/m^2h. This result could be explained by the improvement of the hydrophilicity of membranes by addition of $CaCO_3$ and (Table 4.7) and porosity compared to the pure PSF membranes [108, 229]. As shown in Fig. 4.22, however; the flux declines of C1, C2 and C5 nanocomposite membranes were similar, C10 nanocomposite membrane showed a fast decline.

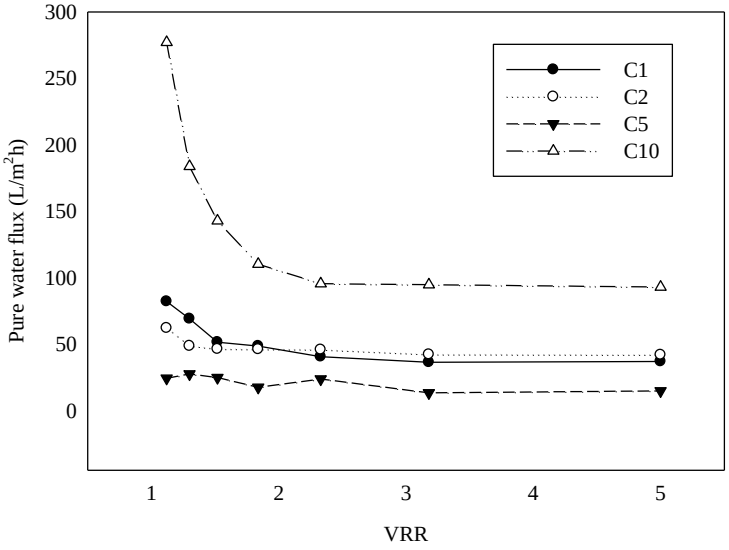

Figure 4.22.Pure water flux of PSF/PEI/$CaCO_3$ nanocomposite membranes

4.4.10. BSA rejection

The BSA flux, BSA rejection and thickness values of prepared PSF/PEI/$CaCO_3$ membranes were given Table 4.9. The BSA rejection values of the pure PSF and PSF/PEI membranes were 94% and 97% with 0.9 and 20.2 L/m^2h BSA flux, respectively. The PSF/PEI membrane had higher BSA rejection than pure PSF; it can be explained by because of PEI hydrophilic and BSA hydrophobic characteristics. All of the prepared $CaCO_3$ nanocomposite membranes rejected more than 90% of the BSA protein and as a result $CaCO_3$ membranes showed UF membrane characteristics.

Table 4.9.The BSA flux, BSA rejection and thickness of PSF (20 wt%), PSF/PEI (20/2 wt%) and PSF/PEI/$CaCO_3$ nanocomposite membranes.

Substrate	BSA flux (L/m^2h)	Rejection (%)	Thickness (µm)
PSF	0.9	94	80±5
PSF/PEI	20.2	97	79±4
C1	7.3	96	68±6
C2	18.1	98	75±3
C5	8.2	95	76±4
C10	78	92	78±5

Fig. 4.23 shows the variation of PSF/PEI/$CaCO_3$ nanocomposite membranes BSA flux values at an operating pressure of 2 bar. As shown in Fig. 4.23, C10 nanocomposite membrane showed a fast decline and then all nanocomposite membranes showed similar permeation rates.

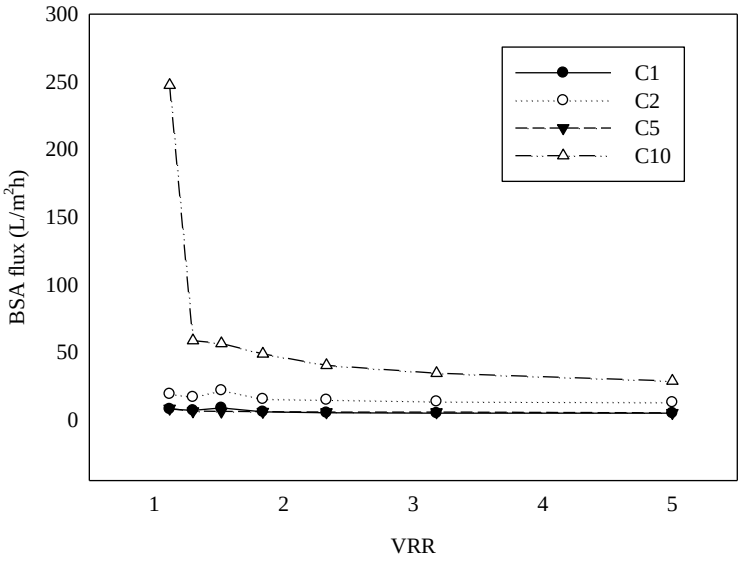

Figure 4.23.BSA flux of PSF/PEI/$CaCO_3$ nanocomposite membranes

4.5. Oil Rejection Experiments

To evaluate the oil rejection performance of Al_2O_3 and $CaCO_3$ nanocomposite membranes, synthetic vacuum oil solution (1000 ppm) and metal equipment production industry wastewaters were used. Oil seperation experiments were carried using dead-end filtration cell under 2 bar TMP with nitrogen gas as driving force, at 25±5 °C and at stirring speed of 300 rpm for all prepared membranes.

Industrial wastewater is obtained from a tank containing a mixture of oily solutions at a metal equipment producing industry in Kayseri with aproximately 500-700 $m^3$of wastewater production per day. The composition of the industrial wastewater is shown in Table 4.10.

Table 4.10.Wastewater characteristics

	Conductivity (mS/cm)	pH	COD (mg/L)
Raw wastewater	6.94	7.6	8167

4.5.1. Oil rejection performance of Al_2O_3 membranes

PSF/PEI/Al_2O_3 membranes have demonstrated that there is a great potential to use these nanocomposite membranes for oily water treatment with higher permeability, porosity and BSA rejection.

4.5.1.1. Oil rejection performance of Al_2O_3 membranes from synthetic wastewater

Vacuum oil solution (1000 ppm) was used to evaluate the separation performance of PSF/PEI/Al_2O_3 nanocomposite membranes. Fig. 4.24 illustrated synthetic oil rejection ratio of Al_2O_3 nanocomposite membranes. As shown, the highest rejection was obtained for 96% for the nanocomposite membranes including 5 wt% Al_2O_3 nanoparticles (80

nm). Synthetic oil rejections demonstrated that, acceptable separation performance was determined.

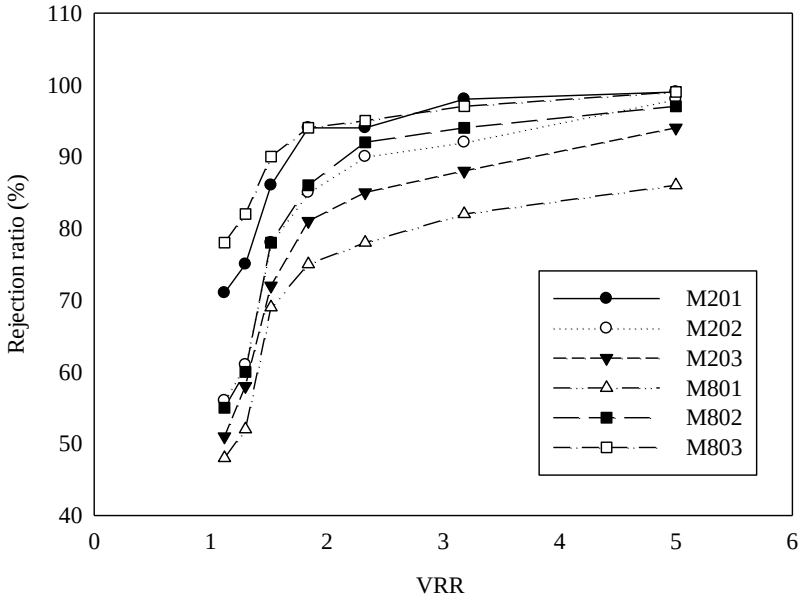

Figure 4.24.Oil rejection ratio of BSA flux of PSF/PEI/Al_2O_3 nanocomposite membranes

The pictures of synthetic oily feed solution and permate was shown in Fig. 4.25. Permeate is so clear after filtration and it seems that oil free and visible.

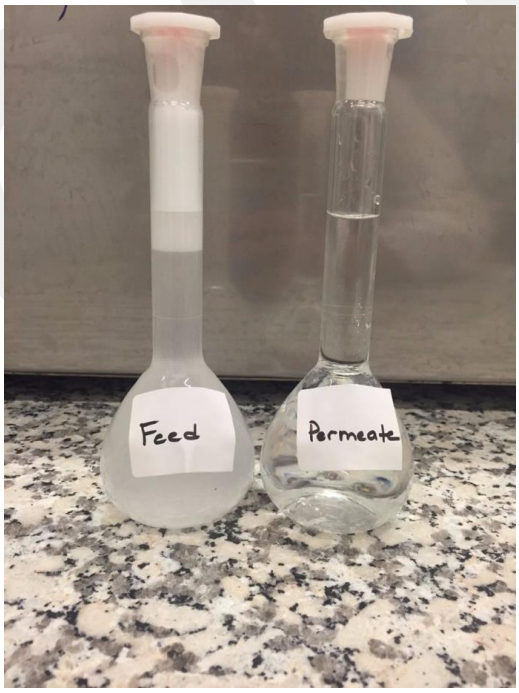

Figure 4.25.Synthetic vacuum oily feed solution and filtreted permeate

4.5.1.2. Oil rejection performance of Al_2O_3 membranes from industrial oily wastewater

The performance of PSF, PSF/PEI and PSF/PEI/Al_2O_3 membranes for the removal of oil from industrial wastewater were tested at 2 bar. The sample pictures of raw oily industrial wastewater and permeates with Al_2O_3 membranes were shown in Fig. 4.26. It is clearly observed that, 0.2 wt% and 1 wt% Al_2O_3 loading nanocomposite membranes were more effective than 5 wt% Al_2O_3 loading for industrial oil removal performance. On the other hand, including 80 nm Al_2O_3 nanoparticle membranes demonstrated just a contrary performance; 80 nm 5 wt% Al_2O_3 permeate was more clear. In terms of COD rejection from industrial oily wastewater, PSF/PEI membrane with 0.2 wt% Al_2O_3 reduces COD from 8167 to 6083 (mg/L).

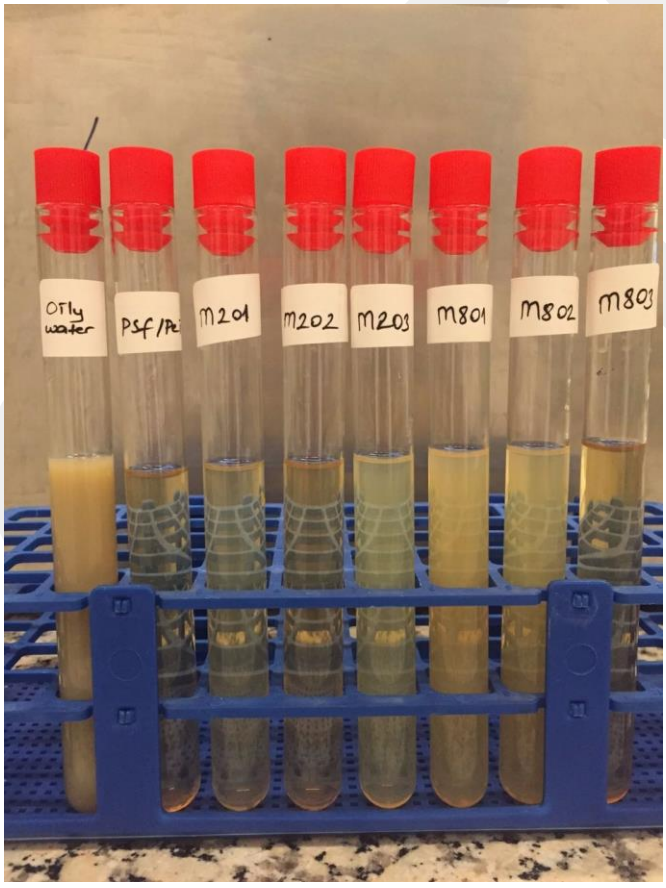

Figure 4.26.Industrial wastewater and filtreted water with Al_2O_3 nanocomposite membranes at 25 ± 5 °C, TMP: 2 bar

pH and conductivity values of permeate are represented in Table 4.11. However, no significant changes were not observed in pH and conductivity. Although for all Al_2O_3 nanocomposite membranes, permate pH were same, conductivities were decreased with increasing Al_2O_3 loading from industrial oily wastewater. It can be related with; real industrial oily wastewater may contain additives such as proteins, inhibitor, heavy metals and that can effect the solution conductivity.

Table 4.11.pH and conductivities of the pemeates in filtrations with PSF/PEI and PSF/PEI/Al_2O_3 membranes

Substrate	Cond.(mS/cm)	pH	COD (mg/L)
Raw wastewater	6.94	7.6	8167
PSF/PEI	6.7	7.5	6136
M201	6.7	7.6	6083
M202	6.8	7.5	6109
M203	6.8	7.6	N/A*
M801	6.6	7.6	N/A*
M802	7.4	7.6	N/A*
M803	6.7	7.5	7174

*N/A: Not acceptable

4.5.2. Oil rejection of $CaCO_3$ membranes

PSF/PEI/$CaCO_3$ membrane characterization results showed that it could be a good candidate for oily water treatment with higher permeability and antifouling capacity.

4.5.2.1. Oil rejection performance of $CaCO_3$ membranes from synthetic wastewater

Fig. 4.27 plots the oily water fluxes for the PSF/PEI/$CaCO_3$ membranes. For VRR <1.1, synthetic oil water fluxes decreased due to the accumulation on the membrane, which shows that water mass transfer limited. In the serial synthetic oily wastewater filtration operation, the deposition and re-suspension of oil reached equilibrium on the membrane surface, so that a stable flux was obtained. All nanocomposite membrane fluxes reached steady state in the permeation rate until VRR >2. The average synthetic oily wastewater fluxes were 65.5, 24.6, 52.5 and 146.1 L/m^2h at 2 bar for the membranes with 1, 2, 5 and 10 wt% $CaCO_3$ nanoparticles loading, respectively.

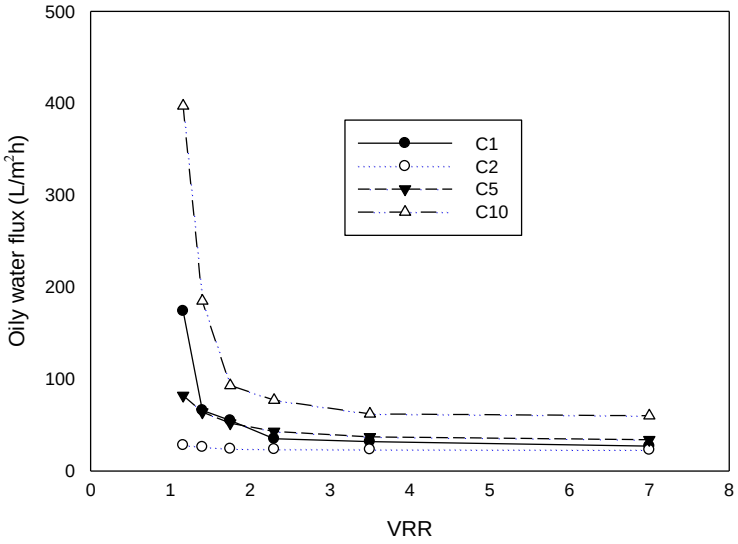

Figure 4.27.Oil rejection ratio of PSF, PSF/PEI and PSF/PEI/$CaCO_3$ membranes of synthetic O/W emulsion and ındustrial wastewater

Fig. 4.28 shows the pure water flux measurements before and after synthetic oily wastewater filtration and synthetic oily water fluxes of PSF, PSF/PEI and PSF/PEI/$CaCO_3$ membranes. The synthetic oily water flux decreased considerably in comparison with pure water flux. This flux decline widely resulted in membrane fouling. Oil droplets adsorption and deposition of the on membrane surface was builded up rapidly, and membrane fouling was caused by the directly. Membranes were claned for 20 min and carried pure water. After that, flux recovery property was calculate to express the antifouling resistance of the membranes [138].

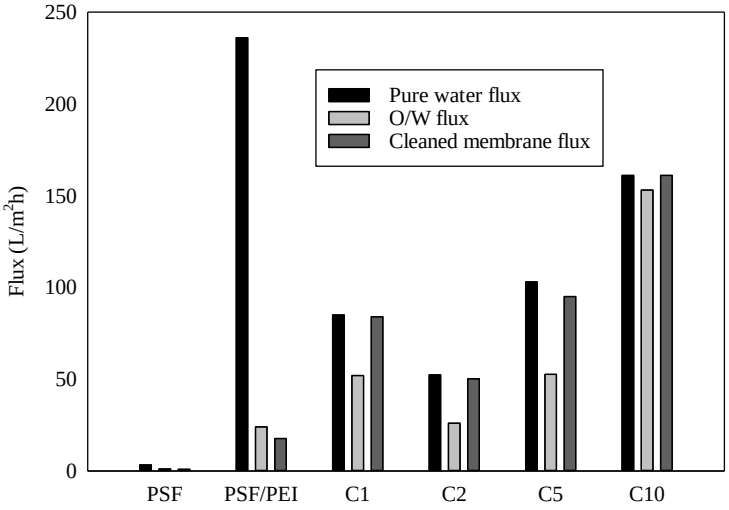

Figure 4.28.Flux changes of PSF, PSF/PEI and PSF/PEI/$CaCO_3$ membranes of pure water, synthetic oily water and cleaned membrane fluxes

The FRR is the determined of antifouling capacity of the membranes [250]. PSF, PSF/PEI and PSF/PEI/$CaCO_3$ membranes FRR, DR and synthetic oil rejection ratio were given in Table 4.12. All $CaCO_3$ nanocomposite membranes showed higher FRR values than pure PSF and PSF/PEI membrane. From Table 4.12, the maximum FRR of 100% was observed incorpareted with 1wt % and 10 wt% of $CaCO_3$ nanoparticles. The hydroxylation of $CaCO_3$ on membrane surface could result increasing hydrophilicity thereby weakening interactions between synthetic oil and membrane surface. 10 wt% of $CaCO_3$ nanoparticles membranes have notable antifouling capacity with the highest FRR and lowest DR values.

Table 4.12.Oil rejection ratio (%), FRR (%) and DR (%) values to PSF, PSF/PEI and PSF/PEI/$CaCO_3$ membranes of synthetic O/W emulsion filtration

	Oil rejection (%)	DR (%)	FRR (%)
PSF	88	65	81
PSF/PEI	99	90	73
C1	>99.9	38	100
C2	>99.9	50	96
C5	>99.9	48	92
C10	>99.9	17	100

4.5.2.2. Oil rejection performance of $CaCO_3$ membranes from industrial wastewaters

Oil separation performance of PSF, PSF/PEI and PSF/PEI/$CaCO_3$ membranes from the real oily industrial wastewater were tested and filtered with $CaCO_3$ nanocomposite membranes were shown in Fig. 4.29. It is clearly observed that, PSF/PEI, 1, 5 and 10 wt% $CaCO_3$ loading nanocomposite membranes were clearer than 2 wt% $CaCO_3$ loading after industrial oily wastewater filtration.

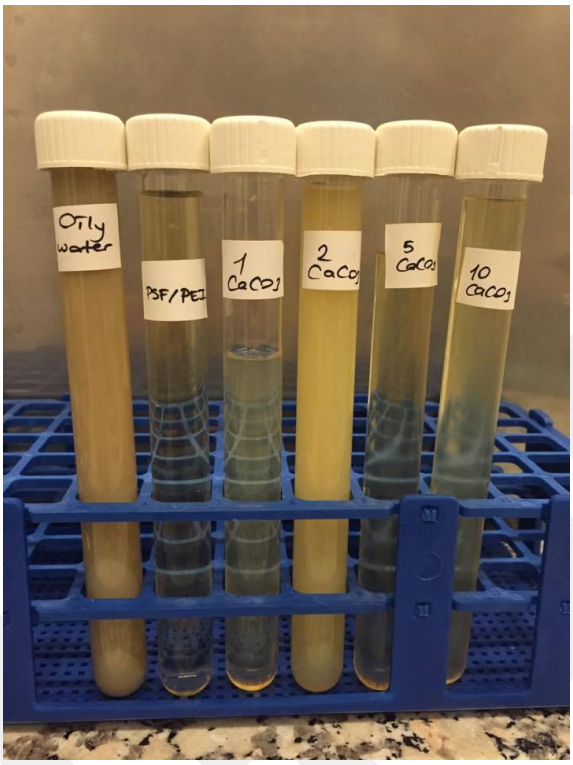

Figure 4.29. Industrial wastewater and filtered water with $CaCO_3$ nanocomposite membranes at 25 ± 5 °C, TMP: 2 bar

Top surface SEM images of PSF/PEI/$CaCO_3$ nanocomposite membranes were shown in Fig.4.30. Compare with clean $CaCO_3$ nanocomposite membranes surface SEM images and the top surface view membranes of after industrial oily wastewater filtration (Fig.4.30); it was clearly observed that membrane surface was fouled. Nanocomposite membrane surfaces were covered by a yellow-brown film after industrial oily wastewater filtration, which was composed of industrial wastewater. The fouled membrane was covered with compact and nonporous gel layer. Consequently, this layer

caused increasing TMP during industrial oily water filtration and membrane fouling [251].

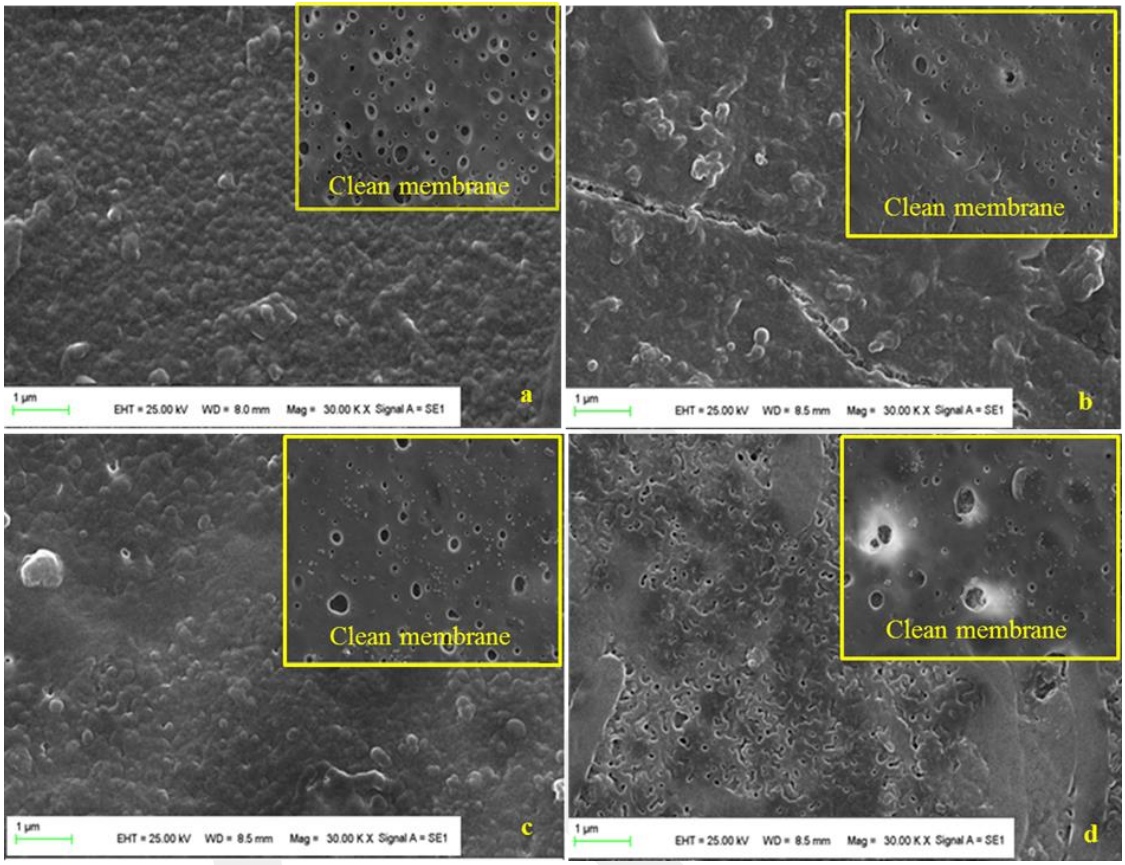

Figure 4.30. SEM images of the top surface view fouled membranes of after industrial oily water filtration; PSF/PEI membrane containing $CaCO_3$ nanoparticles: (a) 0.2 wt%, (b) 1 wt%, (c) 5 wt%, (d) 10 wt%

pH, conductivity and COD values of $CaCO_3$ membranes permeate are given in Table 4.13. However, pH was not effected significantly, conductivities decreased 50% when compared to the raw industrial oily wastewater. The decrease in conductivity can be explained by the tight UF structure of $CaCO_3$ membranes. The highest COD removal was observed for PSF/PEI permeate, and this result is by celar permeate pictures (Fig.4.29) and the lowest FRR value.

Table 4.13.pH and conductivities of the feed of industrial wastewater filtrations with PSF/PEI and PSF/PEI/$CaCO_3$ membranes

	Cond.(mS/cm)	pH	COD(mg/L)
Raw wastewater	6.94	7.6	8167
PSF/PEI	3.16	7.7	5864
C1	3.52	7.9	6004
C2	3.42	8.1	6526
C5	3.75	7.5	6162
C10	3.78	7.5	6203

GCRIS

Chapter 5

5. CONCLUSIONS

In this thesis, new generation of nanocomposite membranes with improved separation performance were developed for oily water treatment. Within thsi context, the flat-sheet PSF membranes fabricated with the corporation of PEI. Then, to improve the membrane performance, nanoparticles with two different sized of Al_2O_3 (20 and 80 nm) and one sized $CaCO_3$ (100 nm) were added into polymeric membrane matrix. Effects of hydrophilic Al_2O_3 and $CaCO_3$ nanoparticles on membrane structure and physicochemical properties were evaluated. The important results obtained for Al_2O_3 and $CaCO_3$ embedded nanocomposite membranes are summarized as;

For PSF/PEI/Al_2O_3 nanocomposite membranes;

- The hydrophilicity, porosity, viscosity, water flux and tensile strength of the PSF/PEI/Al_2O_3 nanocomposite membranes enhanced as the increase of Al_2O_3 content in membrane matrix.
- The smaller sized Al_2O_3 nanoparticles (20 nm) were showed better water flux, porosity, morphological stability and tensile strength because of the high surface area and the higher water adsorption capacity.
- PSF/PEI/Al_2O_3 membranes with 20 nm 5 wt% Al_2O_3 nanoparticles showed excellent water flux of 1336.6 L/m^2h at 0.4 MPa with a contact angle of 56°, porosity of 79% and tensile strength of 4.1 MPa.
- PSF/PEI/Al_2O_3 nanocomposite membranes showed the higher BSA rejection of over 95%.

For PSF/PEI/$CaCO_3$ nanocomposite membranes

- The hydrophilicity, porosity, viscosity, water flux and tensile strength of the nanocomposite membranes improved as the addition of $CaCO_3$ nanoparticle.
- 10 wt% $CaCO_3$ nanoparticles loading exhibited the highest water flux of 197 L/m^2h at 2 bar with a contact angle of 84°, porosity of 70% with 92% BSA rejection.

For the oil removal performance of PSF/PEI/$CaCO_3$ and PSF/PEI/Al_2O_3 nanocomposite membranes;

- All Al_2O_3 and $CaCO_3$ nanocomposite membranes reached similar oil rejection for synthetic wastewater over 90%.
- In spite of it would be early to decide certain effect of nanocomposite membranes in industrial wastewater treatment technology, laboratory-scale experiments will be critical in determining the future position of polymeric membranes incopareted nanomaterials.
- In industrial oily wastewater treatment, the maximum COD reduction was 6083 mg/L for PSF/PEI membrane with 0.2 wt% Al_2O_3 and 6004 mg/L for PSF/PEI membrane with 1 wt% of $CaCO_3$.
- 10 wt% of $CaCO_3$ nanoparticles membranes have notable antifouling capacity with the highest FRR and lowest DR values.

These results have demonstrated that there is a great potential to use these nanocomposite membranes to use oily water treatment with higher permeability and antifouling capacity.

In conclusion, nanocomposite membranes were promising to mitigate or even overcome the intrinsic challenges of current commercial polymeric membranes. The incorporation of nanoparticles with conventional membrane polymers could not only modificate structure and physicochemical properties in terms of hydrophilicity, porosity, thermal, and mechanical stability of membranes, but also introduce unique functionalities into the membranes.

In future work, environmental friendly polymeric membrane fabrication methods and hybrid systems could be used for water and wastewater treatments. It is very important to develop a cost-effective method for scale up in terms of nanomaterial preparation and membrane fabrication, and long-term stability under practical application conditions.

And also thin film nanocomposite membrane will fabricated for desalination and enrgy production processes. Those studies should be implemented on a case by case basis fully considering the environment and the attributes of the system.

GCRIS

BIBLIOGRAPHY

[1] M.B. Ghandashtani, F. Zokaee Ashtiani, M. Karimi, A. Fouladitajar, A novel approach to fabricate high performance nano-SiO2 embedded PES membranes for microfiltration of oil-in-water emulsion, Applied Surface Science, 349 (2015) 393-402.
[2] H. Lotfiyan, F. Zokaee Ashtiani, A. Fouladitajar, S.B. Armand, Computational fluid dynamics modeling and experimental studies of oil-in-water emulsion microfiltration in a flat sheet membrane using Eulerian approach, Journal of Membrane Science, 472 (2014) 1-9.
[3] J. Mueller, Y. Cen, R.H. Davis, Crossflow microfiltration of oily water, Journal of Membrane Science, 129 (1997) 221-235.
[4] P. Kajitvichyanukul, Y.-T. Hung, L.K. Wang, Membrane Technologies for Oil–Water Separation, in: L.K. Wang, J.P. Chen, Y.-T. Hung, N.K. Shammas (Eds.) Membrane and Desalination Technologies, Humana Press, Totowa, NJ, 2011, pp. 639-668.
[5] R.J. Gohari, F. Korminouri, W. Lau, A. Ismail, T. Matsuura, M. Chowdhury, E. Halakoo, M.J. Gohari, A novel super-hydrophilic PSf/HAO nanocomposite ultrafiltration membrane for efficient separation of oil/water emulsion, Separation and Purification Technology, 150 (2015) 13-20.
[6] L. Yan, S. Hong, M.L. Li, Y.S. Li, Application of the Al 2 O 3–PVDF nanocomposite tubular ultrafiltration (UF) membrane for oily wastewater treatment and its antifouling research, Separation and Purification Technology, 66 (2009) 347-352.
[7] D. Lu, T. Zhang, L. Gutierrez, J. Ma, J.-P. Croué, Influence of Surface Properties of Filtration-Layer Metal Oxide on Ceramic Membrane Fouling during Ultrafiltration of Oil/Water Emulsion, Environmental Science & Technology, 50 (2016) 4668-4674.
[8] M.-J. Um, S.-H. Yoon, C.-H. Lee, K.-Y. Chung, J.-J. Kim, Flux enhancement with gas injection in crossflow ultrafiltration of oily wastewater, Water Research, 35 (2001) 4095-4101.
[9] H. Way, B. Forum, D. DT11, The treatment of oily water by coalescing, Filtration & Separation, 29 (1992) 295300-295298.
[10] L. Feng, Z. Zhang, Z. Mai, Y. Ma, B. Liu, L. Jiang, D. Zhu, A Super-Hydrophobic and Super-Oleophilic Coating Mesh Film for the Separation of Oil and Water, Angewandte Chemie, 116 (2004) 2046-2048.
[11] P. Cañizares, F. Martínez, C. Jiménez, C. Sáez, M.A. Rodrigo, Coagulation and electrocoagulation of oil-in-water emulsions, Journal of Hazardous Materials, 151 (2008) 44-51.
[12] Y. Yang, H. Wang, J. Li, B. He, T. Wang, S. Liao, Novel Functionalized Nano-TiO2 Loading Electrocatalytic Membrane for Oily Wastewater Treatment, Environmental Science & Technology, 46 (2012) 6815-6821.
[13] P. Srijaroonrat, E. Julien, Y. Aurelle, Unstable secondary oil/water emulsion treatment using ultrafiltration: fouling control by backflushing, Journal of Membrane Science, 159 (1999) 11-20.
[14] B. Chakrabarty, A. Ghoshal, M. Purkait, Cross-flow ultrafiltration of stable oil-in-water emulsion using polysulfone membranes, Chemical Engineering Journal, 165 (2010) 447-456.
[15] M. Belkacem, M. Bahlouli, A. Mraoui, K. Bensadok, Treatment of oil-water emulsion by ultrafiltration: A numerical approach, Desalination, 206 (2007) 433-439.

[16] X.S. Yi, S.L. Yu, W.X. Shi, N. Sun, L.M. Jin, S. Wang, B. Zhang, C. Ma, L.P. Sun, The influence of important factors on ultrafiltration of oil/water emulsion using PVDF membrane modified by nano-sized TiO2/Al2O3, Desalination, 281 (2011) 179-184.
[17] B. Chakrabarty, A.K. Ghoshal, M.K. Purkait, Ultrafiltration of stable oil-in-water emulsion by polysulfone membrane, Journal of Membrane Science, 325 (2008) 427-437.
[18] X.S. Yi, W.X. Shi, S.L.Yu, C. Ma, N. Sun, S. Wang, L.M. Jin, L.P. Sun, Optimization of complex conditions by response surface methodology for APAM–oil/water emulsion removal from aqua solutions using nano-sized TiO2/Al2O3 PVDF ultrafiltration membrane, Journal of Hazardous Materials, 193 (2011) 37-44.
[19] R. Jamshidi Gohari, E. Halakoo, W.J. Lau, M.A. Kassim, T. Matsuura, A.F. Ismail, Novel polyethersulfone (PES)/hydrous manganese dioxide (HMO) mixed matrix membranes with improved anti-fouling properties for oily wastewater treatment process, RSC Advances, 4 (2014) 17587-17596.
[20] Y. Zhang, P. Cui, T. Du, L. Shan, Y. Wang, Development of a sulfated Y-doped nonstoichiometric zirconia/polysulfone composite membrane for treatment of wastewater containing oil, Separation and Purification Technology, 70 (2009) 153-159.
[21] S. Kasemset, Z. He, D.J. Miller, B.D. Freeman, M.M. Sharma, Effect of polydopamine deposition conditions on polysulfone ultrafiltration membrane properties and threshold flux during oil/water emulsion filtration, Polymer, 97 (2016) 247-257.
[22] R. Jamshidi Gohari, E. Halakoo, N.A.M. Nazri, W.J. Lau, T. Matsuura, A.F. Ismail, Improving performance and antifouling capability of PES UF membranes via blending with highly hydrophilic hydrous manganese dioxide nanoparticles, Desalination, 335 (2014) 87-95.
[23] G. Busca, N. Hilal, B.P. Atkin, Optimisation of washing cycle on ultrafiltration membranes used in treatment of metalworking fluids, Desalination, 156 (2003) 199-207.
[24] N. Maximous, G. Nakhla, W. Wan, K. Wong, Preparation, characterization and performance of Al2O3/PES membrane for wastewater filtration, Journal of Membrane Science, 341 (2009) 67-75.
[25] M.Z. Yunos, Z. Harun, H. Basri, A.F. Ismail, Studies on fouling by natural organic matter (NOM) on polysulfone membranes: Effect of polyethylene glycol (PEG), Desalination, 333 (2014) 36-44.
[26] X.-y. Li, H.P. Chu, Membrane bioreactor for the drinking water treatment of polluted surface water supplies, Water Res., 37 (2003) 4781-4791.
[27] A. Fenu, G. Guglielmi, J. Jimenez, M. Spèrandio, D. Saroj, B. Lesjean, C. Brepols, C. Thoeye, I. Nopens, Activated sludge model (ASM) based modelling of membrane bioreactor (MBR) processes: A critical review with special regard to MBR specificities, Water Res., 44 (2010) 4272-4294.
[28] R. van Reis, A. Zydney, Bioprocess membrane technology, Journal of Membrane Science, 297 (2007) 16-50.
[29] R. Kumar, A.M. Isloor, A.F. Ismail, S.A. Rashid, A.A. Ahmed, Permeation, antifouling and desalination performance of TiO2 nanotube incorporated PSf/CS blend membranes, Desalination, 316 (2013) 76-84.
[30] J.S. Louie, I. Pinnau, I. Ciobanu, K.P. Ishida, A. Ng, M. Reinhard, Effects of polyether–polyamide block copolymer coating on performance and fouling of reverse osmosis membranes, Journal of Membrane Science, 280 (2006) 762-770.
[31] P. Le-Clech, V. Chen, T.A.G. Fane, Fouling in membrane bioreactors used in wastewater treatment, Journal of Membrane Science, 284 (2006) 17-53.

[32] D. Rana, T. Matsuura, Surface Modifications for Antifouling Membranes, Chemical Reviews, 110 (2010) 2448-2471.
[33] L. Zhu, M. Chen, Y. Dong, C.Y. Tang, A. Huang, L. Li, A low-cost mullite-titania composite ceramic hollow fiber microfiltration membrane for highly efficient separation of oil-in-water emulsion, Water Research, 90 (2016) 277-285.
[34] N.A. Ochoa, M. Masuelli, J. Marchese, Effect of hydrophilicity on fouling of an emulsified oil wastewater with PVDF/PMMA membranes, Journal of Membrane Science, 226 (2003) 203-211.
[35] W. Chen, Y. Su, L. Zheng, L. Wang, Z. Jiang, The improved oil/water separation performance of cellulose acetate-graft-polyacrylonitrile membranes, Journal of Membrane Science, 337 (2009) 98-105.
[36] C. Wu, A. Li, L. Li, L. Zhang, H. Wang, X. Qi, Q. Zhang, Treatment of oily water by a poly(vinyl alcohol) ultrafiltration membrane, Desalination, 225 (2008) 312-321.
[37] L.-Q. Shen, Z.-K. Xu, Z.-M. Liu, Y.-Y. Xu, Ultrafiltration hollow fiber membranes of sulfonated polyetherimide/polyetherimide blends: preparation, morphologies and anti-fouling properties, Journal of Membrane Science, 218 (2003) 279-293.
[38] S.P. Nunes, M.L. Sforça, K.-V. Peinemann, Dense hydrophilic composite membranes for ultrafiltration, Journal of Membrane Science, 106 (1995) 49-56.
[39] R. Jamshidi Gohari, W.J. Lau, T. Matsuura, A.F. Ismail, Effect of surface pattern formation on membrane fouling and its control in phase inversion process, Journal of Membrane Science, 446 (2013) 326-331.
[40] D. Lu, W. Cheng, T. Zhang, X. Lu, Q. Liu, J. Jiang, J. Ma, Hydrophilic Fe 2 O 3 dynamic membrane mitigating fouling of support ceramic membrane in ultrafiltration of oil/water emulsion, Separation and Purification Technology, 165 (2016) 1-9.
[41] E. Yuliwati, A.F. Ismail, Effect of additives concentration on the surface properties and performance of PVDF ultrafiltration membranes for refinery produced wastewater treatment, Desalination, 273 (2011) 226-234.
[42] K.A. DeFriend, M.R. Wiesner, A.R. Barron, Alumina and aluminate ultrafiltration membranes derived from alumina nanoparticles, Journal of Membrane Science, 224 (2003) 11-28.
[43] S.-H. Zhi, R. Deng, J. Xu, L.-S. Wan, Z.-K. Xu, Composite membranes from polyacrylonitrile with poly(N,N-dimethylaminoethyl methacrylate)-grafted silica nanoparticles as additives, Reactive and Functional Polymers, 86 (2015) 184-190.
[44] J.-e. Zhou, Q. Chang, Y. Wang, J. Wang, G. Meng, Separation of stable oil–water emulsion by the hydrophilic nano-sized ZrO 2 modified Al 2 O 3 microfiltration membrane, Separation and Purification Technology, 75 (2010) 243-248.
[45] C.R. Kellenberger, F.C. Pfleiderer, R.A. Raso, C.H. Burri, C.M. Schumacher, R.N. Grass, W.J. Stark, Limestone nanoparticles as nanopore templates in polymer membranes: narrow pore size distribution and use as self-wetting dialysis membranes, RSC Advances, 4 (2014) 61420-61426.
[46] D. Wu, Y. Huang, S. Yu, D. Lawless, X. Feng, Thin film composite nanofiltration membranes assembled layer-by-layer via interfacial polymerization from polyethylenimine and trimesoyl chloride, Journal of Membrane Science, 472 (2014) 141-153.
[47] S.-J. Park, R.K. Cheedrala, M.S. Diallo, C. Kim, I.S. Kim, W.A. Goddard, Nanofiltration membranes based on polyvinylidene fluoride nanofibrous scaffolds and crosslinked polyethyleneimine networks, J. Nanopart. Res., 14 (2012) 884.
[48] C. Ba, J. Langer, J. Economy, Chemical modification of P84 copolyimide membranes by polyethylenimine for nanofiltration, Journal of Membrane Science, 327 (2009) 49-58.

[49] G. Zhang, S. Lu, L. Zhang, Q. Meng, C. Shen, J. Zhang, Novel polysulfone hybrid ultrafiltration membrane prepared with TiO2-g-HEMA and its antifouling characteristics, J. Membr. Sci., 436 (2013) 163-173.
[50] M. Sianipar, S.H. Kim, C. Min, L.D. Tijing, H.K. Shon, Potential and performance of a polydopamine-coated multiwalled carbon nanotube/polysulfone nanocomposite membrane for ultrafiltration application, J. Ind. Eng. Chem., 34 (2016) 364-373.
[51] M.K. Sinha, M.K. Purkait, Increase in hydrophilicity of polysulfone membrane using polyethylene glycol methyl ether, J. Membr. Sci., 437 (2013) 7-16.
[52] A. Sotto, A. Boromand, R. Zhang, P. Luis, J.M. Arsuaga, J. Kim, B. Van der Bruggen, Effect of nanoparticle aggregation at low concentrations of TiO2 on the hydrophilicity, morphology, and fouling resistance of PES–TiO2 membranes, Journal of Colloid and Interface Science, 363 (2011) 540-550.
[53] T.A. Saleh, V.K. Gupta, Synthesis and characterization of alumina nano-particles polyamide membrane with enhanced flux rejection performance, Separation and Purification Technology, 89 (2012) 245-251.
[54] Effects of Inorganic Nano-Additives on Properties and Performance of Polymeric Membranes in Water Treatment, Separ. Purif. Rev., 45 (2016) 141-167.
[55] M.C. Porter, Handbook of industrial membrane technology, (1989).
[56] M.T. Ravanchi, T. Kaghazchi, A. Kargari, Application of membrane separation processes in petrochemical industry: a review, Desalination, 235 (2009) 199-244.
[57] R.W. Baker, Membrane technology, Wiley Online Library, 2000.
[58] J. Mulder, Basic principles of membrane technology, Springer Science & Business Media, 2012.
[59] R. Rautenbach, R. Albrecht, Membrane separation processes, (1989).
[60] C.J. Geankoplis, Transport processes and separation process principles:(includes unit operations), Prentice Hall Professional Technical Reference, 2003.
[61] M. Hlavacek, F. Bouchet, Constant flowrate blocking laws and an example of their application to dead-end microfiltration of protein solutions, Journal of Membrane Science, 82 (1993) 285-295.
[62] T. Moritz, S. Benfer, P. Arki, G. Tomandl, Influence of the surface charge on the permeate flux in the dead-end filtration with ceramic membranes, Separation and Purification Technology, 25 (2001) 501-508.
[63] B. Tansel, J. Sager, T. Rector, J. Garland, R.F. Strayer, L. Levine, M. Roberts, M. Hummerick, J. Bauer, Significance of hydrated radius and hydration shells on ionic permeability during nanofiltration in dead end and cross flow modes, Separation and Purification Technology, 51 (2006) 40-47.
[64] L. Song, Flux decline in crossflow microfiltration and ultrafiltration: mechanisms and modeling of membrane fouling, Journal of membrane science, 139 (1998) 183-200.
[65] H. Kyllönen, P. Pirkonen, M. Nyström, J. Nuortila-Jokinen, A. Grönroos, Experimental aspects of ultrasonically enhanced cross-flow membrane filtration of industrial wastewater, Ultrasonics sonochemistry, 13 (2006) 295-302.
[66] S. Loeb, S. Sourirajan, Sea Water Demineralization by Means of an Osmotic Membrane, in: Saline Water Conversion—II, AMERICAN CHEMICAL SOCIETY, 1963, pp. 117-132.
[67] Y. Pouliot, Membrane processes in dairy technology—From a simple idea to worldwide panacea, International Dairy Journal, 18 (2008) 735-740.
[68] R.W. Baker, Membrane Technology and Applications, Third Edition ed., 2012.
[69] E. Saljoughi, M. Amirilargani, T. Mohammadi, Effect of PEG additive and coagulation bath temperature on the morphology, permeability and thermal/chemical stability of asymmetric CA membranes, Desalination, 262 (2010) 72-78.

[70] R. Singh, Hybrid Membrane Systems for Water Purification, Elsevier, 2006.
[71] M. Murder, Kluwer Academic Publishers, 1997.
[72] H. Strathmann, L. Giorno, E. Drioli, Introduction to membrane science and technology, Wiley-VCH Weinheim, 2011.
[73] S. Nakao, H. Osada, H. Kurata, T. Tsuru, S. Kimura, Separation of proteins by charged ultrafiltration membranes, Desalination, 70 (1988) 191-205.
[74] A.-S. Jönsson, G. Trägårdh, Ultrafiltration applications, Desalination, 77 (1990) 135-179.
[75] W. Gao, H. Liang, J. Ma, M. Han, Z.-l. Chen, Z.-s. Han, G.-b. Li, Membrane fouling control in ultrafiltration technology for drinking water production: A review, Desalination, 272 (2011) 1-8.
[76] M. Rumeau, F. Persin, V. Sciers, M. Persin, J. Sarrazin, Separation by coupling ultrafiltration and complexation of metallic species with industrial water soluble polymers. Application for removal or concentration of metallic cations, Journal of membrane science, 73 (1992) 313-322.
[77] A.G. Vishtal, A. Kraslawski, Challenges in industrial applications of technical lignins, BioResources, 6 (2011) 3547-3568.
[78] J.M. Laîné, D. Vial, P. Moulart, Status after 10 years of operation — overview of UF technology today, Desalination, 131 (2000) 17-25.
[79] L. Fiksdal, T. Leiknes, The effect of coagulation with MF/UF membrane filtration for the removal of virus in drinking water, Journal of Membrane Science, 279 (2006) 364-371.
[80] J. Cadotte, R. Forester, M. Kim, R. Petersen, T. Stocker, Nanofiltration membranes broaden the use of membrane separation technology, Desalination, 70 (1988) 77-88.
[81] E.M. Vrijenhoek, S. Hong, M. Elimelech, Influence of membrane surface properties on initial rate of colloidal fouling of reverse osmosis and nanofiltration membranes, Journal of membrane science, 188 (2001) 115-128.
[82] B. Van der Bruggen, C. Vandecasteele, Removal of pollutants from surface water and groundwater by nanofiltration: overview of possible applications in the drinking water industry, Environmental pollution, 122 (2003) 435-445.
[83] S. Alami-Younssi, A. Larbot, M. Persin, J. Sarrazin, L. Cot, Rejection of mineral salts on a gamma alumina nanofiltration membrane Application to environmental process, Journal of Membrane Science, 102 (1995) 123-129.
[84] K.P. Lee, T.C. Arnot, D. Mattia, A review of reverse osmosis membrane materials for desalination—Development to date and future potential, Journal of Membrane Science, 370 (2011) 1-22.
[85] R. Sheikholeslami, Strategies for future research and development in desalination – Challenges ahead, Desalination, 248 (2009) 218-224.
[86] A. Zhu, P.D. Christofides, Y. Cohen, On RO membrane and energy costs and associated incentives for future enhancements of membrane permeability, Journal of Membrane Science, 344 (2009) 1-5.
[87] D. Hofmann, L. Fritz, J. Ulbrich, C. Schepers, M. Böhning, Detailed-atomistic molecular modeling of small molecule diffusion and solution processes in polymeric membrane materials, Macromolecular theory and simulations, 9 (2000) 293-327.
[88] W.J. Koros, G.K. Fleming, S.M. Jordan, T.H. Kim, H.H. Hoehn, Polymeric membrane materials for solution-diffusion based permeation separations, Progress in Polymer Science, 13 (1988) 339-401.
[89] P. Shao, R.Y.M. Huang, Polymeric membrane pervaporation, Journal of Membrane Science, 287 (2007) 162-179.

[90] E. Fernández, J.M. Benito, C. Pazos, J. Coca, Ceramic membrane ultrafiltration of anionic and nonionic surfactant solutions, Journal of Membrane Science, 246 (2005) 1-6.
[91] J. Randon, P. Blanc, R. Paterson, Modification of ceramic membrane surfaces using phosphoric acid and alkyl phosphonic acids and its effects on ultrafiltration of BSA protein, Journal of Membrane Science, 98 (1995) 119-129.
[92] S. Uemiya, State-of-the-art of supported metal membranes for gas separation, Separation and purification Methods, 28 (1999) 51-85.
[93] D.J. Edlund, J. McCarthy, The relationship between intermetallic diffusion and flux decline in composite-metal membranes: implications for achieving long membrane lifetime, Journal of Membrane Science, 107 (1995) 147-153.
[94] S. Uemiya, Brief Review of Steam Reforming Using a Metal Membrane Reactor, Topics in Catalysis, 29 (2004) 79-84.
[95] J.W. Phair, R. Donelson, Developments and Design of Novel (Non-Palladium-Based) Metal Membranes for Hydrogen Separation, Industrial & Engineering Chemistry Research, 45 (2006) 5657-5674.
[96] X. Chai, T. Kobayashi, N. Fujii, Ultrasound-associated cleaning of polymeric membranes for water treatment, Separation and Purification Technology, 15 (1999) 139-146.
[97] G.-d. Kang, Y.-m. Cao, Development of antifouling reverse osmosis membranes for water treatment: A review, Water Research, 46 (2012) 584-600.
[98] H. Huang, K. Schwab, J.G. Jacangelo, Pretreatment for Low Pressure Membranes in Water Treatment: A Review, Environmental Science & Technology, 43 (2009) 3011-3019.
[99] M.-J. Han, S.-T. Nam, Thermodynamic and rheological variation in polysulfone solution by PVP and its effect in the preparation of phase inversion membrane, Journal of Membrane Science, 202 (2002) 55-61.
[100] H. Lohokare, Y. Bhole, S. Taralkar, U. Kharul, Poly (acrylonitrile) based ultrafiltration membranes: Optimization of preparation parameters, Desalination, 282 (2011) 46-53.
[101] G. Arthanareeswaran, P. Thanikaivelan, K. Srinivasn, D. Mohan, M. Rajendran, Synthesis, characterization and thermal studies on cellulose acetate membranes with additive, European polymer journal, 40 (2004) 2153-2159.
[102] L. Phelane, F.N. Muya, H.L. Richards, P.G.L. Baker, E.I. Iwuoha, Polysulfone Nanocomposite Membranes with improved hydrophilicity, Electrochimica Acta, 128 (2014) 326-335.
[103] M.R. Esfahani, H.A. Stretz, M.J. Wells, Comparing humic acid and protein fouling on polysulfone ultrafiltration membranes: Adsorption and reversibility, Journal of Water Process Engineering, 6 (2015) 83-92.
[104] V.T. Magalad, G.S. Gokavi, C. Ranganathaiah, M.H. Burshe, C. Han, D.D. Dionysiou, M.N. Nadagouda, T.M. Aminabhavi, Polymeric blend nanocomposite membranes for ethanol dehydration—effect of morphology and membrane–solvent interactions, Journal of Membrane Science, 430 (2013) 321-329.
[105] V. Vatanpour, S.S. Madaeni, A.R. Khataee, E. Salehi, S. Zinadini, H.A. Monfared, TiO2 embedded mixed matrix PES nanocomposite membranes: Influence of different sizes and types of nanoparticles on antifouling and performance, Desalination, 292 (2012) 19-29.
[106] H. Cong, M. Radosz, B.F. Towler, Y. Shen, Polymer–inorganic nanocomposite membranes for gas separation, Separation and Purification Technology, 55 (2007) 281-291.

[107] A.K. Mishra, S. Bose, T. Kuila, N.H. Kim, J.H. Lee, Silicate-based polymer-nanocomposite membranes for polymer electrolyte membrane fuel cells, Progress in Polymer Science, 37 (2012) 842-869.
[108] E.-S. Kim, G. Hwang, M. Gamal El-Din, Y. Liu, Development of nanosilver and multi-walled carbon nanotubes thin-film nanocomposite membrane for enhanced water treatment, Journal of Membrane Science, 394 (2012) 37-48.
[109] K. Ebert, D. Fritsch, J. Koll, C. Tjahjawiguna, Influence of inorganic fillers on the compaction behaviour of porous polymer based membranes, Journal of Membrane Science, 233 (2004) 71-78.
[110] J.M. Arsuaga, A. Sotto, G. del Rosario, A. Martínez, S. Molina, S.B. Teli, J. de Abajo, Influence of the type, size, and distribution of metal oxide particles on the properties of nanocomposite ultrafiltration membranes, Journal of membrane science, 428 (2013) 131-141.
[111] X. Cao, J. Ma, X. Shi, Z. Ren, Effect of TiO 2 nanoparticle size on the performance of PVDF membrane, Applied Surface Science, 253 (2006) 2003-2010.
[112] S. Madaeni, S. Zinadini, V. Vatanpour, A new approach to improve antifouling property of PVDF membrane using in situ polymerization of PAA functionalized TiO 2 nanoparticles, Journal of membrane science, 380 (2011) 155-162.
[113] B.-H. Jeong, E.M. Hoek, Y. Yan, A. Subramani, X. Huang, G. Hurwitz, A.K. Ghosh, A. Jawor, Interfacial polymerization of thin film nanocomposites: a new concept for reverse osmosis membranes, Journal of Membrane Science, 294 (2007) 1-7.
[114] D. Rana, Y. Kim, T. Matsuura, H.A. Arafat, Development of antifouling thin-film-composite membranes for seawater desalination, Journal of Membrane Science, 367 (2011) 110-118.
[115] E.-S. Kim, G. Hwang, M.G. El-Din, Y. Liu, Development of nanosilver and multi-walled carbon nanotubes thin-film nanocomposite membrane for enhanced water treatment, Journal of Membrane Science, 394 (2012) 37-48.
[116] W.J. Lau, A.F. Ismail, N. Misdan, M.A. Kassim, A recent progress in thin film composite membrane: A review, Desalination, 287 (2012) 190-199.
[117] C. Bellona, J.E. Drewes, P. Xu, G. Amy, Factors affecting the rejection of organic solutes during NF/RO treatment—a literature review, Water research, 38 (2004) 2795-2809.
[118] I.J. Roh, A.R. Greenberg, V.P. Khare, Synthesis and characterization of interfacially polymerized polyamide thin films, Desalination, 191 (2006) 279-290.
[119] A.K. Ghosh, B.-H. Jeong, X. Huang, E.M.V. Hoek, Impacts of reaction and curing conditions on polyamide composite reverse osmosis membrane properties, Journal of Membrane Science, 311 (2008) 34-45.
[120] J. Glater, S.-k. Hong, M. Elimelech, The search for a chlorine-resistant reverse osmosis membrane, Desalination, 95 (1994) 325-345.
[121] Y.-N. Kwon, S. Hong, H. Choi, T. Tak, Surface modification of a polyamide reverse osmosis membrane for chlorine resistance improvement, Journal of membrane science, 415 (2012) 192-198.
[122] S. Low, C. Liping, L.S. Hee, Water softening using a generic low cost nano-filtration membrane, Desalination, 221 (2008) 168-173.
[123] S. Kim, L. Chen, J.K. Johnson, E. Marand, Polysulfone and functionalized carbon nanotube mixed matrix membranes for gas separation: Theory and experiment, Journal of Membrane Science, 294 (2007) 147-158.
[124] M.A. Aroon, A.F. Ismail, T. Matsuura, M.M. Montazer-Rahmati, Performance studies of mixed matrix membranes for gas separation: A review, Separation and Purification Technology, 75 (2010) 229-242.

[125] A.C. Balazs, T. Emrick, T.P. Russell, Nanoparticle polymer composites: where two small worlds meet, Science, 314 (2006) 1107-1110.
[126] X.-F. Sun, J. Qin, P.-F. Xia, B.-B. Guo, C.-M. Yang, C. Song, S.-G. Wang, Graphene oxide–silver nanoparticle membrane for biofouling control and water purification, Chemical Engineering Journal, 281 (2015) 53-59.
[127] Effect of metal and metal oxide nanoparticle impregnation route on structure and liquid filtration performance of polymeric nanocomposite membranes: a comprehensive review, Desalin. Water. Treat., 51 (2013) 3295-3316.
[128] A. Rahimpour, M. Jahanshahi, S. Khalili, A. Mollahosseini, A. Zirepour, B. Rajaeian, Novel functionalized carbon nanotubes for improving the surface properties and performance of polyethersulfone (PES) membrane, Desalination, 286 (2012) 99-107.
[129] X. Cao, J. Ma, X. Shi, Z. Ren, Effect of TiO2 nanoparticle size on the performance of PVDF membrane, Appl. Surf. Sci., 253 (2006) 2003-2010.
[130] J. Vanneste, A. Sotto, C.M. Courtin, V. Van Craeyveld, K. Bernaerts, J. Van Impe, J. Vandeur, S. Taes, B. Van der Bruggen, Application of tailor-made membranes in a multi-stage process for the purification of sweeteners from Stevia rebaudiana, J. Food. Eng., 103 (2011) 285-293.
[131] A. Rahimpour, M. Jahanshahi, B. Rajaeian, M. Rahimnejad, TiO2 entrapped nano-composite PVDF/SPES membranes: Preparation, characterization, antifouling and antibacterial properties, Desalination, 278 (2011) 343-353.
[132] S. Balta, A. Sotto, P. Luis, L. Benea, B. Van der Bruggen, J. Kim, A new outlook on membrane enhancement with nanoparticles: The alternative of ZnO, J. Membr. Sci., 389 (2012) 155-161.
[133] N. Maximous, G. Nakhla, W. Wan, K. Wong, Performance of a novel ZrO2/PES membrane for wastewater filtration, J. Membr. Sci., 352 (2010) 222-230.
[134] B. Cheng, M. Lei, J. Yu, X. Zhao, Preparation of monodispersed cubic calcium carbonate particles via precipitation reaction, Materials Letters, 58 (2004) 1565-1570.
[135] D. Hao, S.-c. Lu, Y.-x. Deng, G.-x. Du, Mechano-activated surface modification of calcium carbonate in wet stirred mill and its properties, Transactions of Nonferrous Metals Society of China, 17 (2007) 1100-1104.
[136] C. Wang, C. Piao, X. Zhai, F.N. Hickman, J. Li, Synthesis and characterization of hydrophobic calcium carbonate particles via a dodecanoic acid inducing process, Powder Technology, 198 (2010) 131-134.
[137] X. Gao, Y. Zhu, S. Zhou, W. Gao, Z. Wang, B. Zhou, Preparation and characterization of well-dispersed waterborne polyurethane/CaCO3 nanocomposites, Colloids and Surfaces A: Physicochemical and Engineering Aspects, 377 (2011) 312-317.
[138] L. Yan, Y.S. Li, C.B. Xiang, Preparation of poly(vinylidene fluoride)(pvdf) ultrafiltration membrane modified by nano-sized alumina (Al2O3) and its antifouling research, Polymer, 46 (2005) 7701-7706.
[139] M. Homayoonfal, M.R. Mehrnia, S. Rahmani, Y. Mohades Mojtahedi, Fabrication of alumina/polysulfone nanocomposite membranes with biofouling mitigation approach in membrane bioreactors, Journal of Industrial and Engineering Chemistry, 22 (2015) 357-367.
[140] Y.M. Mojtahedi, M.R. Mehrnia, M. Homayoonfal, Fabrication of Al2O3/PSf nanocomposite membranes: efficiency comparison of coating and blending methods in modification of filtration performance, Desalination and Water Treatment, 51 (2013) 6736-6742.

[141] J. Dai, K. Xiao, H. Dong, W. Liao, X. Tang, Z. Zhang, S. Cai, Preparation of Al2O3/PU/PVDF composite membrane and performance comparison with PVDF membrane, PU/PVDF blending membrane, and Al2O3/PVDF hybrid membrane, Desalination and Water Treatment, 57 (2016) 487-494.
[142] D. Hou, G. Dai, H. Fan, J. Wang, C. Zhao, H. Huang, Effects of calcium carbonate nano-particles on the properties of PVDF/nonwoven fabric flat-sheet composite membranes for direct contact membrane distillation, Desalination, 347 (2014) 25-33.
[143] K. Fujihara, M. Kotaki, S. Ramakrishna, Guided bone regeneration membrane made of polycaprolactone/calcium carbonate composite nano-fibers, Biomaterials, 26 (2005) 4139-4147.
[144] S.-H. Zhi, L.-S. Wan, Z.-K. Xu, Poly(vinylidene fluoride)/poly(acrylic acid)/calcium carbonate composite membranes via mineralization, Journal of Membrane Science, 454 (2014) 144-154.
[145] J.E. Cadotte, R.J. Petersen, R.E. Larson, E.E. Erickson, A new thin-film composite seawater reverse osmosis membrane, Desalination, 32 (1980) 25-31.
[146] B.J.A. Tarboush, D. Rana, T. Matsuura, H.A. Arafat, R.M. Narbaitz, Preparation of thin-film-composite polyamide membranes for desalination using novel hydrophilic surface modifying macromolecules, Journal of Membrane Science, 325 (2008) 166-175.
[147] S. Veríssimo, K.V. Peinemann, J. Bordado, Influence of the diamine structure on the nanofiltration performance, surface morphology and surface charge of the composite polyamide membranes, Journal of Membrane Science, 279 (2006) 266-275.
[148] S.-H. Huang, C.-L. Li, C.-C. Hu, H.A. Tsai, K.-R. Lee, J.-Y. Lai, Polyamide thin-film composite membranes prepared by interfacial polymerization for pervaporation separation, Desalination, 200 (2006) 387-389.
[149] A.P. Korikov, P.B. Kosaraju, K.K. Sirkar, Interfacially polymerized hydrophilic microporous thin film composite membranes on porous polypropylene hollow fibers and flat films, Journal of Membrane Science, 279 (2006) 588-600.
[150] A. Prakash Rao, N.V. Desai, R. Rangarajan, Interfacially synthesized thin film composite RO membranes for seawater desalination, Journal of Membrane Science, 124 (1997) 263-272.
[151] I.J. Roh, A.R. Greenberg, V.P. Khare, Synthesis and characterization of interfacially polymerized polyamide thin films, Desalination, 191 (2006) 279-290.
[152] R.J. Petersen, Composite reverse osmosis and nanofiltration membranes, Journal of Membrane Science, 83 (1993) 81-150.
[153] T. Sarada, L. Sawyer, M. Ostler, Three dimensional structure of Celgard® microporous membranes, Journal of Membrane Science, 15 (1983) 97-113.
[154] W. Zhu, X. Zhang, C. Zhao, W. Wu, J. Hou, M. Xu, A novel polypropylene microporous film, Polymers for Advanced Technologies, 7 (1996) 743-748.
[155] K. Trommer, B. Morgenstern, Nonrigid microporous PVC sheets: Preparation and properties, Journal of applied polymer science, 115 (2010) 2119-2126.
[156] L. Dauginet-De Pra, E. Ferain, R. Legras, S. Demoustier-Champagne, Fabrication of a new generation of track-etched templates and their use for the synthesis of metallic and organic nanostructures, Nuclear Instruments and Methods in Physics Research Section B: Beam Interactions with Materials and Atoms, 196 (2002) 81-88.
[157] R. Fleischer, P. Price, E. Symes, Novel filter for biological materials, Science, 143 (1964) 249-250.
[158] M.E. Toimil-Molares, Characterization and properties of micro- and nanowires of controlled size, composition, and geometry fabricated by electrodeposition and ion-track technology, Beilstein Journal of Nanotechnology, 3 (2012) 860-883.

[159] S. Ramakrishna, R. Jose, P. Archana, A. Nair, R. Balamurugan, J. Venugopal, W. Teo, Science and engineering of electrospun nanofibers for advances in clean energy, water filtration, and regenerative medicine, Journal of materials science, 45 (2010) 6283-6312.
[160] K. Yoon, B.S. Hsiao, B. Chu, Functional nanofibers for environmental applications, Journal of Materials Chemistry, 18 (2008) 5326-5334.
[161] J.A. Prince, G. Singh, D. Rana, T. Matsuura, V. Anbharasi, T.S. Shanmugasundaram, Preparation and characterization of highly hydrophobic poly(vinylidene fluoride) – Clay nanocomposite nanofiber membranes (PVDF–clay NNMs) for desalination using direct contact membrane distillation, Journal of Membrane Science, 397–398 (2012) 80-86.
[162] B.S. Lalia, E. Guillen-Burrieza, H.A. Arafat, R. Hashaikeh, Fabrication and characterization of polyvinylidenefluoride-co-hexafluoropropylene (PVDF-HFP) electrospun membranes for direct contact membrane distillation, Journal of Membrane Science, 428 (2013) 104-115.
[163] R. Gopal, S. Kaur, Z. Ma, C. Chan, S. Ramakrishna, T. Matsuura, Electrospun nanofibrous filtration membrane, Journal of Membrane Science, 281 (2006) 581-586.
[164] N. Bhardwaj, S.C. Kundu, Electrospinning: a fascinating fiber fabrication technique, Biotechnology advances, 28 (2010) 325-347.
[165] X. Zong, K. Kim, D. Fang, S. Ran, B.S. Hsiao, B. Chu, Structure and process relationship of electrospun bioabsorbable nanofiber membranes, Polymer, 43 (2002) 4403-4412.
[166] P. Burmann, B. Zornoza, C. Téllez, J. Coronas, Mixed matrix membranes comprising MOFs and porous silicate fillers prepared via spin coating for gas separation, Chemical Engineering Science, 107 (2014) 66-75.
[167] I.C. Kim, H.G. Yoon, K.H. Lee, Formation of integrally skinned asymmetric polyetherimide nanofiltration membranes by phase inversion process, Journal of applied polymer science, 84 (2002) 1300-1307.
[168] H. Kim, R. Tyagi, A. Fouda, K. Jonasson, The kinetic study for asymmetric membrane formation via phase-inversion process, Journal of applied polymer science, 62 (1996) 621-629.
[169] M. Ulbricht, Advanced functional polymer membranes, Polymer, 47 (2006) 2217-2262.
[170] G.J. Gittens, P.A. Hitchcock, D.C. Sammon, G.E. Wakley, The structure of cellulose acetate membranes for reverse osmosis. Part I. Membranes prepared from a dioxan based dope, Desalination, 8 (1970) 369-391.
[171] R.W. Baker, Membrane technology and applications, John Wiley & Sons, Ltd, (2004) 96-103.
[172] L.Y. Lafreniere, F.D. Talbot, T. Matsuura, S. Sourirajan, Effect of poly (vinylpyrrolidone) additive on the performance of poly (ether sulfone) ultrafiltration membranes, Industrial & engineering chemistry research, 26 (1987) 2385-2389.
[173] J.-F. Blanco, J. Sublet, Q.T. Nguyen, P. Schaetzel, Formation and morphology studies of different polysulfones-based membranes made by wet phase inversion process, Journal of Membrane Science, 283 (2006) 27-37.
[174] A.S. More, S.K. Pasale, P.P. Wadgaonkar, Synthesis and characterization of polyamides containing pendant pentadecyl chains, European Polymer Journal, 46 (2010) 557-567.
[175] S.X. Liu, J.-T. Kim, Characterization of surface modification of polyethersulfone membrane, Journal of adhesion science and technology, 25 (2011) 193-212.

[176] I. Pinnau, B.D. Freeman, Formation and Modification of Polymeric Membranes: Overview, in: Membrane Formation and Modification, American Chemical Society, 1999, pp. 1-22.
[177] I. Pinnau, B.D. Freeman, Formation and modification of polymeric membranes: overview, in, ACS Publications, 2000.
[178] H.J. Lee, J. Won, H. Lee, Y.S. Kang, Solution properties of poly(amic acid)–NMP containing LiCl and their effects on membrane morphologies, Journal of Membrane Science, 196 (2002) 267-277.
[179] D. Wang, K. Li, W. Teo, Porous PVDF asymmetric hollow fiber membranes prepared with the use of small molecular additives, Journal of Membrane Science, 178 (2000) 13-23.
[180] N.A. Ochoa, P. Prádanos, L. Palacio, C. Pagliero, J. Marchese, A. Hernández, Pore size distributions based on AFM imaging and retention of multidisperse polymer solutes, Journal of Membrane Science, 187 (2001) 227-237.
[181] M.-J. Han, Effect of propionic acid in the casting solution on the characteristics of phase inversion polysulfone membranes, Desalination, 121 (1999) 31-39.
[182] D.A. Musale, A. Kumar, G. Pleizier, Formation and characterization of poly(acrylonitrile)/Chitosan composite ultrafiltration membranes, Journal of Membrane Science, 154 (1999) 163-173.
[183] J.-H. Kim, K.-H. Lee, Effect of PEG additive on membrane formation by phase inversion, Journal of Membrane Science, 138 (1998) 153-163.
[184] I.-C. Kim, K.-H. Lee, Effect of various additives on pore size of polysulfone membrane by phase-inversion process, Journal of Applied Polymer Science, 89 (2003) 2562-2566.
[185] Y.S. Li, L. Yan, C.B. Xiang, L.J. Hong, Treatment of oily wastewater by organic–inorganic composite tubular ultrafiltration (UF) membranes, Desalination, 196 (2006) 76-83.
[186] F.L. Hua, Y.F. Tsang, Y.J. Wang, S.Y. Chan, H. Chua, S.N. Sin, Performance study of ceramic microfiltration membrane for oily wastewater treatment, Chemical Engineering Journal, 128 (2007) 169-175.
[187] M. Cheryan, N. Rajagopalan, Membrane processing of oily streams. Wastewater treatment and waste reduction, Journal of Membrane Science, 151 (1998) 13-28.
[188] Z. Xue, Y. Cao, N. Liu, L. Feng, L. Jiang, Special wettable materials for oil/water separation, Journal of Materials Chemistry A, 2 (2014) 2445-2460.
[189] H.-C. Yang, K.-J. Liao, H. Huang, Q.-Y. Wu, L.-S. Wan, Z.-K. Xu, Mussel-inspired modification of a polymer membrane for ultra-high water permeability and oil-in-water emulsion separation, Journal of Materials Chemistry A, 2 (2014) 10225-10230.
[190] Y. Yang, H. Zhang, P. Wang, Q. Zheng, J. Li, The influence of nano-sized TiO2 fillers on the morphologies and properties of PSF UF membrane, Journal of Membrane Science, 288 (2007) 231-238.
[191] M. Padaki, R. Surya Murali, M.S. Abdullah, N. Misdan, A. Moslehyani, M.A. Kassim, N. Hilal, A.F. Ismail, Membrane technology enhancement in oil–water separation. A review, Desalination, 357 (2015) 197-207.
[192] Y. Zhang, F. Liu, Y. Lu, L. Zhao, L. Song, Investigation of phosphorylated TiO2–SiO2 particles/polysulfone composite membrane for wastewater treatment, Desalination, 324 (2013) 118-126.
[193] Y. Zhang, X. Shan, Z. Jin, Y. Wang, Synthesis of sulfated Y-doped zirconia particles and effect on properties of polysulfone membranes for treatment of wastewater containing oil, Journal of Hazardous Materials, 192 (2011) 559-567.

[194] A. Ahmad, M. Majid, B. Ooi, Functionalized PSf/SiO 2 nanocomposite membrane for oil-in-water emulsion separation, Desalination, 268 (2011) 266-269.
[195] V. Vatanpour, S.S. Madaeni, R. Moradian, S. Zinadini, B. Astinchap, Novel antibifouling nanofiltration polyethersulfone membrane fabricated from embedding TiO2 coated multiwalled carbon nanotubes, Separation and Purification Technology, 90 (2012) 69-82.
[196] S. Jamal, S. Chang, H. Zhou, Filtration behaviour and fouling mechanisms of polysaccharides, Membranes, 4 (2014) 319-332.
[197] S. Zhao, Z. Wang, X. Wei, B. Zhao, J. Wang, S. Yang, S. Wang, Performance improvement of polysulfone ultrafiltration membrane using PANiEB as both pore forming agent and hydrophilic modifier, Journal of Membrane Science, 385 (2011) 251-262.
[198] H. Lohokare, Y. Bhole, S. Taralkar, U. Kharul, Poly(acrylonitrile) based ultrafiltration membranes: Optimization of preparation parameters, Desalination, 282 (2011) 46-53.
[199] C.L. Wu, M.Q. Zhang, M.Z. Rong, K. Friedrich, Tensile performance improvement of low nanoparticles filled-polypropylene composites, Composites Science and Technology, 62 (2002) 1327-1340.
[200] H. Lohokare, Y. Bhole, U. Kharul, Effect of support material on ultrafiltration membrane performance, Journal of applied polymer science, 99 (2006) 3389-3395.
[201] Z. Chen, M. Deng, Y. Chen, G. He, M. Wu, J. Wang, Preparation and performance of cellulose acetate/polyethyleneimine blend microfiltration membranes and their applications, Journal of Membrane Science, 235 (2004) 73-86.
[202] A. Ananth, G. Arthanareeswaran, H. Wang, The influence of tetraethylorthosilicate and polyethyleneimine on the performance of polyethersulfone membranes, Desalination, 287 (2012) 61-70.
[203] Q. Wei, F. Wang, Z.-R. Nie, C.-L. Song, Y.-L. Wang, Q.-Y. Li, Highly hydrothermally stable microporous silica membranes for hydrogen separation, The Journal of Physical Chemistry B, 112 (2008) 9354-9359.
[204] H.B.T. Jeazet, C. Staudt, C. Janiak, A method for increasing permeability in O2/N2 separation with mixed-matrix membranes made of water-stable MIL-101 and polysulfone, Chemical Communications, 48 (2012) 2140-2142.
[205] P.V. Chai, E. Mahmoudi, Y.H. Teow, A.W. Mohammad, Preparation of novel polysulfone-Fe3O4/GO mixed-matrix membrane for humic acid rejection, Journal of Water Process Engineering, 15 (2017) 83-88.
[206] I.M. Wienk, R.M. Boom, M.A.M. Beerlage, A.M.W. Bulte, C.A. Smolders, H. Strathmann, Recent advances in the formation of phase inversion membranes made from amorphous or semi-crystalline polymers, J. Membr. Sci., 113 (1996) 361-371.
[207] A. Alpatova, E.-S. Kim, X. Sun, G. Hwang, Y. Liu, M.G. El-Din, Fabrication of porous polymeric nanocomposite membranes with enhanced anti-fouling properties: effect of casting composition, J. Membr. Sci., 444 (2013) 449-460.
[208] P. Aerts, E. Van Hoof, R. Leysen, I.F.J. Vankelecom, P.A. Jacobs, Polysulfone–Aerosil composite membranes: Part 1. The influence of the addition of Aerosil on the formation process and membrane morphology, J. Membr. Sci., 176 (2000) 63-73.
[209] J.L. White, J.W. Crowder, The influence of carbon black on the extrusion characteristics and rheological properties of elastomers: Polybutadiene and butadiene–styrene copolymer, J. Appl. Polym. Sci., 18 (1974) 1013-1038.
[210] J.S. Taurozzi, C.A. Crock, V.V. Tarabara, C60-polysulfone nanocomposite membranes: Entropic and enthalpic determinants of C60 aggregation and its effects on membrane properties, Desalination, 269 (2011) 111-119.

[211] M. Alhoshan, J. Alam, L.A. Dass, N. Al-Homaidi, Fabrication of polysulfone/ZnO membrane: influence of ZnO nanoparticles on membrane characteristics, Adv. Polym. Tech., 32 (2013).
[212] S. Zhao, W. Yan, M. Shi, Z. Wang, J. Wang, S. Wang, Improving permeability and antifouling performance of polyethersulfone ultrafiltration membrane by incorporation of ZnO-DMF dispersion containing nano-ZnO and polyvinylpyrrolidone, J. Membr. Sci., 478 (2015) 105-116.
[213] T.M. Costa, M.R. Gallas, E.V. Benvenutti, J.A. da Jornada, Study of nanocrystalline γ-Al2O3 produced by high-pressure compaction, J. Phys. Chem. B, 103 (1999) 4278-4284.
[214] Z. Zhang, Q. An, Y. Ji, J. Qian, C. Gao, Effect of zero shear viscosity of the casting solution on the morphology and permeability of polysulfone membrane prepared via the phase-inversion process, Desalination, 260 (2010) 43-50.
[215] A. Khalid, A.A. Al-Juhani, O.C. Al-Hamouz, T. Laoui, Z. Khan, M.A. Atieh, Preparation and properties of nanocomposite polysulfone/multi-walled carbon nanotubes membranes for desalination, Desalination, 367 (2015) 134-144.
[216] N. Meng, Z. Wang, Z.-X. Low, Y. Zhang, H. Wang, X. Zhang, Impact of trace graphene oxide in coagulation bath on morphology and performance of polysulfone ultrafiltration membrane, Sep. Purif. Technol., 147 (2015) 364-371.
[217] J. Hong, Y. He, Polyvinylidene fluoride ultrafiltration membrane blended with nano-ZnO particle for photo-catalysis self-cleaning, Desalination, 332 (2014) 67-75.
[218] W. Pu, X. He, L. Wang, C. Jiang, C. Wan, Preparation of PVDF–HFP microporous membrane for Li-ion batteries by phase inversion, Journal of Membrane Science, 272 (2006) 11-14.
[219] R. Rezaee, S. Nasseri, A.H. Mahvi, R. Nabizadeh, S.A. Mousavi, A. Rashidi, A. Jafari, S. Nazmara, Fabrication and characterization of a polysulfone-graphene oxide nanocomposite membrane for arsenate rejection from water, J. Environ. Health., 13 (2015) 61.
[220] M.-J. Han, S.-T. Nam, Thermodynamic and rheological variation in polysulfone solution by PVP and its effect in the preparation of phase inversion membrane, Journal of Membrane Science, 202 (2002) 55-61.
[221] J.-H. Choi, J. Jegal, W.-N. Kim, Fabrication and characterization of multi-walled carbon nanotubes/polymer blend membranes, J. Membr. Sci., 284 (2006) 406-415.
[222] K. Wang, A.A. Abdalla, M.A. Khaleel, N. Hilal, M.K. Khraisheh, Mechanical properties of water desalination and wastewater treatment membranes, Desalination, 401 (2017) 190-205.
[223] M. Kumar, D. McGlade, M. Ulbricht, J. Lawler, Quaternized polysulfone and graphene oxide nanosheet derived low fouling novel positively charged hybrid ultrafiltration membranes for protein separation, RSC Adv., 5 (2015) 51208-51219.
[224] M. Kumar, Z. Gholamvand, A. Morrissey, K. Nolan, M. Ulbricht, J. Lawler, Preparation and characterization of low fouling novel hybrid ultrafiltration membranes based on the blends of GO−TiO2 nanocomposite and polysulfone for humic acid removal, J. Membr. Sci., 506 (2016) 38-49.
[225] A. Ouradi, Q.T. Nguyen, A. Benaboura, Polysulfone–AN69 blend membranes and its surface modification by polyelectrolyte-layer deposit—Preparation and characterization, J. Membr. Sci., 454 (2014) 20-35.
[226] G.L. Jadav, P.S. Singh, Synthesis of novel silica-polyamide nanocomposite membrane with enhanced properties, Journal of Membrane Science, 328 (2009) 257-267.

[227] A. Dehghani Kiadehi, A. Rahimpour, M. Jahanshahi, A.A. Ghoreyshi, Novel carbon nano-fibers (CNF)/polysulfone (PSf) mixed matrix membranes for gas separation, J. Ind. Eng. Chem., 22 (2015) 199-207.
[228] N.N. Rupiasih, H. Suyanto, M. Sumadiyasa, N. Wendri, Study of effects of low doses UV radiation on microporous polysulfone membranes in sterilization process, (2013).
[229] E. Celik, L. Liu, H. Choi, Protein fouling behavior of carbon nanotube/polyethersulfone composite membranes during water filtration, water research, 45 (2011) 5287-5294.
[230] A. Mollahosseini, A. Rahimpour, M. Jahamshahi, M. Peyravi, M. Khavarpour, The effect of silver nanoparticle size on performance and antibacteriality of polysulfone ultrafiltration membrane, Desalination, 306 (2012) 41-50.
[231] S. Majeed, D. Fierro, K. Buhr, J. Wind, B. Du, A. Boschetti-de-Fierro, V. Abetz, Multi-walled carbon nanotubes (MWCNTs) mixed polyacrylonitrile (PAN) ultrafiltration membranes, J. Membr. Sci., 403–404 (2012) 101-109.
[232] H. Wu, B. Tang, P. Wu, Novel ultrafiltration membranes prepared from a multi-walled carbon nanotubes/polymer composite, J. Membr. Sci., 362 (2010) 374-383.
[233] B.D. McCloskey, H.B. Park, H. Ju, B.W. Rowe, D.J. Miller, B.J. Chun, K. Kin, B.D. Freeman, Influence of polydopamine deposition conditions on pure water flux and foulant adhesion resistance of reverse osmosis, ultrafiltration, and microfiltration membranes, Polymer, 51 (2010) 3472-3485.
[234] M.R. Esfahani, J.L. Tyler, H.A. Stretz, M.J.M. Wells, Effects of a dual nanofiller, nano-TiO2 and MWCNT, for polysulfone-based nanocomposite membranes for water purification, Desalination, 372 (2015) 47-56.
[235] S. Saksena, A.L. Zydney, Effect of solution pH and ionic strength on the separation of albumin from immunoglobulins (IgG) by selective filtration, Biotechnology and bioengineering, 43 (1994) 960-968.
[236] B. Yu, J. Liu, S. Liu, F. Zhou, Pdop layer exhibiting zwitterionicity: a simple electrochemical interface for governing ion permeability, Chemical Communications, 46 (2010) 5900-5902.
[237] A.K. Nair, A.M. Isloor, R. Kumar, A.F. Ismail, Antifouling and performance enhancement of polysulfone ultrafiltration membranes using CaCO3 nanoparticles, Desalination, 322 (2013) 69-75.
[238] A.P. Lim, A.Z. Aris, A review on economically adsorbents on heavy metals removal in water and wastewater, Reviews in Environmental Science and Bio/Technology, 13 (2014) 163-181.
[239] Z.G. Cui, K.Z. Shi, Y.Z. Cui, B.P. Binks, Double phase inversion of emulsions stabilized by a mixture of CaCO3 nanoparticles and sodium dodecyl sulphate, Colloids and Surfaces A: Physicochemical and Engineering Aspects, 329 (2008) 67-74.
[240] C.-M. Chan, J. Wu, J.-X. Li, Y.-K. Cheung, Polypropylene/calcium carbonate nanocomposites, Polymer, 43 (2002) 2981-2992.
[241] Functionalization of zinc oxide (ZnO) nanoparticles and its effects on polysulfone-ZnO membranes, Desalin. Water. Treat., 57 (2016) 7801-7811.
[242] H.-D. Yu, S.Y. Tee, M.-Y. Han, Preparation of porosity-controlled calcium carbonate by thermal decomposition of volume content-variable calcium carboxylate derivatives, Chemical Communications, 49 (2013) 4229-4231.
[243] M. Abebe, N. Hedin, Z. Bacsik, Spherical and Porous Particles of Calcium Carbonate Synthesized with Food Friendly Polymer Additives, Crystal Growth & Design, 15 (2015) 3609-3616.

[244] M.A. Osman, A. Atallah, U.W. Suter, Influence of excessive filler coating on the tensile properties of LDPE–calcium carbonate composites, Polymer, 45 (2004) 1177-1183.
[245] R.S. Lam, J.M. Charnock, A. Lennie, F.C. Meldrum, Synthesis-dependant structural variations in amorphous calcium carbonate, CrystEngComm, 9 (2007) 1226-1236.
[246] A. Stoica-Guzun, M. Stroescu, S. Jinga, I. Jipa, T. Dobre, L. Dobre, Ultrasound influence upon calcium carbonate precipitation on bacterial cellulose membranes, Ultrasonics Sonochemistry, 19 (2012) 909-915.
[247] M. Khayet, Membrane surface modification and characterization by X-ray photoelectron spectroscopy, atomic force microscopy and contact angle measurements, Applied Surface Science, 238 (2004) 269-272.
[248] J.S.d.C. Campos, A.A. Ribeiro, C.X. Cardoso, Preparation and characterization of PVDF/CaCO 3 composites, Materials Science and Engineering: B, 136 (2007) 123-128.
[249] F. Morel, V. Bounor-Legaré, E. Espuche, O. Persyn, M. Lacroix, Surface modification of calcium carbonate nanofillers by fluoro- and alkyl-alkoxysilane: Consequences on the morphology, thermal stability and gas barrier properties of polyvinylidene fluoride nanocomposites, European Polymer Journal, 48 (2012) 919-929.
[250] S.B. Teli, S. Molina, E.G. Calvo, A.E. Lozano, J. de Abajo, Preparation, characterization and antifouling property of polyethersulfone–PANI/PMA ultrafiltration membranes, Desalination, 299 (2012) 113-122.
[251] Z. Ma, T. Lei, X. Ji, X. Gao, C. Gao, Submerged Membrane Bioreactor for Vegetable Oil Wastewater Treatment, Chemical Engineering & Technology, 38 (2015) 101-109.